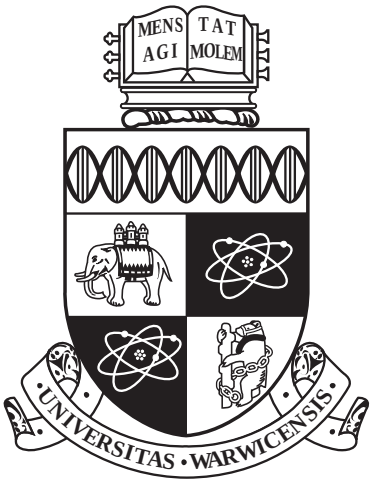

Variability of Structurally Constrained and Unconstrained Functional Connectivity in Schizophrenia

by

Ye Yao

Thesis

Submitted to the University of Warwick

for the degree of

Doctor of Philosophy

Computer Science

February 2016

THE UNIVERSITY OF
WARWICK

Contents

List of Tables

List of Figures

Acknowledgments

I am heartily thankful to my supervisor, Jianfeng Feng, whose encouragement, guidance and support from the initial to the final level enabled me to develop an understanding of the subject.

Secondly, I offer my regards and blessings to all of those who supported me including Prof. Edmund Rolls, Prof. David Waxman, Prof. Lena Palaniyappan and Prof. Thomas Nichols in any respect during the completion of the project.

Lastly, I would like to thank my family for their wonderful help.

Declarations

The MRI data of this thesis has been previously reported in some earlier study (Palaniyappan et al., 2013), University of Nottingham, UK.

The thesis is my own work except some parts are based on the collaborative research with Dr. Bing Xu, Prof. Edmund Rolls, Prof. David Waxman, Prof. Lena Palaniyappan and my supervisor, Prof. Jianfeng Feng. In the collaborative research, Prof. Jianfeng Feng raised the Functional Connectivity Entropy (FCE) idea. Dr. Bing Xu, Prof. Edmund Rolls, Prof. David Waxman, Prof. Jianfeng Feng and I discussed this idea and tried to go further. I got the structurally constrained and unconstrained functional connectivity idea, did the processing, finished the analysis and wrote most of the paper writing. Prof. Edmund Rolls, Prof. David Waxman and Prof. Lena Palaniyappan helped me to do paper writings to publish the results in better journals. For the computational model part in the thesis, Prof. Gustavo Deco wrote the raw code, Dr. Bing Xu revised the codings in the FCE model, and I did data analysis. Furthermore, Dr. Ting Li, Prof. Chunbo Li and I applied the FCE idea in cognitive training area.

The thesis includes materials arising from work which has appeared in print. The functional connectivity entropy idea is firstly published on Yao et al. [2014], which is published before the beginning of the PhD period. Since the idea is crucial in this thesis, I just introduce this idea in Section 1.4.1, 2.8 and 3.1. The key story of this thesis has already been published on Yao et al. [2015], and several figures and tables are reproduced or modified from the article, which have been clarified well in the

main text. Functional connectivity entropy idea could also be applied in cognitive training area, which is demonstrated in Section 4.6, has been published on Li et al. [2016]. Some texts and figures are reproduced or modified from this article. Finally, in the thesis include a list of functional connectivity entropy work in Schizophrenia area, which is still in preparation and will be submitted soon.

The thesis has not been submitted for a degree at another university.

Abstract

In this thesis, entropy is used to characterize intrinsic ageing properties of the human brain. Analysis of fMRI data from a large dataset of individuals, using resting state BOLD signals, demonstrated that a functional connectivity entropy associated with brain activity increases with age. During an average lifespan, the entropy, which was calculated from a population of individuals, increased by approximately 0.1 bits, due to correlations in BOLD activity becoming more widely distributed. This is attributed to the number of excitatory neurons and the excitatory conductance decreasing with age. Incorporating these properties into a computational model leads to quantitatively similar results to the fMRI data. The dataset involved males and females and significant differences were found between them. The entropy of males at birth was lower than that of females. However, the entropies of the two sexes increase at different rates, and intersect at approximately 50 years; after this age, males have a larger entropy.

In addition, the connectivity between different brain areas provides evidence about normal function and dysfunction. Changes are described in the distribution of these connectional strengths in schizophrenia using a large sample of resting-state fMRI data. The functional connectivity entropy, which measures the dispersion of the functional connectivity distribution, was lower in patients with schizophrenia than in controls, reflecting a reduction in both strong positive and negative correlations between brain regions. The decrease in the functional connectivity entropy was strongly associated with an increase in the positive, negative, and general symptoms. Using an integrate-and-fire simulation model based on anatomical connectivity, it is

shown that a reduction in the efficacy of the NMDA mediated excitatory synaptic inputs can reduce the functional connectivity entropy to resemble the pattern seen in schizophrenia.

Spatial variation in connectivity is an integral aspect of the brain's architecture. In the absence of this variability, the brain may act as a single homogenous entity without regional specialization. In this thesis, We investigate the variability in functional links categorized on the basis of the presence of direct structural paths (primary) or indirect paths mediated by one (secondary) or more (tertiary) brain regions ascertained by diffusion tensor imaging. We quantified the variability in functional connectivity using an unbiased estimate of unpredictability (functional connectivity entropy) in a neuropsychiatric disorder where structure-function relationship is considered to be abnormal. 34 patients and 32 healthy controls underwent DTI and resting state functional MRI scans. Less than one-third (27.4% in patients, 27.85% in controls) of functional links between brain regions were regarded as direct primary links on the basis of DTI tractography, while the rest were secondary or tertiary. The most significant changes in the distribution of functional connectivity in schizophrenia occur in indirect tertiary paths with no direct axonal linkage in both early ($p=0.0002$, $d=1.46$) and late ($p=1\times10^{-17}$, $d=4.66$) stages of schizophrenia, and are not altered by the severity of symptoms, suggesting that this is an invariant feature of this illness. Unlike those with early stage illness, patients with chronic illness show some additional reduction in the distribution of connectivity among functional links that have direct structural paths ($p=0.08$, $d=0.44$). Our findings address a critical gap in the literature linking structure and function in schizophrenia, and demonstrate for the first time that the abnormal state of functional connectivity preferentially affects structurally unconstrained links in schizophrenia. It also raises the question of a continuum of dysconnectivity ranging from less direct (structurally unconstrained) to more direct (structurally constrained) brain pathways underlying the clinical severity and persistence of schizophrenia.

Keywords Schizophrenia Functional MRI Diffusion Tensor Imaging

FC Functional Connectivity

SC Structurally Constrained

SU Structurally Unconstrained

FCE Functional Connectivity Entropy

Abbreviations

MRI	Magnetic resonance imaging
fMRI	functional Magnetic resonance imaging
BOLD	Blood-oxygen-level dependent
rsfMRI	Resting state fMRI
DTI	Diffusion Tensor Imaging
FCE	Functional Connectivity Entropy
SCZD	Schizophrenia
RSN	Resting State Network

Chapter 1

Introduction

1.1 MRI, functional MRI and Diffusion MRI

1.1.1 Magnetic resonance imaging

Magnetic resonance imaging (MRI) is a medical imaging technique used in radiology to image the anatomy and the physiological processes of the body in both health and disease. The basic principle of MRI scanners is using strong magnetic fields, radio waves, and field gradients to form images of the body [Edelman and Warach, 1993].

All hydrogen atoms have nuclear spins, which are associated with a magnetic dipole moment (analogous to a compass needle) and detectable by MRI, as shown in Figure 1.1. The human body is roughly 70-percent water with full of hydrogen atoms, and most MRI scans essentially measure the spatial distribution of water in the object being imaged. MRI is widely used in hospitals and clinics for medical diagnosis, staging of disease and follow-up without exposing the body to ionizing radiation [Brown et al., 2014].

It should be emphasized that Reflecting the fundamental importance and applicability of MRI in medicine, Dr. Paul Lauterbur of the University of Illinois at Urbana-Champaign and Sir Peter Mansfield of the University of Nottingham were awarded the 2003 Nobel Prize in Physiology or Medicine for their 'discoveries concerning magnetic resonance imagin'.

In all kinds of MRI medical applications, MRI of the nervous system is the most interesting one, which uses magnetic fields and radio waves to produce high quality two- or three-dimensional images of nervous system structures [Dousset et al., 1999]. After the first MR images of a human brain were obtained in 1978 by two groups of researchers at EMI Laboratories led by Dr. Ian Robert Young and

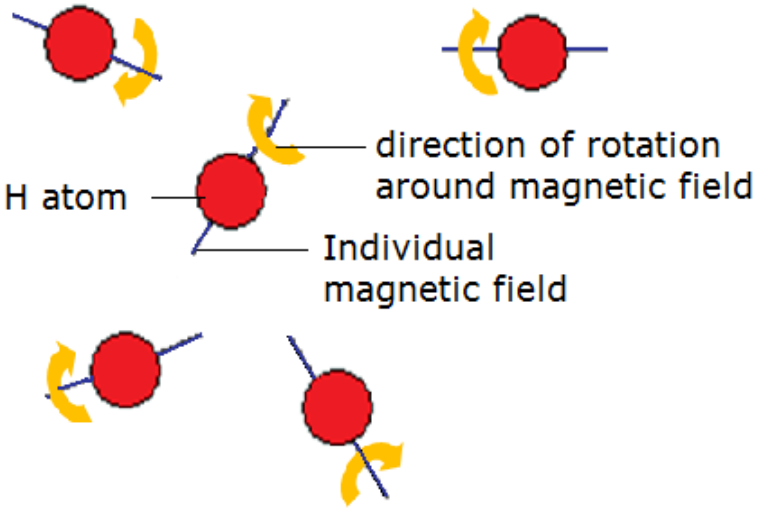

Figure 1.1: Nuclear spins of hydrogen atoms

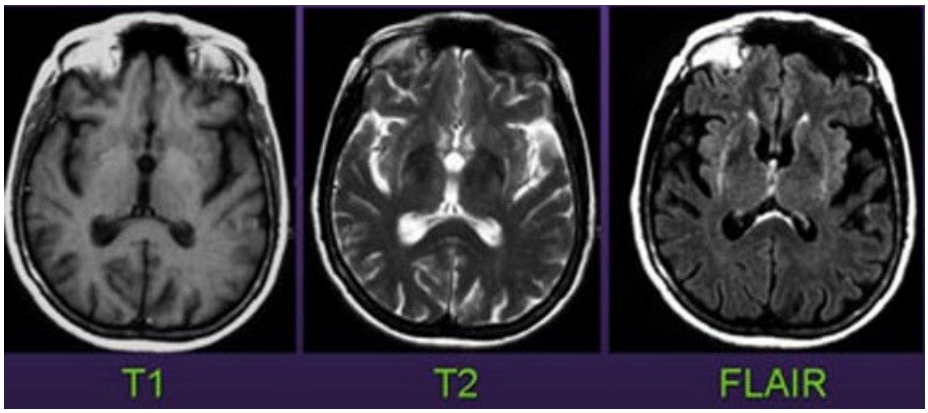

Figure 1.2: Different types of MRI imaging modes

Dr. Hugh Clow [Clow and Young, 1978], a number of different imaging modes can be used with imaging the nervous system: T1, T2, Flair (fluid attenuated inversion recovery), fMRI and Diffusion MRI [Edelman and Warach, 1993][Johansen-Berg and Behrens, 2013][Brown et al., 2014], as shown in Figure 1.2:
T1: It is useful and common for visualizing normal anatomy. Cerebrospinal fluid area is dark.
T2: It is useful and common for visualizing pathology. Cerebrospinal fluid area is light, while white matter is darker than that with T1.
FLAIR: It is useful for evaluation of white matter plaques near the ventricles and identifying demyelination.
fMRI: Functional magnetic resonance imaging is to measure brain activity, which will be described in detail in Section 1.1.2.
Diffusion MRI: It allows the mapping of the diffusion process of water molecules, in vivo and non-invasively, which will be described in detail in Section 1.1.3.

1.1.2 Functional Magnetic resonance imaging

Functional magnetic resonance imaging (fMRI) is a functional neuroimaging procedure using MRI technology that measures brain activity by detecting changes associated with blood flow [Huettel et al., 2004]. The primary form of fMRI uses the blood-oxygen-level dependent (BOLD) contrast, discovered by Dr. Seiji Ogawa [Ogawa et al., 1990]. This is a type of specialized brain and body scan used to map neural activity in the brain by imaging the change in blood flow (hemodynamic response) related to energy use by brain cells [Huettel et al., 2004], as illustrated in Figure 1.3.

The fMRI mainly detect the differences in magnetic properties between arterial (oxygen-rich) and venous (oxygen-poor) blood [Huettel et al., 2004]. The change in the fMRI signal from neuronal activity is called the hemodynamic response (HDR). It lags the neuronal events triggering it by 1 to 2 seconds, since it takes that long for the vascular system to respond to the brain's need for glucose. From this point it typically rises to a peak at about 5 seconds after the stimulus. If the neurons keep firing, say from a continuous stimulus, the peak spreads to a flat plateau while the neurons stay active. After activity stops, the BOLD signal falls below the original level, the baseline, a phenomenon called the undershoot. Over time the signal recovers to the baseline [Huettel et al., 2004][Ogawa et al., 1990][Ogawa and Sung, 2007].

There are mainly two types of fMRI scanning, task fMRI and resting state fMRI (rsfMRI) [Ogawa and Sung, 2007]. Task fMRI lets the subject do one or

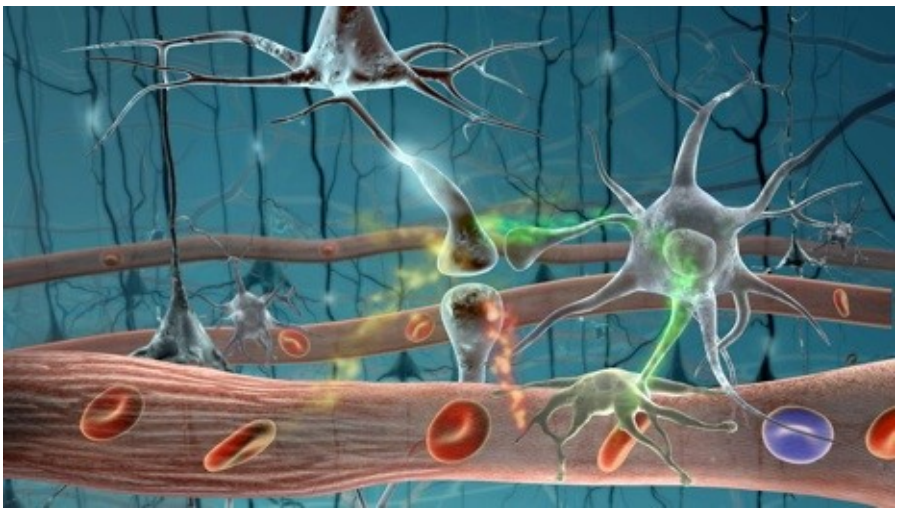

Figure 1.3: Blood-oxygen-level dependent (BOLD) demonstration

several specific and explicit tasks during MRI acquisition, while resting state fMRI just asks the subject to be at rest. In this thesis,we only use resting state fMRI data. Resting state fMRI is a method of functional brain imaging that can be used to evaluate regional interactions [Biswal, 2012].

Functional connectivity is the connectivity between brain regions that share functional properties. More specifically, it can be defined as the temporal correlation between two resting state BOLD signals [Biswal et al., 1997].

1.1.3 Diffusion MRI

Diffusion MRI is MRI method which allows the mapping of the diffusion process of water molecules in biological tissues like human beings, in vivo and non-invasively [Johansen-Berg and Behrens, 2013]. Molecular diffusion in tissues is not free, but reflects interactions with many obstacles like fibers [Hagmann et al., 2006]. That's why Diffusion MRI could reflect anatomical structures of brain.

There are lots of different types of diffusion MRI including Diffusion Tensor Imaging (DTI) [Le Bihan et al., 2001], High angular resolution diffusion imaging (HARDI) [Tuch et al., 2002] and Diffusion spectrum magnetic resonance imaging (DSI) [Wedeen et al., 2008]. In this thesis,we mainly use DTI data to do analysis. DTI is a magnetic resonance imaging technique that enables the measurement of the restricted diffusion of water in tissue in order to produce neural tract images [Johansen-Berg and Behrens, 2013]. After a list of processing, tractography results could be extracted for every subject [Basser et al., 2000], as shown in Figure 1.4.

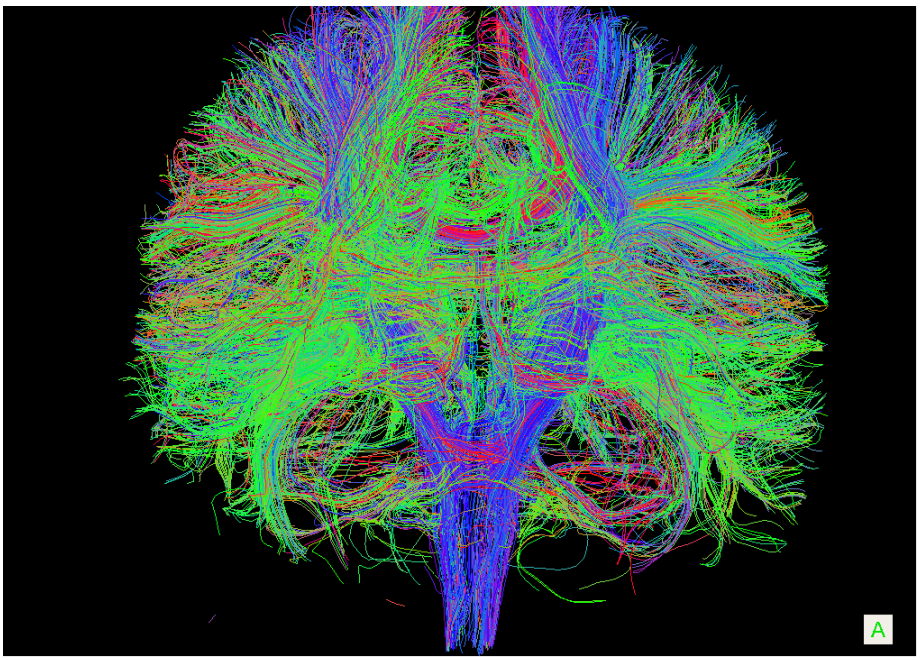

Figure 1.4: Diffusion MRI (Diffusion Tensor Imaging) tractography demonstration

1.2 Schizophrenia Brief Introduction

Schizophrenia is a mental disorder characterized by abnormal social behavior and failure to recognize what is real [Gottesman, 1991]. Common symptoms include false beliefs, unclear or confused thinking, hearing voices, reduced social engagement and emotional expression, and a lack of motivation [Kay et al., 1987]. Symptoms typically come on gradually, begin in young adulthood, and last a long time [First, 1994]. In this thesis,we tried to do some analysis on the schizophrenia effects on the brain.

Schizophrenia affects around $0.3\% \sim 0.7\%$ of people at some point in their life [van den Heuvel et al., 2009]. The incidence is comparatively quite high and schizophrenia does affect our society. For example, the winner of the 1994 Nobel Prize for Economics and one of the best mathematician in our history, John Nash got schizophrenia and fight against it for around half a century.

A number of attempts have been made to explain the link between altered brain function and schizophrenia [Gottesman, 1991]. Studies using neuropsychological tests and brain imaging technologies to examine functional differences in brain activity have shown that differences seem to most commonly occur in the frontal lobes, hippocampus and temporal lobes [Kircher and Thienel, 2005]. Unfortunately,

the authentic understanding of schizophrenia is still in mystery [Andreasen et al., 2012].

1.3 Schizophrenia Effects on Brain

Optimal function of the human brain relies on the cooperation of constituent brain regions. The degree of cooperative activity between two brain regions at rest, measured using functional connectivity [Friston, 1994], varies greatly across the brain. A complete lack of spatial variability in functional connectivity indicates that the entire brain is either acting as a single homogenous unit without regional specialization, or the constituent brain regions are entirely asynchronous, without integration. In contrast, optimum spatial variability in connectional strength reflects simultaneous integration and segregation across distributed brain regions. This diversity forms the core of the overall topology of the complex functional architecture of human brain [Bullmore and Sporns, 2009][Tononi et al., 1994] altered in neuropsychiatric disorders such as schizophrenia [Alexander-Bloch et al., 2010][Fornito et al., 2012][Rubinov and Bullmore, 2013][van den Heuvel et al., 2013].

In healthy controls, presence of structural connectivity (putative axonal linkage assessed using diffusion tensor imaging) strongly predicts the strength of functional connectivity [Damoiseaux and Greicius, 2009][Honey et al., 2009][Skudlarski et al., 2010][van den Heuvel et al., 2009]. Nevertheless, most of the pairwise functional connections exist in the absence of a direct axonal linkage between two regions [Adachi et al., 2012][Damoiseaux and Greicius, 2009][Honey et al., 2009]. In general, functional links that have a structural basis are stronger and involve anatomically more proximal regions [Honey et al., 2009]. In contrast, functional links between regions that do not share direct axonal linkage appear to be weaker, and involve spatially distant regions [Adachi et al., 2012][Honey et al., 2009]. Functional links in the absence of one-to-one axonal connections may emerge from directed polysynaptic connections or shared inputs/outputs involving a third region [Adachi et al., 2012]. Such indirect, weaker functional links may represent a connectional architecture that is physiologically distinct from the links with a more direct structural basis.

Several studies observe a reduction in overall strength of functional connectivity in schizophrenia [Argyelan et al., 2014][Bassett et al., 2012][Lynall et al., 2010], while both increased [Skudlarski et al., 2010][Whitfield-Gabrieli et al., 2009] and decreased [Bluhm et al., 2007][Liang et al., 2006] connectivity involving different regional connections are noted across the brain [Karbasforoushan and Wood-

ward, 2012][Pettersson-Yeo et al., 2011][Rubinov and Bullmore, 2013]. The presence of both hyper- and hypoconnectivity involving different regional connections [Guo et al., 2014][Skudlarski et al., 2010][Venkataraman et al., 2012][Woodward et al., 2012] indicates a large diversity in the distribution of connectivity across the functional links in schizophrenia. If such a diversification lies at the core of the dynamic pathophysiological process defining the presence of schizophrenia in an individual, then for a randomly chosen pair of brain regions, the connectional strength is likely to be less predictable in a patient compared to a healthy control.

Moreover, schizophrenia is characterized by the co-occurrence of positive, negative and cognitive symptoms [Rolls and Deco, 2010] which appear to be related to altered glutamatergic and GABAergic synaptic connectivity in several cortical areas [Coyle, 2006][Rolls, 2012][Rolls et al., 2008][Stan and Lewis, 2012]. Over the last two decades, much neuroimaging evidence for structural and functional deficits in the brain has strengthened the notion of dysconnectivity in schizophrenia [Friston and Frith, 1995][Frith, 1995]. The bulk of evidence for pathological dysconnectivity in schizophrenia comes from functional Magnetic Resonance Imaging (fMRI) studies [Bluhm et al., 2007][Meyer-Lindenberg et al., 2005][Whitfield-Gabrieli et al., 2009][Zhou et al., 2007]. These numerous small to medium-sized studies have indicated that schizophrenia is unlikely to be a disorder of a single or small-set of functional connections. Instead, the emerging picture is suggestive of a widespread change in the brain's network architecture, affecting the diversity (or complexity) that is characteristic of normal brain functions [Bassett et al., 2013][Lynall et al., 2010].

1.4 Functional Connectivity Entropy (FCE)

1.4.1 Functional Connectivity Entropy Origin

There is now a consensus that ageing is multifactorial; it is the joint outcome of genetics, the accumulation of random accidents and irreparable losses in molecular fidelity [Hayflick, 2007]. There is ample evidence that the genetic component alone plays a critical role in longevity determination [Christensen et al., 2006]. This is shown in regulatory and structural changes that occur with age in miRNA [Lanceta et al., 2010], mRNA [Rea and Johnson, 2003], ncRNA [Bates et al., 2009], protein expression [Morrow et al., 2004] and functional MRI [Zuo et al., 2010] in many species. Intuitively, these changes could be expected to correspond to changes in the functioning of the brain. But in what precise sense? This is the question we address in this work. The answer involves an explicitly quantitative way of characterizing

the intrinsic ageing process of the human brain.

We used entropy to quantify the functioning of the brain in individuals of different ages. Accordingly, we shall describe this as the functional connectivity entropy (FCE).

To motivate the definition of functional connectivity entropy, let us consider the following example of an analysis.

We parcellated the whole brain of three individuals into 90 regions, based on the AAL atlas [Tzourio-Mazoyer et al., 2002]. These were healthy males aged 24, 49 and 69 years, which we describe as 'young', 'middle-aged' and 'elderly'. For these, we calculated the correlation coefficient between the BOLD signal of the thalamus in the right hemisphere and each of 45 brain regions in the left hemisphere (Table 2.2). These signals are represented in the left-hand of panels (a), (b) and (c) of Figure 1.5. Differences between the three individuals show up which are found in more extensive analyses.

The distribution of the correlation coefficients of the elderly male (red histogram in Figure 1.5d) is more widely spread than that of the young male (blue histogram) and middle-aged male (white histogram). This leads to the elderly male having a larger functional connectivity entropy than that of the middle aged male, who has a yet larger functional connectivity entropy than that of the young male (see Figure 1.5d). This implies that the dispersion of correlations, between the right thalamus and a region of the brain in the left hemisphere, is typically an increasing function of age. This conclusion is found to hold in a full analysis, where a pairwise comparison of all regions in the brain is used, rather than just comparing regions in the left hemisphere with the right hemispheric thalamus.

Entropy characterizes the degree of underlying randomness of a random variable. Random variables with small entropies have a high level of predictability and hence a low level of randomness. By contrast, large entropies correspond to low levels of predictability and high levels of randomness [Vaseghi, 2008].

As outlined in Section 2.5, we view the brain as being divided (parcellated) into a number of distinct regions. For each pair of distinct brain regions, we calculated the correlation coefficient of their neuronal activity; this characterizes the functional coupling of the two brain regions. The resulting set of correlation coefficients generates a frequency distribution. The correlation coefficient of a distinct pair of brain regions, that have been randomly selected, can be regarded as a random variable that follows this frequency distribution. we use the dispersion or variability of this random variable as a measure of the functional connectivity entropy (c.f., complexity) of the neuronal dynamics of the brain.

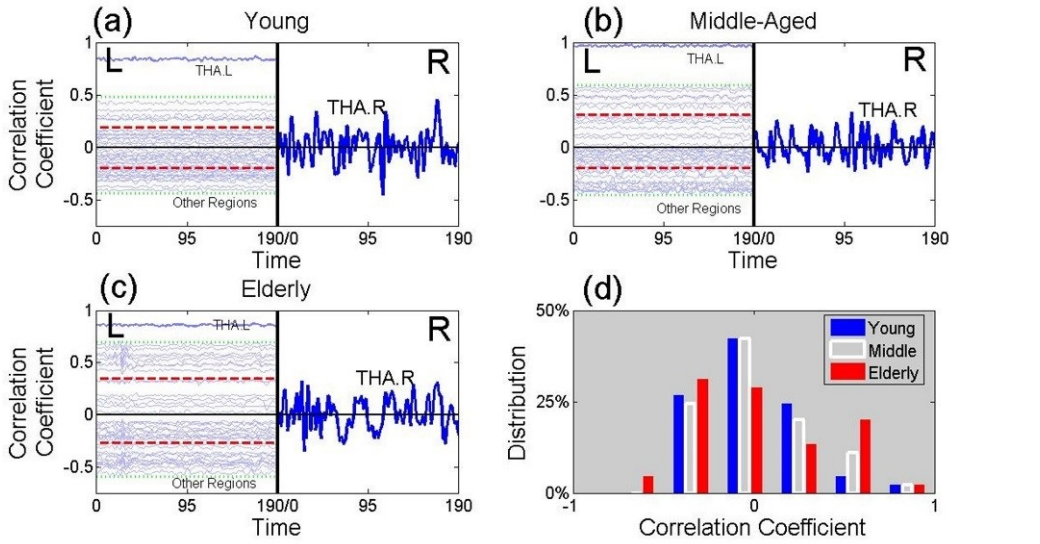

Figure 1.5: The Origin of the Functional Connectivity Entropy
This figure presents time series from BOLD signals. The left-hand sides of panels (a), (b) and (c) contain 45 time series from brain regions of the left hemisphere. The vertical location of a time series, from a given brain region, is given by value of the correlation coefficient of that region with the right thalamus. Panel (a) is from a healthy young male (age 24 years), panel (b) is from a healthy middle-aged male (age 49 years) and panel (c) is from a healthy elderly male (age 69 years). The two horizontal red lines in panels (a), (b) and (c) give, separately, the mean over either positive or negative correlation coefficients. Thus the separation of these lines is a measure of the width of the distribution. In the right halves of panels (a), (b) and (c), the time series of the right thalamus is plotted (using a different vertical scale). Panel (d) gives a histogram of the correlation coefficients of the young male (in blue), the middle-aged male (in white) and the elderly male (in red).
This figure is reproduced from Yao et al. [2014].

The functional connectivity entropy effectively measures the dispersion (or spread) of functional connectivities that exist within the brain. we initiated this research under the assumption that the dispersion of functional connectivities is related to the age of the brain.

We collected fMRI data from 1248 individuals, ranging from 6 to 76 years of age. This provided a unique opportunity to characterize the ageing process of the human brain.

In the analysis of the fMRI dataset of differently aged individuals, we found that, at the population level, the functional connectivity entropy of the human brain has a definite tendency to increase over time. This can be viewed as there being a higher level of randomness in the way different brain-regions functionally interact with one another.

This section is modified from Yao et al. [2014].

1.4.2 Functional Connectivity Entropy in Schizophrenia

Most functional imaging studies in schizophrenia have predominantly focused on how the strength or magnitude of correlations between brain regions is affected in patients when compared to controls. Considering the overall variability in the connectional strength within the brain can capture significant amount of information on normal and abnormal brain function. we have shown that the information obtained using a measure of entropy predicts age-related changes to the connectional architecture of the brain [Yao et al., 2014]. Similarly, measuring the entropy of the functional connectivity dispersion can provide a systems neuroscience perspective to the neurobiological basis of schizophrenia. Furthermore, most studies of large-scale networks in psychiatry have investigated abnormalities pertaining exclusively to connections surviving a specified correlation threshold, thus ignoring the weaker links. The shortcoming of such approaches was recently highlighted by Bassett et al. [2013], who showed that in a relatively small sample of 29 subjects with schizophrenia, the region-specific diversity of connectional strength and the state of organization of weak (rather than strong) connections were the crucial factors to discriminate patients with schizophrenia from controls.

The unpredictability of bivariate functional connectivity across the entire brain can be quantified using an index of entropy based on the principles of information theory (Shannon). Functional Connectivity Entropy (FCE) is a measure of randomness of the strength of functional connectivity, across all possible pairwise interregional connections in the brain [Yao et al., 2014]. This is different from the unpredictability or complexity across time that has been investigated previously in

schizophrenia [Bassett et al., 2012][Fernndez et al., 2013]. Higher FCE represents the presence of increased variability in connectional strength and has been observed in association with healthy ageing [Yao et al., 2014]. On the basis of a computational model, altered FCE has been attributed to a reduction in the pool of excitatory neurons [Yao et al., 2014], an observation that is highly relevant to the study of schizophrenia [Anticevic et al., 2013].

1.5 Hypothesis

Recent observations also suggest that weak (rather than strong) [Bassett et al., 2012] and long-distance (rather than short distance) functional links [Guo et al., 2014] are crucial to discriminate patients with schizophrenia from controls. This raises the possibility that the connectional architecture involving functional links that have no direct structural connectivity may be preferentially affected in schizophrenia.

In this thesis, we firstly showed the meanings of Functional Connectivity Entropy (FCE). Afterwards, we represented the FCE property in schizophrenia. Then, we tested the hypothesis that the randomness of functional connectivity (measured using FCE) is abnormal in schizophrenia, and this abnormality is specific to functional links with no direct structural connectivity. we also investigated the relationship between FCE and symptom burden in patients. Given its onset around adolescence, various dynamic changes coinciding with brain maturation take place in the initial few years in the course of schizophrenia, giving rise to several unstable and inconsistent neurobiological patterns that stabilized during the later stage of the illness [Pantelis et al., 2009]. In particular, the architecture of functional connectivity in patients is significantly affected by duration of illness. Patients with longer duration of illness show reduced segregation and integration [Liu et al., 2008], and reduced connectivity among core brain hubs [Collin et al., 2014]. In light of these observations, we expected a moderating effect of illness duration on FCE.

The key story of this thesis has already been published on Yao et al. [2015].

Chapter 2

Research Methodology

The information in Section 2.1, 2.2 and 2.11 have been also demonstrated in Yao et al. [2015], while those in Section 2.5.1, 2.7.1 and 2.8 have been mentioned in Yao et al. [2014].

2.1 Participants

This sample has been previously reported in a published article [Palaniyappan et al., 2013]. Thirty-four patients satisfying DSM-IV (Diagnostic and Statistical Manual of Mental Disorders) criteria for schizophrenia (n = 28) or schizoaffective disorder (n = 6) and thirty-two age, gender and parental socio-economic status [Rose and Pevalin, 2003] matched healthy controls were included. Patients were recruited from the community-based mental health teams (including Early Intervention in Psychosis teams) in Nottinghamshire and Leicestershire, UK. The diagnosis was made in a clinical consensus meeting in accordance with the procedure of Leckman et al. [1982], using all available information including a review of case files and a standardized clinical interview (SSPI) [Liddle et al., 2002]. All patients were in a stable phase of illness (defined as a change of no more than ten points in their Global Assessment of Function [GAF] score, assessed 6 weeks prior and immediately prior to study participation). The study was given ethical approval by the National Research Ethics Committee, Derbyshire, UK. All volunteers gave written informed consent. Clinical and demographic characteristics of this sample are presented in Table 2.1.

Patients were interviewed on the same day as the scan by a research psychiatrist and clinical severity of psychosis over the previous week was assessed on the basis of total SSPI scores. Duration of illness was estimated from the time of

reported onset of psychotic symptoms (Criterion A of DSM-IV schizophrenia), on the basis of information from case notes and clinical interview. The patient sample was divided into early-stage (<5 years duration) and later-stage (>5 years) illness, based on the clinical notion of 'critical period' of psychosis during which interventions can modify outcome [Crumlish et al., 2009][McGorry, 2002][Mcgorry et al., 2008] and clinical stability is achieved [Levie, 1979]. Thirty-two out of Thirty-four patients were receiving antipsychotic treatment at the time of scan. The chlorpromazine equivalent doses were calculated using data presented by Woods [2003] and Chong et al. [2000] (for clozapine). In addition, 25 mg risperidone depot injection every 14 days was considered equivalent to 4 mg oral risperidone per day, in accordance with the recommendation of the British National Formulary [Committee and of Great Britain, 2012].

Table 2.1: Clinical and demographic features
NS-SEC: National Statistics Socio-economic Classification
CPZ equivalents: Chlorpromazine equivalents
This table is modified from Yao et al. [2015].

	Patients (n=34)	Controls (n=32)	t/χ^2, p
Age	34.1 ± 9.1	33.4 ± 9.1	t=0.30, p=0.76
Gender	25/9	22/10	χ^2=0.18, p=0.67
Mean,parental NS-SEC (SD)	2.45 ± 1.5	2.22 ± 1.4	t=0.24, p=0.51
Handedness,(right/left)	29/5	28/4	χ^2=0.07, p=0.79
SOFAS score	54.4 ± 13.2	-	-
Antipsychotic,dose (CPZ equivalents)	694.5 ± 715.8	-	-
Median,duration of illness in years (range)	6.0(28)	-	-
Total,SSPI score	11.8 ± 7.7	-	-

2.1.1 Excluded subjects

The original sample consisted of 42 patients and 40 controls, but (3 patients, 5 controls) subjects were excluded due to movement artefacts in fMRI, 1 patient had poor quality DTI due to excessive movement, 2 patients aborted scans (1 DTI, 1 fMRI), and in 2 patients and 3 controls tractography was not successful due to image acquisition errors. There were no differences in the duration of illness (mean (SD) in years in the excluded group=8.9(4.5), included group=9.6(8.1), p=0.8), total SSPI score (mean (SD) in the included group=11.8(7.7), excluded group=11.6(6.2), p=0.94) or antipsychotic dose (mean (SD) in the excluded group=694.5(716), included group=485.7(357), p=0.46) between patients who were included or excluded in the analysis.

2.2 MRI Acquisition

Diffusion-weighted images were acquired using a single-shot, spin-echo, echo planar imaging (EPI) sequence in alignment with the anterior commissure - posterior commissure (AC-PC) plane. The acquisition parameters were as follows: Repetition Time (TR) = 8.63 s, Echo Time (TE) = 56.9 ms, voxel size = 2mm isotropic, 112 × 112 matrix, Field of View (FoV) = 224 × 224 × 104, flip angle = 90^o, 52 slices, 32 directions with a b-factor of 1000s/mm^2, EPI Factor = 59, total scan time = 6.29 min.

For resting-state fMRI, 240 time points were acquired during the 10 minutes resting phase wherein the subjects were instructed to keep their eyes open and to relax, without the need to focus on any particular task. Dual-echo gradient-echo echo-planar images (GE-EPI) were acquired to enhance sensitivity, using 8-channel SENSE head coil (SENSE factor 2, anterior-posterior direction, TE1/TE2 25/53 ms, flip angle 85^o, 255 × 255 mm field of view, in-plane resolution = 3 mm × 3 mm, slice thickness = 4 mm, TR = 2500 ms; 40 descending axial slices, 240 time points per acquisition). Scans were inspected immediately after each acquisition, and if motion was detected, scans were repeated.

A magnetisation prepared rapid acquisition gradient echo image (MPRAGE T1) with 1 mm isotropic resolution, 256 × 256 × 160 matrix, TR/TE 8.1/3.7 ms, shot interval 3 s, flip angle 8^o, SENSE factor 2 was also acquired for each participant for image registration and to define anatomical regions for tractography.

2.3 DTI processing

For DTI images, we first used FMRIB Software Library v5.0 (`http://fsl.fmrib.ox.ac.uk/fsl`) [Jenkinson et al., 2012] to remove the eddy-current and extract the brain mask from the B0 image. Then, we used TrackVis [Wang et al., 2007] to obtain the fiber images by the deterministic tracking method, with anatomical regions defined using the AAL convention [Tzourio-Mazoyer et al., 2002] (Table 2.2) on the basis of co-registered T1 image from each subject. This enabled us me to determine the presence of streamlines connecting every pair of brain regions. All the processes were performed using the PANDA suite [Cui et al., 2013].

If two brain regions A and B have one or more streamlines directly connecting each other, then this link AB is regarded as a direct or primary structural path. In contrast, if two brain regions X and Y have no direct connections, but share a direct connection with a common third region Z, then the link XY can be regarded as

indirect secondary structural path. If two brain regions K and L have neither direct connections, nor a common third region, but are connected to each other indirectly by virtue of being connected a common direct link (for example, K connects directly to A, A connects directly to B, B connects directly to L), then the link KL can be regarded as indirect tertiary structural path. To study the effect of the minimum streamline threshold, we varied the minimum from one to three and repeated the primary analysis (group comparisons). The results, shown in Section 4.5.3, indicated that the structural paths were robust across these thresholds.

Thus, for every subject, we identified primary, secondary and tertiary paths on the basis of the DTI fiber streamlines. An illustration of these paths is shown in Figure 2.1.

Table 2.2: Names and abbreviations of AAL brain regions

Regions	**Abbr.**	**Regions**	**Abbr.**
Amygdala	AMYG	Orbitofrontal cortex (middle)	ORBmid
Angular gyrus	ANG	Orbitofrontal cortex (superior)	ORBsup
Anterior cingulate gyrus	ACG	Pallidum	PAL
Calcarine cortex	CAL	Paracentral lobule	PCL
Caudate	CAU	Parahippocampal gyrus	PHG
Cuneus	CUN	Postcentral gyrus	PoCG
Fusiform gyrus	FFG	Posterior cingulate gyrus	PCG
Heschl gyrus	HES	Precentral gyrus	PreCG
Hippocampus	HIP	Precuneus	PCUN
Inferior occipital gyrus	IOG	Putamen	PUT
Inferior frontal gyrus (opercula)	IFGoperc	Rectus gyrus	REC
Inferior frontal gyrus (triangular)	IFGtriang	Rolandic operculum	ROL
Inferior parietal lobule	IPL	Superior occipital gyrus	SOG
Inferior temporal gyrus	ITG	Superior frontal gyrus (dorsal)	SFGdor
Insula	INS	Superior frontal gyrus (medial)	SFGmed
Lingual gyrus	LING	Superior parietal gyrus	SPG
Middle cingulate gyrus	MCG	Superior temporal gyrus	STG
Middle occipital gyrus	MOG	Supplementary motor area	SMA
Middle frontal gyrus	MFG	Supramarginal gyrus	SMG
Middle temporal gyrus	MTG	Temporal pole (middle)	TPOmid
Olfactory	OLF	Temporal pole (superior)	TPOsup
Orbitofrontal cortex (inferior)	ORBinf	Thalamus	THA
Orbitofrontal cortex (medial)	ORBmed		

2.3.1 Brain structural networks

In this thesis, we used diffusion tensor imaging (DTI), but not High angular resolution diffusion imaging (HARDI) or diffusion spectrum magnetic resonance imaging (DSI) to detect structural connectivity. The main reason is that DTI images is easier to be acquired with simpler requirement for sequence designing in MRI machine and shorter scanning time, compared with HARDI and DSI. Moreover, DTI scan-

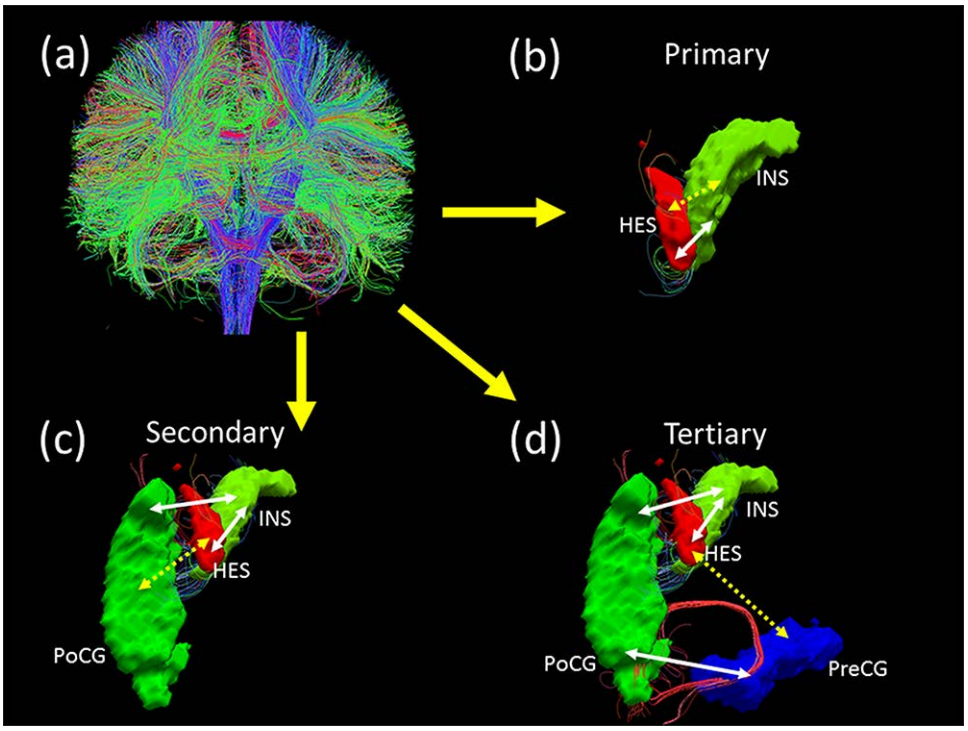

Figure 2.1: Three types of structural paths defined using diffusion tractography (a): whole-brain fiber connection network construction by Diffusion Tensor Imaging data; (b): Heschl gyrus (HES) and Insula (INS) are directly connected with each other through white matter tracts. HES $\leftrightarrow$ INS link is a primary structural path (c): Heschl gyrus and Postcentral gyrus (PoCG) are indirectly linked (discontinuous arrow) through white matter tracts (continuous arrows) that connect HES and PoCG with the Insula. Though there are no direct connections between HES and PoCG, INS acts as a common third region. HES $\leftrightarrow$ PoCG link is termed as a secondary structural path. (d): Heschl gyrus and Precentral gyrus (PreCG) are indirectly linked (discontinuous arrow) through white matter tracts (continuous arrows) that connect HES with INS, INS with PoCG and PoCG with PreCG. There are no direct connections or a single common third region between HES and PreCG. HES $\leftrightarrow$ PreCG link is termed as a tertiary structural path.
This figure is reproduced from Yao et al. [2015].

ning is comparatively technology with fewer noises [Johansen-Berg and Behrens, 2013] to get access to more reliable analysis. Thus, DTI images were chosen here to extract brain structural connectivity. The preprocessings of DTI imaging have been described in details in the last section, Section 2.3. We used streamline deterministic tracking method to detect structural connectivity for it is simple and stable [Johansen-Berg and Behrens, 2013]. However, the streamline results sometimes show large variances in the same link of different subjects [Savadjiev et al., 2008]. For some specific links, some subjects hold only several streamlines, while the others have hundreds of or even more than one thousand of streamlines in our data analysis. Thus, we used a binary network, but not the raw data to do analysis with a streamline threshold. The streamline threshold is ONE in the Results sections, which is also discussed in Section 4.5.3. We wrote a Matlab code to extract indirect pathways including secondary and tertiary links as described in the last section, Section 2.3, which is mainly based on matrix multiplication. Thus, we determined all primary, secondary and tertiary pathways for all brain connecitivies. It should be emphasized that all path calculations are based on structural (not functional) connectivity.

2.4 fMRI processing

Weighted summation of the dual-echo images produced a single set of low-artefact functional images [Posse et al., 1999]. Retrospective physiological correction was then performed [Glover et al., 2015]. The first five volumes of fMRI datasets were discarded, to allow for scanner stabilization. Further processing was then conducted by Statistical Parametric Mapping (SPM8) (`http://www.fil.ion.ucl.ac.uk/spm`) [Friston, 2007] and Data Processing Assistant for Resting-State fMRI (DPARSF) [Yan and Zang, 2010]. After slice-timing correction and realignment to the middle volume, the functional scans were spatially normalized using the unified segmentation approach to a standard template (Montreal Neurological Institute) and resampled to $3 \times 3 \times 3$ mm^3. Data was then smoothed using a Gaussian kernel of 8 mm full-width at half- maximum, detrended, and then passed through a band-pass filter (0.01-0.08 Hz) to reduce low-frequency drift and high-frequency physiological noise.

Nuisance covariates including head motion, global mean signals, white matter signals and cerebrospinal signals were regressed out from the time series. Regional time series were extracted in each of the 90 automated anatomical labelling atlas (AAL) [Tzourio-Mazoyer et al., 2002] based brain regions by averaging the signals of all voxels within a region. The names of the 90 brain regions are listed in Table

2.2, along with further details of fMRI preprocessing in Section 4.5.

2.4.1 Brain functional networks

After data preprocessing, the time series were extracted in each ROI by averaging the signals of all voxels within the region. The 90 regions were based on the AAL Template [Tzourio-Mazoyer et al., 2002]. After that, the Pearson's correlation coefficient of every pair of regions was calculated. Since the atlas is the AAL template with 90 ROIs, 4005 functional connectivity links were obtained connecting every pair of regions. Thus a whole brain functional network was constructed.

2.5 Entropy Calculation

2.5.1 Functional Connectivity Entropy Meanings

We used entropy to quantify the functioning of the brain. Accordingly, we shall describe this as the functional connectivity entropy (FCE).

As outlined below, the brain was viewed as being divided (parcellated) into a number of distinct regions. For each pair of distinct brain regions, we calculated the correlation coefficient of their neuronal activity; this characterizes the functional coupling of the two brain regions. The resulting set of correlation coefficients generates a frequency distribution. The correlation coefficient of a distinct pair of brain regions, that have been randomly selected, can be regarded as a random variable that follows this frequency distribution. we use the dispersion or variability (measured using Shannon's entropy, see below) of this random variable as a measure of the FCE (c.f., complexity) of the neuronal dynamics of the brain. we investigated, in this work, how this measure of the FCE changes with age and in Figure 2.2, we illustrated the behaviours of the brain's dynamics that it captures.

Figure 2.2 (top row) shows the situation where every brain region fluctuates over time, but is totally correlated with all other regions. In such a case, the FCE of correlation coefficients is zero; all correlation coefficients are unity, and hence their distribution exhibits no randomness, just predictability. A case of non-zero FCE occurs when a range of different correlation coefficients are found between different pairs of brain regions. An example of this case is given by the second row in Figure 2.2. In the opposite case of completely independent or incoherent activity in all regions, the correlation coefficients will all be zero and their dispersion (FCE) will again be zero. This means the entropy measure is sensitive to co-ordinated activity that is most interesting, namely activity that is intermediate between fully

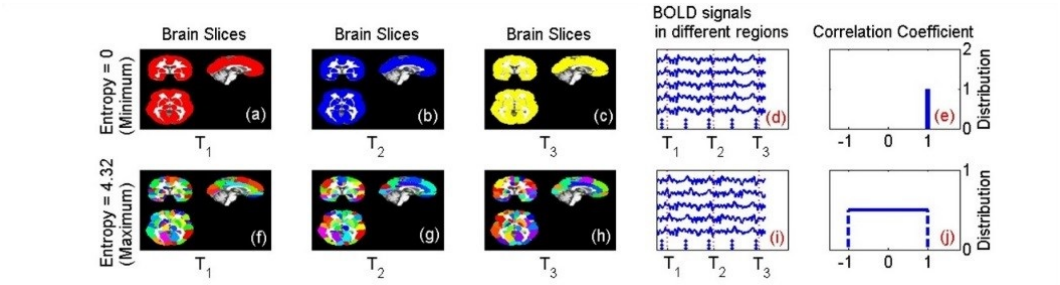

Figure 2.2: Illustration of the Functional Connectivity Entropy of the Brain
In this figure, the brain is parcellated into a number of distinct regions. Different levels of brain activity (as measured by BOLD signals) are illustrated by different colors in the brain slices of the figure. we use two artificial data sets of BOLD signals to illustrate what the functional connectivity entropy captures about brain activity. Panels (a), (b) and (c) show brain activities of brain slices at three different times (T1, T2, T3), when the correlation coefficients between all regions of the brain are unity. In this case, all regions of the brain have the same color since they are behaving synchronously. Panel (d) shows the BOLD signals in different brain regions, for this case. Panel (e) shows the corresponding distribution of the correlation coefficients (a 'spike' located at a correlation coefficient of unity). The functional connectivity entropy for this case is zero (the minimum possible value).
Panels (f), (g) and (h) show the brain activities at three different times (T1, T2, T3), when all correlation coefficients are generally different (so all regions have different colors, indicating that all regions are behaving asynchronously. Panel (i) shows BOLD signals in different brain regions, for this case. Panel (j) shows the corresponding distribution of the correlation coefficients (a uniform distribution). The functional connectivity entropy in this case is the maximum possible value.
This figure is reproduced from Yao et al. [2014].

synchronised and fully incoherent brain-region dynamics.

2.5.2 Functional Connectivity Entropy Calculation Method

After data preprocessing, the time series were extracted in each ROI by averaging the signals of all voxels within the region. The 90 regions were based on a selected atlas, say the AAL Template. After that, we calculated the Pearson Correlation Coefficient of every pair of regions. Since the atlas was the AAL template, we had 4005 function links connecting every two regions. Thus we constructed a whole brain functional network.

Given 4005 different correlation numbers, we considered the values of the correlation coefficients as a realization of a random variable. The range of this was [-1,1]. we then defined the brain functional connectivity entropy as the relative en-

tropy, i.e., the KL (Kullback-Leibler) divergence from the correlation distribution to a reference Lebesgue measure. In practice, we did not have a continuous distribution of correlation coefficients, but 4005 correlations values from each individual. we thus separated all 4005 realizations into 20 class intervals of equal width, and determined the frequency (pi) of each class. These frequencies were used to calculate the Shannon entropy (sum of -pi*log(pi)) of the whole brain. This can be considered as the functional connectivity entropy (FCE).

2.6 Statistical inference

We applied linear regression model [Seber and Lee, 2012] to remove age, sex and dose effects for patients and controls, which was applied in Figure 3.10, 3.11, 4.2 and 4.3. We used Cohen's d [Cohen, 1992] to quantify the effect size of the mean differences.

2.7 Computational Model

2.7.1 Computational model of brain networks

A computational model from Deco et al.'s work [Deco and Jirsa, 2012] could be used to verify the results about functional connectivity entropy.

Neuron dynamics

The global structure of the model is illustrated in Figure 2.3. Every brain region served as a node in a large scale network, which consists of a population of excitatory pyramidal neurons and a population of GABAergic inhibitory neurons, which are all-to-all connected. The communication between every two nodes is through synaptic connections between excitatory neurons in those areas.

For each brain area, an integrate-and-fire neuron model with excitatory (AMPA and NMDA) and inhibitory (GABA) synaptic receptors was applied. The dynamics of the membrane potential $V(t)$ are described by:

$$\begin{cases} C_m \frac{\mathrm{d}V(t)}{\mathrm{d}t} = -g_m(V(t) - V_L) - I_{syn}(t), & V(t) < V_{thr}, \\ V(t) = V_{reset}, & V(t) \geq V_{thr}. \end{cases} \tag{2.1}$$

The total synaptic current I_{syn} is given by the sum of glutamatergic AMPA external background excitatory currents ($I_{AMPA,EXT}$), AMPA ($I_{AMPA,REC}$) and

NMDA ($I_{NMDA,REC}$) recurrent excitatory currents, and GABAergic recurrent inhibitory currents (I_{GABA}):

$$I_{syn} = I_{AMPA,ext} + I_{AMPA,rec} + I_{NMDA,rec} + I_{GABA}, \tag{2.2}$$

where,

$$\begin{cases} I_{AMPA,ext}(t) = g_{AMPA,ext}(V(t) - V_E) \sum_j s_j^{AMPA,ext}(t), \\ I_{AMPA,rec}(t) = g_{AMPA,rec}(V(t) - V_E) \sum_j \omega_j^{AMPA} s_j^{AMPA,rec}(t), \\ I_{NMDA,rec}(t) = \frac{g_{NMDA,rec}(V(t)-V_E)}{1+\gamma e^{-\beta V(t)}} \sum_j \omega_j^{NMDA} s_j^{NMDA,rec}(t), \\ I_{GABA}(t) = g_{GABA}(V(t) - V_I) \sum_j \omega_j^{GABA} s_j^{GABA}(t), \end{cases} \tag{2.3}$$

The gating variables $s_j(t)$ are the fractions of open channels of neurons and are given by:

$$\begin{cases} \frac{\mathrm{d}s_j^{AMPA,ext}(t)}{\mathrm{d}t} = -\frac{s_j^{AMPA,ext}(t)}{\tau_{AMPA}} + \sum_k \delta(t - t_j^k), \\ \frac{\mathrm{d}s_j^{AMPA,rec}(t)}{\mathrm{d}t} = -\frac{s_j^{AMPA,rec}(t)}{\tau_{AMPA}} + \sum_k \delta(t - t_j^k), \\ \frac{\mathrm{d}s_j^{NMDA,rec}(t)}{\mathrm{d}t} = -\frac{s_j^{NMDA,rec}(t)}{\tau_{NMDA,decay}} + \alpha x_j^{NMDA,rec}(t)(1 - s_j^{NMDA,rec}(t)), \\ \frac{\mathrm{d}x_j^{NMDA,rec}(t)}{\mathrm{d}t} = -\frac{s_j^{NMDA,rec}(t)}{\tau_{NMDA,rise}} + \sum_k \delta(t - t_j^k), \\ \frac{\mathrm{d}s_j^{GABA}(t)}{\mathrm{d}t} = -\frac{s_j^{GABA}(t)}{\tau_{GABA}} + \sum_k \delta(t - t_j^k), \end{cases} \tag{2.4}$$

The sums over the k index represent all of the spikes emitted by presynaptic neuron j (at times t_j^k). The description and value of most parameters are shown in Table 2.3.

Each local area contains 100 excitatory neurons and 100 inhibitory neurons. The connection strengths between and within the populations are determined by dimensionless strength ω. Illustrated in Figure 2.3, there are 4 different intra-connection strength: ① excitation (AMPA and NMDA) within excitatory neurons ω^1; ② excitation (AMPA and NMDA) from excitatory neuron to inhibitory neuron $\omega^2 = 1$; ③ inhibition (GABA) from inhibitory neuron to excitatory neuron $\omega^3 = 1$; ④ inhibition (GABA) within inhibitory neurons $\omega^4 = 1$. we vary ω^1 systematically to see the implications for the global functional connectivity entropy. The inter-regional connection strength ω^{inter} is proportional to number of fibers linking every two regions. The neuroanatomical matrix whose element is fiber number, is obtained by Diffusion Tensor Imaging. Here, we used averaged structural matrix

from 46 healthy people, which is showed in Figure 2.4.

All neurons always received an external background input from $N_{ext} = 800$ external neurons emitting independent Poisson spike trains at a rate of 3Hz. More specifically, for all neurons inside a given population p, the resulting global spike train, which is still Poissonian, had a time-varying rate $\nu^p_{ext}(t)$, governed by,

$$\tau_n \frac{\mathrm{d}\nu^p_{ext}(t)}{\mathrm{d}t} = -(\nu^p_{ext}(t) - \nu_0) + \sigma\sqrt{2\tau_n}\xi^p(t), \tag{2.5}$$

where $\tau_n = 300ms$, $\nu_0 = 2.4k$Hz, $\sigma_\nu = 0.2$ is the standard deviation of $\nu^p_{ext}(t)$, and $\xi^p(t)$ is normalized Gaussian white noise.

Table 2.3: Neural and synaptic parameters

		Excitatory neuron	Inhibitory neuron		
Membrane capacitance C_m		0.5 nF	0.2 nF	Excitatory reversal potential V_E	0 mV
Leak conductance g_m		25 nS	20 nS	Inhibitory reversal potential V_I	-70 mV
Resting potential V_L		-70 mV	-70 mV	Decay time τ_{AMPA}	2 ms
Threshold potential V_{thr}		-50 mV	-50 mV	Rise time $\tau_{NMDA,rise}$	2 ms
Reset potential V_{reset}		-55 mV	-55 mV	Decay time $\tau_{NMDA,decay}$	100 ms
Refractory time τ_{ref}		2 ms	1 ms	Decay time τ_{GABA}	10 ms
Synaptic conductance	$g_{AMPA,ext}$	2.496 nS	1.944 nS	α	0.5 kHz
	$g_{AMPA,rec}$	0.104 nS	0.081 nS	β	0.062
	$g_{NMDA,rec}$	0.327 nS	0.258 nS	γ	0.28
	g_{GABA}	2.45 nS	1.2 nS		

BOLD signal

The simulation of the fMRI BOLD signal is computed by means of the Balloon-Windkessel hemodynamic model Friston et al. [2003]. The BOLD-signal of each region is driven by the level of neuronal activity summed over all neurons in both populations (excitatory and inhibitory populations) in that particular region. In all simulations, neuronal activity is given by the rate of spiking activity in a time window of 1 ms. In brief, for the i'th region, neuronal activity z_i causes an increase in a vasodilator signal s_i that is subject to autoregulatory feedback. Inflow f_i responds in proportion to this signal with concomitant changes in blood volume ν_i and deoxyhemoglobincontent q_i. The equations relating these biophysical variables are:

$$\begin{cases} \frac{\mathrm{d}s_i(t))}{\mathrm{d}t} = \varepsilon_i z_i - k_i s_i - \gamma_i(f_i - 1), \\ \frac{\mathrm{d}f_i(t)}{\mathrm{d}t} = s_i, \\ \tau_i \frac{\mathrm{d}\nu_i(t)}{\mathrm{d}t} = fi - \nu_i^{1/\alpha}, \\ \tau_i \frac{\mathrm{d}q_i(t)}{\mathrm{d}t} = \frac{f_i[1-(1-\rho_i)^{1/f_i}]}{\rho_i} - \frac{q_i \nu_i^{1/\alpha}}{\nu_i}, \end{cases} \tag{2.6}$$

where ρ is the resting oxygen extraction fraction. The BOLD signal is taken to

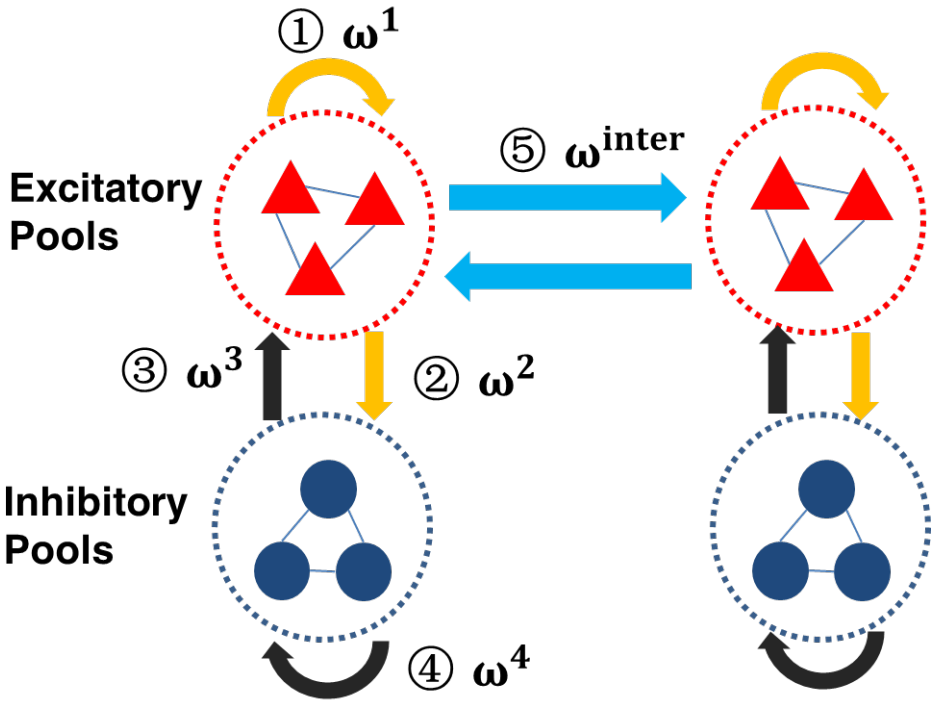

Figure 2.3: Schematic representation of the brain network
Each brain area is comprised of excitatory neurons (red triangles) and inhibitory interneurons (blue circles). ①②③④ represent the four different intra-connection during each brain area, and ⑤ describes the inter-connection between different brain area, which depends on DTI.

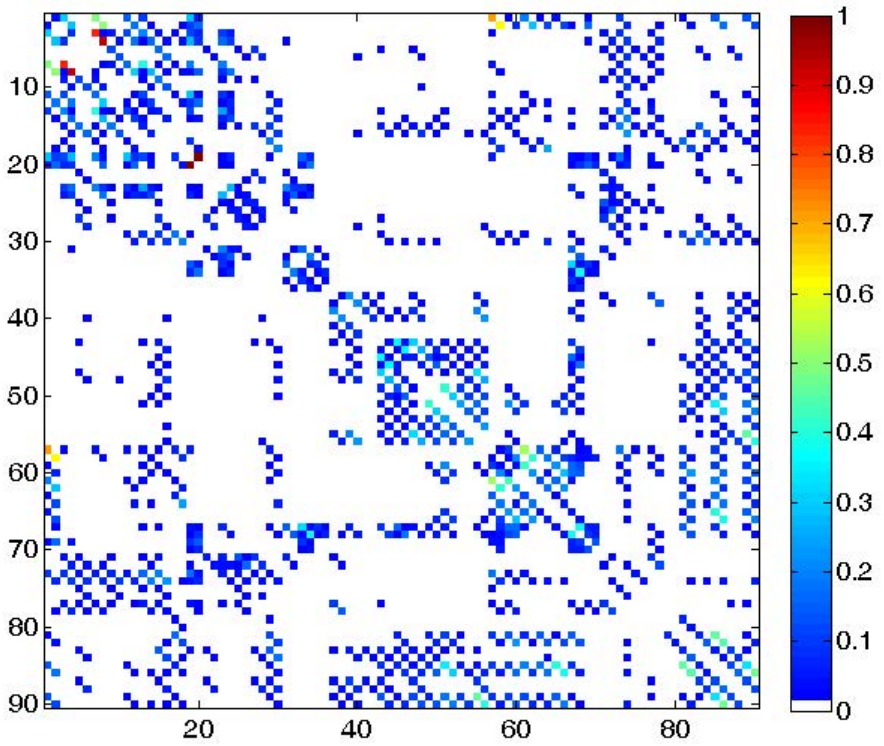

Figure 2.4: Neuroanatomical connectivity matrix
Neuroanatomical connectivity matrix, obtained by DTI after averaging across 46 human subjects.

be a static nonlinear function of volume and deoxyhemoglobin that comprises a volume-weighted sum of extra- and intravascular signals:

$$y_i = V_0[7\rho_i(1-q_i) + 2(1-\frac{q_i}{\nu_i}) + (2\rho_i - 0.2)(1-\nu_i)], \tag{2.7}$$

where $V_0 = 0.02$ is the resting blood volume fraction. The biophysical parameters were taken as $\varepsilon_i = 0.2$, $k_i = 0.65$, $\gamma_i = 0.41$, $\tau_i = 0.98$, $\alpha = 0.32\rho_i = 0.34$.

Simulation of the functional connectivity entropy

After the simulated BOLD time series were obtained, the global signal (average over all regions) was regressed out. Figure 2.5 shows typical temporal evolution of the simulated BOLD signal (after regression) for several brain regions. we then calculated the simulated functional connectivity by calculating the correlation matrix of the BOLD time series. Figure 2.6 and 2.7 plot an example of stimulated functional connectivity matrix and corresponding distribution of correlation, respectively. Using the calculation method of functional connectivity entropy, we could compare the simulated functional connectivity entropy with that from fMRI data.

When we increase intra-excitatory connection strength ω^1 with other parameters fixed, the firing rate of excitatory neurons in the whole brain increase. (Firing-rate amplification of inhibitory neurons can be ignored compared to that of excitatory neurons.) Based on the fact that the firing rate of one excitatory neuron, in resting state, is about 3Hz and that the model of one neuron here could also described the dynamics of several neurons or a neuron mass, we can calculate the actual excitatory neuron number in each brain region by the 100 times mean firing rate divided by 3Hz. (Here we just use the averaged firing rate of all excitatory neurons in the whole brain, not in each brain region.) Figure 2.8 illustrates the positive correlation between actual excitatory neuron number and intra-excitatory connection strength. The two red dashed lines show the range of connection strength $[1.78, 1.81]$, which makes the corresponding entropy match the human data. Based on the least squares line (black dashed line), the neuron number range is limited to $[888, 1130]$ (indicated by green text arrows).

2.7.2 Computational model in Schizophrenia

When we reduced the excitatory NMDA connection strength from the excitatory population to the inhibitory population within each brain region with the other parameters fixed, the firing rate of the excitatory neurons averaged across the whole brain increased, as illustrated in Figure 2.9.

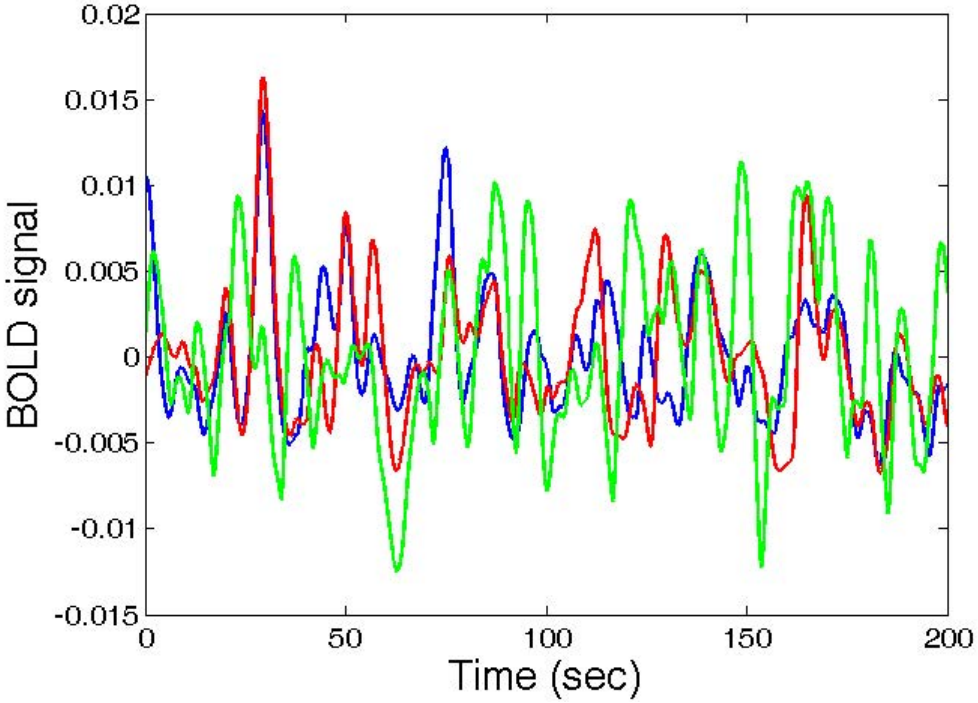

Figure 2.5: Simulated BOLD signals
Simulated BOLD signal for thalamus (blue), Inferior temporal gyrus (red) and Insula(green) when intra-excitatory connection strength ω^1=1.81.

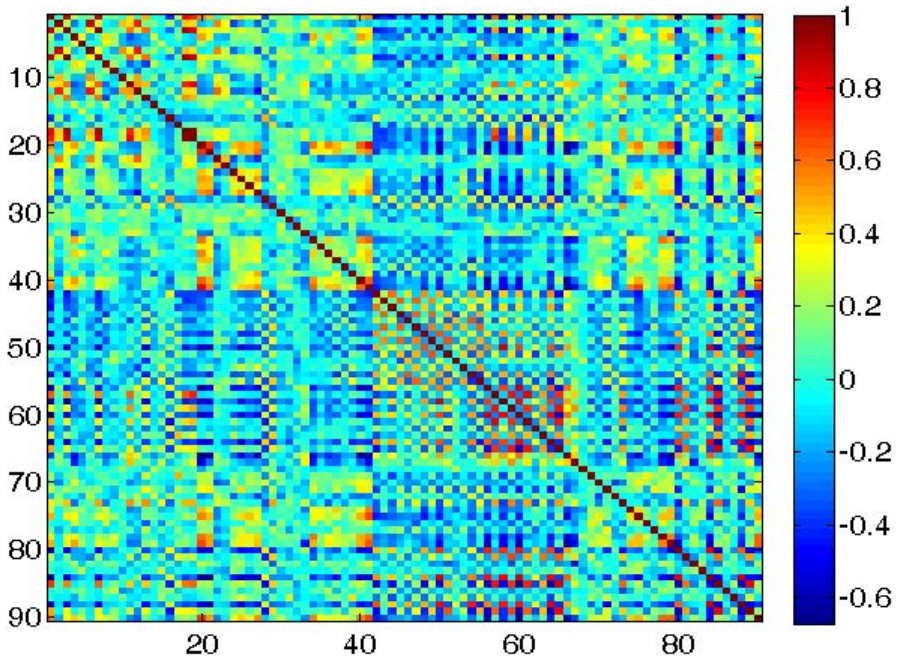

Figure 2.6: Simulated functional connectivity matrix
Simulated functional connectivity matrix when intra-excitatory connection strength ω^1=1.81.

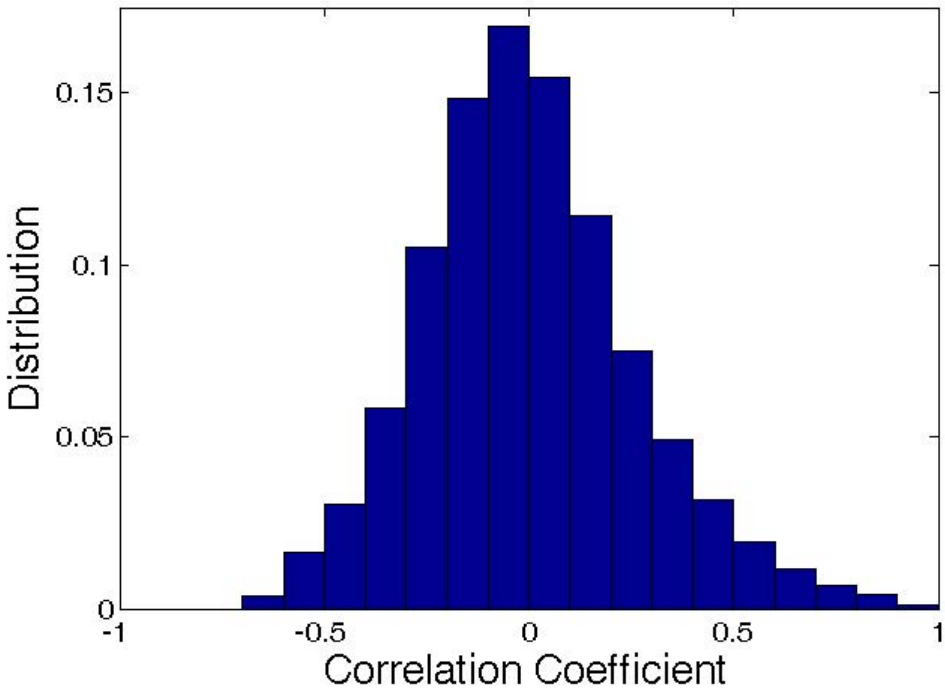

Figure 2.7: The distribution of correlation coefficients
The distribution of correlation coefficients when the intra-excitatory connection strength ω^1=1.81.

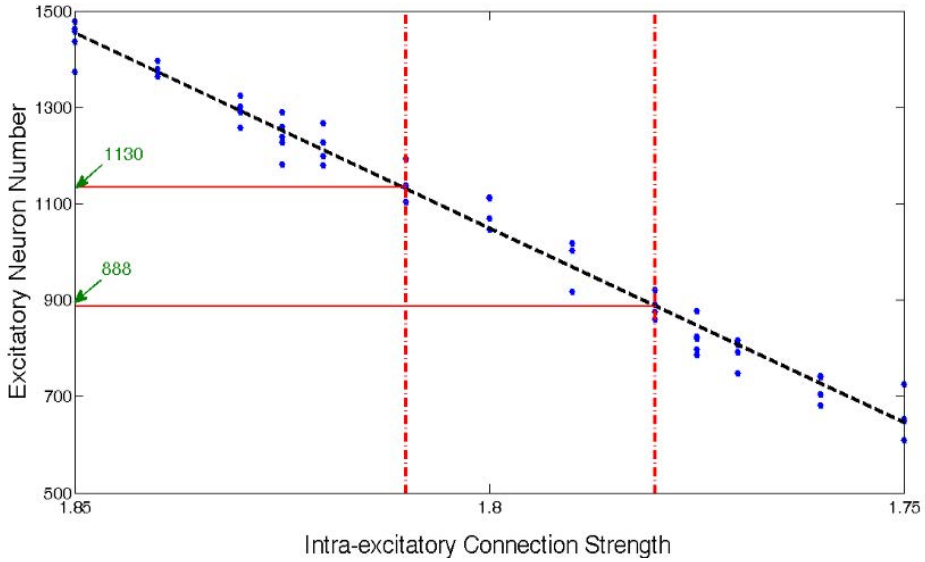

Figure 2.8: Excitatory neuron number versus intra-excitatory connection strength ω^1

When we reduced the excitatory NMDA connection strength from all excitatory neurons (i.e. E-to-E and E-to-I, where E indicates excitatory and we indicates inhibitory) by 8%, the firing rate of the excitatory neurons averaged across the whole brain decreased by 50%.

2.8 Methods for Functional Connectivity Entropy Origin: Ageing Problem (Section 3.1)

2.8.1 Subjects

Our meta-analysis included 26 datasets, with a total of 1248 samples. These covered a range of individuals from 6 to 76 years of age. Samples of poor quality were excluded.

Note that 22 of these datasets came from the 1000 Functional Connectomes Project (`http://fcon_1000.projects.nitrc.org/`), where data came from all over the world including China, Britain and United States. In these 22 data sets, there were 842 samples, with ages ranging from 18 to 73 years, with 357 of them male. The mean age was 28.3±12.3 years. Details are listed in Table 2.4. The fMRI scans performed by 1000 Functional Connectomes Project were carried out in accordance with the guidelines issued by the local ethical committees of the various

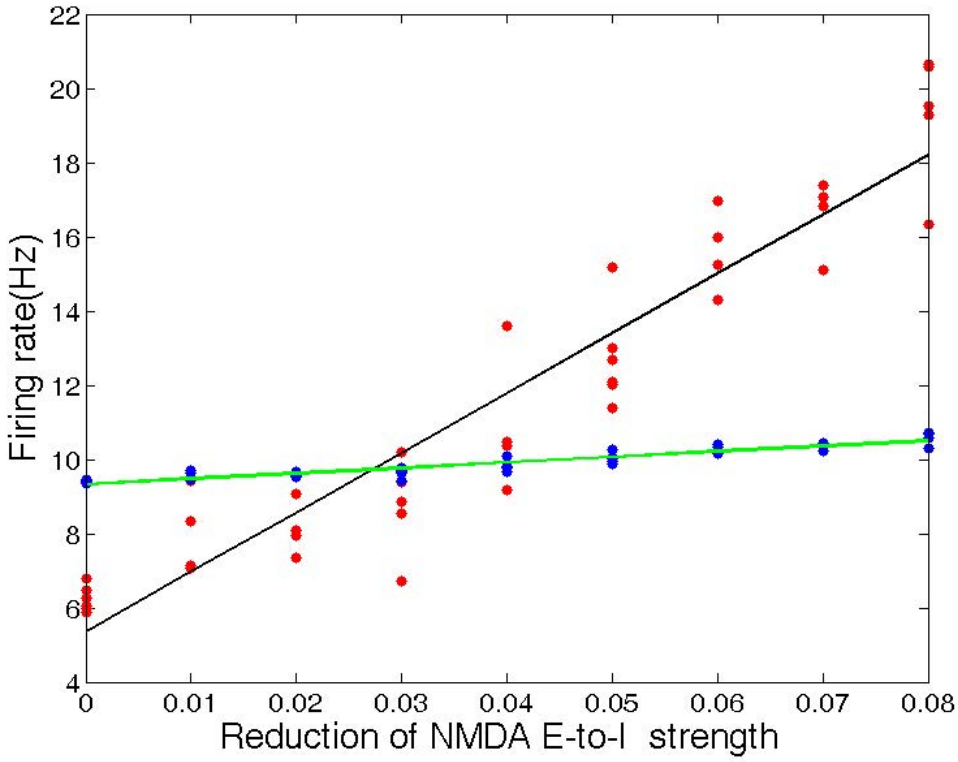

Figure 2.9: Average firing rate versus percent reduction of NMDA strength from the excitatory to inhibitory (E-to-I) population
Here red and blue dots represent different trials for excitatory and inhibitory neurons, respectively. The black and green lines are the corresponding least-squares fit. The linear correlation between the excitatory firing rate and the connection strength is statistically significant (10^{-20}), while this is not the case for the inhibitory neurons.

research institutes, which can be found in their website. And informed consent was obtained from all subjects.

Table 2.4: Detailed information of 22 databases from the FCON 1000 Project This table is modified from Yao et al. [2014].

Database	**Quantity**	**Male/Female**	**Age (years)**
Atlanta	27	12/15	29.9±8.6
Baltimore	23	8/15	29.3±5.5
Beijing_Zang	193	75/118	21.2±1.8
Berlin_Margulies	23	12/11	30.1±5.1
Cambridge_Buckner	192	71/121	21.1±2.3
Cleveland	31	11/20	43.5±11.1
Dallas	24	12/12	42.6±20.1
ICBM	36	15/21	38.2±17.6
Leiden_2180	10	10/0	23.4±2.5
Leiden_2200	19	11/8	21.7±2.6
Leipzig	37	16/21	26.2±5.0
Milwaukee_b	46	15/31	53.5±5.8
Munchen	11	6/5	66.6±3.4
NewHeaven_a	18	10/8	31.6±10.3
NewHeaven_b	16	8/8	26.9±6.3
Newark	18	9/9	24.3±4.0
Orangeburg	20	15/5	40.7±11.0
Oulu	22	7/15	21.3±0.6
PaloAlto	17	2/15	32.5±8.1
Pittsburgh	14	8/6	36.0±8.6
Queensland	18	11/7	26.3±3.7
Saintlouis	27	13/14	25.3±2.3
Whole Database	842	357/485	28.3±12.3

Another 2 datasets were from the ADHD-200 Consortium for the global competition (`http://fcon_1000.projects.nitrc.org/indi/adhd200/`). One of these was from the Phyllis Green and Randolph Cowen Institute for Pediatric Neuroscience at the Child Study Center, New York University Langone Medical Center, New York, New York and the Nathan Kline Institute for Psychiatric Research, Orangeburg, NY, USA. The other came from the Institute of Mental Health, Peking University and the National Key Laboratory of Cognitive Neuroscience and Learning, Beijing University. Since they were both concerned about ADHD classification, their data were ADHD patients versus controls (normal individuals). we cannot apply the data from individuals with ADHD disorder, since their brains may be different from normal people, and we used only the controls, namely the normal people from the 2 datasets. In total, there were 241 samples, with 134 of them male. Their mean age was 11.83±2.47 years, so they were teenagers/children. Since most samples in the other dataset were more than 18 years old, we selected the two

datasets to complete the analysis about ageing in the range of 6 years to 18 years old. The fMRI study in Peking University was approved by the Research Ethics Review Board of Institute of Mental Health, Peking University. Informed consent was also obtained from the parent of each subject and all of the children agreed to participate in the study. The fMRI scans from NYU were carried out in accordance with the guidelines issued by the local ethical committee, and informed consent was obtained from all subjects.

There was also one dataset of elderly people, covering 117 samples from the Department of Psychiatry, Tongji Hospital, Tongji University School of Medicine and Department of Biological Psychiatry, Shanghai Mental Health Centre, Shanghai Jiao Tong University School of Medicine. In this dataset, 73 were male. The mean age was 70.42±3.52 years. With a designed health status checklist, we excluded individuals with: obvious cognitive decline, a diagnosis of AD, serious functional decline (having difficulty with independent living), as well as individuals with major medical or psychiatric conditions such as cancer, current chemotherapy/radiation treatment, major depression, and schizophrenia. This study was approved by the Human Research Ethics Board of Tongji Hospital in Shanghai, China and all participants gave written informed consent before being enrolled in this part.

The last dataset was from the Department of Biomedical Imaging and Radiological Sciences, National Yang-Ming University, Taipei, Taiwan and the Brain Connectivity Laboratory, Institute of Neuroscience, National Yang-Ming University, Taipei, Taiwan. There were 48 samples in the dataset. All were male and covered a range of ages from 21 to 76 years. The mean age was 43.8±17.0 years and all individuals were normal and healthy. Moreover, the T1-image and DTI data of these 48 samples were also applied in this thesis. The fMRI scans from National Yang-Ming University were carried out in accordance with the guidelines issued by the local ethical committee, and informed consent was obtained from all subjects.

2.8.2 Data Acquisition

The various ways that data were acquired in the 22 datasets from the 1000 Functional Connectomes project can be found in their website, `http://fcon_1000.projects.nitrc.org/`. Moreover, the acquisition of the two datasets from the ADHD-200 Consortium for the global competition was in their website, `http://fcon_1000.projects.nitrc.org/indi/adhd200/`.

In the dataset from Shanghai, all people underwent functional scanning using a Siemens Trio 3T scanner at East China Normal University, Shanghai, China. Foam padding was used to minimize head motion for all subjects. Functional images

were acquired using a single-shot, gradient-recalled echo planar imaging sequence (repetition time = 2000 ms, echo time = 25 ms and flip angle = 90 degrees). Thirty-two transverse slices (field of view = 240 × 240 mm^2, in-plane matrix = 64 × 64, slice thickness = 5 mm, voxel size = 3.75 × 3.75 × 5 mm^3), aligned along the anterior commissureCposterior commissure line were acquired. For each subject, a total of 155 volumes were acquired, resulting in a total scan time of 310s. Subjects were instructed simply to rest with their eyes closed, not to think of anything in particular, and not to fall asleep.

At last, in the dataset from Taiwan, all people underwent structural, functional and diffusion tensor imaging scanning using a Siemens Trio 3T scanner at National Yang-Ming University, Taiwan. Foam padding was used to minimize head motion for all subjects. Functional images were acquired using a single-shot, gradient-recalled echo planar imaging sequence (repetition time = 2500 ms, echo time = 27 ms and flip angle = 77). Fourty-three transverse slices (field of view = 220 × 220 mm^2, in-plane matrix = 64 × 64, slice thickness = 3.4 mm, voxel size = 3.44 × 3.44 × 3.4 mm^3), aligned along the anterior commissureCposterior commissure line were acquired. For each subject, a total of 200 volumes were acquired, resulting in a total scan time of 500s. Subjects were instructed simply to rest with their eyes closed, not to think of anything in particular, and not to fall asleep. The diffusion tensor images covering the whole brain were obtained using spin echo-based echo planar imaging sequence, including 30 volumes with diffusion gradients applied along 30 non-collinear directions (b = 1000 s/mm^2) and three volumes without diffusion weighting (b = 0 s/mm^2). Each volume consisted of 63 contiguous axial slices (repetition time = 11000 ms, echo time = 104 ms, flip angle = 90 degrees, field of view = 100 × 100 mm^2, matrix size = 128 × 128, voxel size = 2 × 2 × 2 mm^3). To improve the signal to noise ratio, the entire sequence was repeated three times. Subsequently, high-resolution T1-weighted anatomical images were acquired in the sagittal orientation using a magnetization-prepared rapid gradient-echo sequence (repetition time = 3500 ms, echo time = 3.5 ms, flip angle = 7, field of view = 256 × 256 mm^2, matrix size = 256 × 256, slice thickness = 1 mm, voxel size = 1 × 1 × 1 mm^3 and 192 slices)on each subject.

2.8.3 Data Preprocessing

Firstly, we dealt with the two datasets from the controls of ADHD 200 Consortium. Before functional image preprocessing, the first four volumes were discarded, to allow for scanner stabilization. Briefly, the remaining functional scans were first corrected for within-scan acquisition time differences between slices, and are then

realigned to the middle volume, to correct for inter-scan head motions. The functional scans were then spatially normalized to a standard template [Fonov et al., 2011] (Montreal Neurological Institute) and resampled at 4 mm 4 mm $\times$ 4 mm voxel resolution. After normalization, the Blood Oxygenation Level Dependent (BOLD) signal of each voxel was first detrended to remove any linear trend and then passed through a bandpass filter (0.009 Hz $<$ f $<$ 0.08 Hz) to reduce low-frequency drift and high-frequency physiological noise. Finally, nuisance covariates including head motions, global mean signals, white matter signals, and cerebrospinal fluid signals were regressed out. An automated anatomical labeling (AAL) atlas [Tzourio-Mazoyer et al., 2002] was used to parcellate the brain into 90 regions of interest (ROIs), with 45 in each hemisphere. The names of the ROIs and their corresponding abbreviations are listed in Table 2.2. we thank Carlton Chu, Virginia Tech's ARC, the ADHD-200 consortium, and the Neuro Bureau for what they have done for us.

Let us now consider all other datasets. The first 10 volumes of these datasets were discarded, to allow for scanner stabilization and the subjects' adaptation to the environment. fMRI data preprocessing was then conducted by Statistical Parametric Mapping [Frackowiak et al., 2003] (SPM8) and a Data Processing Assistant for Resting-State fMRI [Yan and Zang, 2010] (DPARSF). The remaining functional scans were first corrected for within-scan acquisition time differences, between slices, and then realigned to the middle volume, to correct for inter-scan head motions. Subsequently, the functional scans were spatially normalized to a standard template [Fonov et al., 2011] (Montreal Neurological Institute) and resampled to 3 $\times$ 3 $\times$ 3 mm^3. Data was then smoothed, and after normalization and smoothing, BOLD signals of each voxel were firstly detrended, to remove any linear trend, and then passed through a band-pass filter (0.01-0.08 Hz) to reduce low-frequency drift and high-frequency physiological noise. Finally, nuisance covariates including head motions, global mean signals, white matter signals and cerebrospinal signals were regressed out from the BOLD signals. After data preprocessing, the time series were extracted in each ROI by averaging the signals of all voxels within that region and then linearly regressing out the influence of head motion and global signals. In this thesis, the automated anatomical labeling atlas Tzourio-Mazoyer et al. [2002] (AAL) was used to parcellate the brain into 90 regions of interest (ROIs) (45 per hemisphere). The names of the ROIs and their corresponding abbreviations are listed in Table 2.2.

On the other hand, we also applied the DTI data of the 48 samples from Taiwan to construct the connection matrix in this neuron model. we first applied the FSL [Jenkinson et al., 2012] to remove the eddy-current and extract the brain

mask of B0 image. Then, we used the TrackVis [Wang et al., 2007] (`http://www.trackvis.org/`) to obtain the fiber images by the deterministic tracking method. After that, we used the T1 data to extract the native template for every person by FSL. Thus, we could count the number of fibers connecting every two brain regions. All the processes were performed by a pipeline named PANDA [Cui et al., 2013] from Beijing Normal University.

2.8.4 Statistical inference

We used Pearson product-moment correlation coefficient [Rodgers and Nicewander, 1988] to describe the relationship the connection between the functional connectivity entropy with ageing. In addition, we also used partial correlations [Rodgers and Nicewander, 1988]. Moreover, we applied a linear regression analysis [Seber and Lee, 2012] to determine any trends of the functional connectivity entropy of normal people, with age.

2.9 Methods for Functional Connectivity Entropy Results in Schizophrenia (Section 3.2)

2.9.1 Subjects

This schizophrenia analysis contained three schizophrenia datasets. Two of the three datasets had information about the symptom severity. One of these was recruited at the National Taiwan University Hospital, and the other from the Second Xiangya Hospital of Central South University in China. In total there were 152 patients in these two datasets with schizophrenia (84 males / 68 females, aged 27.11 $\pm$ 9.57 years, illness duration 4.06 $\pm$ 5.43 years), identified using DSM-IV diagnostic criteria. None of the patients had co-morbidities with other Axis-1 disorders. Two patients were left handed and 150 right handed (Edinburgh Handedness Inventory). Symptom severity was measured using the Positive and Negative Syndrome Scale (PANSS) administered either one week before or after the MRI scan. However, 26 patients could not complete their PANSS assessment due to poor health. Only 22 patients were treatment naive, the remaining 130 were all taking antipsychotic medication.

The third schizophrenia dataset also came from Second Xiangya Hospital of Central South University in China, but had no severity information. It contained 63 patients with schizophrenia (34 males / 29 females). The patients had a mean age of 25.00 $\pm$ 6.59 years. we wished to use the two datasets from the Second

Xiangya Hospital to test for differences between the controls and the patients with schizophrenia as these patients are within five years after their first onset. Thus, we called the two datasets from the Second Xiangya Hospital the 'Xiangya dataset'. The two datasets with symptom severity information from the PANSS were used to extract the relation with the brain features and the symptom severity information, and we termed these two combined datasets the 'PANSS dataset'.

For the controls, a total of 322 individuals were included ranging from 22 to 28 years old. These had a mean age of 24.1 ± 1.9 years old. The patients with schizophrenia from the Second Xiangya Hospital (mean age: 24.1 ± 7.3 years) and healthy control groups used in the main analyses were well matched by age (two-sample t test, $p = 0.95$). Of the healthy controls, 142 were males. Samples with poor data quality were excluded. 20 of these datasets came from the 1000 Functional Connectomes Project (`http://fcon_1000.projects.nitrc.org/`), where data came from all over the world including China, Britain and United States. In these 20 data sets, there were 312 samples, with 132 of them male. The mean age was 24.1 ± 1.9 years. Details are listed in Table 2.5. The controls also included a 21st dataset of 10 healthy individuals from the Department of Biomedical Imaging and Radiological Sciences, National Yang-Ming University, Taipei, Taiwan and the Brain Connectivity Laboratory, Institute of Neuroscience, National Yang-Ming University, Taipei, Taiwan. All were male. The mean age was 24.5 ± 1.4 years. Moreover, the T1-images and DTI data of these 10 individuals were used for the anatomical connectivity analyses described.

Table 2.5: Detailed information of the 21 databases for the normal controls

Database	**Quantity**	**fMRI Information (TR(s) /Slices /Timepoints)** (TR(s)/Slices/Timepoints)	**Male/Female**	**Age (years)**
Atlanta	15	2, 20, 205	6/9	23.0 ±2.4
Baltimore	8	2.5, 47, 123	1/7	22.0 ±2.0
Beijing_Zang	69	2, 33, 225	25/44	22.0 ±1.2
Berlin_Margulies	12	2.3, 34, 195	4/8	23.0 ±1.2
Cambridge_Buckner	64	3, 47, 119	22/42	25.0 ±1.4
Cleveland	3	2.8, 31, 127	0/3	22.0 ±2.3
Dallas	7	2, 31, 115	3/4	27.0 ±1.7
ICBM	7	2, 23, 128	3/4	27.0 ±2.0
Leiden_2180	7	2.18, 38, 215	7/0	27.0 ±1.7
Leiden_2200	7	2.2, 38, 215	3/4	27.0 ±2.4
Leipzig	25	2.3, 34, 195	11/14	25.0 ±1.9
NewHaven_a	5	1, 16, 249	4/1	23.4 ±1.1
NewHaven_b	9	1.5, 22, 181	4/5	24.4 ±2.2
Newark	16	2, 32, 135	7/9	23.6 ±1.4
Orangeburg	2	2, 22, 165	2/0	25.5 ±0.7
Oulu	8	1.8, 28, 245	3/5	22.0 ±0.0
PaloAlto	6	2, 29, 235	1/5	24.2 ±1.7
Pittsburgh	5	1.5, 29, 275	5/0	26.6 ±1.5
Queensland	14	2.1, 36, 190	8/6	25.1 ±1.7
Saintlouis	23	2.5, 32, 127	13/10	25.7 ±1.8
Yang-Ming	10	2.5, 43, 200	10/0	24.5 ±1.4
Whole Database	322	N/A	142/180	24.1 ±1.9

Table 2.6: Detailed information for the patients

Database	Quantity	Male/Female	Age (years)	PANSS Severity Symptoms
Second XiangYa Hospital	63	34 / 29	25.00 ± 6.59	No
Second XiangYa Hospital	83	49 / 34	23.37 ± 7.83	Yes
Taiwan National Hospital	69	35 / 34	31.59 ± 9.60	Yes

2.9.2 Data Acquisition

In the dataset from the National Taiwan University Hospital, all subjects underwent a functional MRI scan in a single session using a 3T MR system (TIM Trio, Siemens, Germany). A 32 channel head coil was used as the RF signal receiver. Sponges were used to fix subjects' heads within the coil to prevent motion artifacts. All images were acquired parallel to anterior-commissure-posterior-commissure line with an auto-align technique. The total scan time for each subject was about 6 minutes. The resting-state fMRI was performed with a gradient-echo echo planar sequence. Subjects were asked to relax and think of nothing in particular and to keep their eyes closed, although they were requested not to fall asleep. Wakefulness was assessed throughout the recording via an intercom link to the scanner chamber. The exact parameters were as follows: repetition time (TR) 2000 ms, echo time (TE) 24 ms, field of view (FOV) 256 × 256 mm^2, matrix 64 × 64, slice thickness 3 mm and flip angle 90. For each participant, 34 trans-axial slices with no gap were acquired to encompass the whole brain volume.

In the dataset from the Second Xiangya Hospital with severe symptoms, all image data were acquired using a 1.5T Siemens MRI scanner. A total of 180 volumes of Echo Planar Imagining (EPI) images were obtained axially (repetition time, 2000 ms; echo time, 40 ms; slices thickness, 5mm; gap, 1mm; field of view (FOV), 24 × 24 mm^2; resolution, 64 × 64; flip angle, 90). On the other hand, the samples without severe symptoms from the Second Xiangya Hospital were from a 3T Philips MRI scanner with a total of 240 volumes of Echo Planar Imaging (EPI) images were obtained axially (repetition time, 2000 ms; echo time, 30 ms; slices thickness, 4mm; resolution, 64 × 64; flip angle, 90).

For the healthy controls, the data acquisition details for the 20 datasets from the 1000 Functional Connectomes Project are provided on their website, `http://fcon_1000.projects.nitrc.org/`. In the 21st young healthy control dataset, from the National Yang-Ming University, Taiwan, all 10 people underwent structural, functional and diffusion tensor imaging scanning using a Siemens Trio 3T scanner at the National Yang-Ming University, Taiwan. Foam padding was used to minimize head motion for all subjects. Functional images were acquired using a single-shot,

gradient-recalled echo planar imaging sequence (repetition time = 2500 ms, echo time = 27 ms and flip angle = 77). Fourty-three transverse slices (field of view = 220 $\times$ 220 mm^2, in-plane matrix = 64 $\times$ 64, slice thickness = 3.4 mm, voxel size = 3.44 $\times$ s3.44 $\times$ 3.4 mm^3), aligned along the anterior commissureCposterior commissure line were acquired. For each subject, a total of 200 volumes were acquired, resulting in a total scan time of 500s. Subjects were instructed simply to rest with their eyes closed, not to think of anything in particular, and not to fall asleep. The diffusion tensor images covering the whole brain were obtained using spin echo-based echo planar imaging sequence, including 30 volumes with diffusion gradients applied along 30 non-collinear directions (b = 1000 s/mm^2) and three volumes without diffusion weighting (b = 0 s/mm^2). Each volume consisted of 63 contiguous axial slices (repetition time = 11000 ms, echo time = 104 ms, flip angle = 90 degrees, field of view = 100 $\times$ 100 mm^2, matrix size = 128 $\times$ 128, voxel size = 2 $\times$ 2 $\times$ 2 mm^3). To improve the signal to noise ratio, the entire sequence was repeated three times. Subsequently, high-resolution T1-weighted anatomical images were acquired in the sagittal orientation using a magnetization-prepared rapid gradient-echo sequence (repetition time = 3500 ms, echo time = 3.5 ms, flip angle = 7, field of view = 256 $\times$ 256 mm^2, matrix size = 256 $\times$ 256, slice thickness = 1 mm, voxel size = 1 $\times$ 1 $\times$ 1 mm^3 and 192 slices).

2.9.3 Data Preprocessing

Firstly, we deal with the resting-state BOLD signal. The first 10 volumes of these datasets were discarded, to allow for scanner stabilization and the subjects' adaptation to the environment. fMRI data preprocessing was then conducted by Statistical Parametric Mapping (SPM8) [Frackowiak et al., 2003] and a Data Processing Assistant for Resting-State fMRI (DPARSF) [Yan and Zang, 2010]. The remaining functional scans were first corrected for within-scan acquisition time differences, between slices, and then realigned to the middle volume, to correct for inter-scan head motions. Subsequently, the functional scans were spatially normalized to a standard template (Montreal Neurological Institute) [Fonov et al., 2011] and resampled to 3 $\times$ 3 $\times$ 3 mm^3. Data was then smoothed, and after normalization and smoothing, BOLD signals of each voxel were firstly detrended, to remove any linear trend, and then passed through a band-pass filter (0.01-0.08 Hz) to reduce low-frequency drift and high-frequency physiological noise. Finally, nuisance covariates including head motion, global mean signals, white matter signals and cerebrospinal signals were regressed out from the BOLD signals. After data preprocessing, the time series were extracted in each ROI by averaging the signals of all voxels within that region. In

this theis, the automated anatomical labelling atlas (AAL) [Tzourio-Mazoyer et al., 2002] was used to parcellate the brain into 90 regions of interest (ROIs) (45 per hemisphere). The names of the ROIs and their corresponding abbreviations are listed in Table 2.2.

For DTI images, we first used FSL [Jenkinson et al., 2012] to remove the eddy-current and extract the brain mask from the B0 image. Then, we used TrackVis [Wang et al., 2007] to obtain the fiber images by the deterministic tracking method. After that, we used the T1 data to extract the native template for every person by FSL. Thus, we could count the number of fibers connecting every pair of brain regions. All the processes were performed using a pipeline named PANDA [Cui et al., 2013] from Beijing Normal University.

2.9.4 Statistical inference

Two-sample t tests [Mendenhall et al., 2008] were used to test the differences between the groups in FCE and in the functional connectivity of every link. we also utilized a Kolmogorov-Smirnov test to compare the differences between two distributions of the functional connectivity [Feldman and Valdez-Flores, 2009]. The relation between the functional connectivity entropy and the different PANSS subscores was measured with the Pearson correlation coefficient with Bonferroni correction, followed by partial Pearson correlation [Rodgers and Nicewander, 1988] to remove age effects. Moreover, we used permutation tests [Rédei, 2008] to clarify the robustness of the findings.

2.10 Functional Connectivity Entropy Properties

2.10.1 Entropy will grow higher with more intervals in $[-1, 1]$

In this thesis, we separated $[-1, 1]$ into 20 intervals. If we separate it into more parts, the entropy will be larger.

Proof

According to the property of Shannon entropy,

$$\begin{aligned}\mathrm{H}(P_{11}, \cdots, P_{m1}, \cdots, P_{1n}, \cdots, P_{mn}) &= \mathrm{H}(P_{11} + \cdots + P_{m1}, \cdots, P_{1n} + \cdots + P_{mn}) \\ &+ \sum_{i=1}^{n} (P_{1i} + \cdots + P_{mi}) \mathrm{H}\left(\frac{P_{1i}}{\sum_{j=1}^{m} P_{ji}}, \cdots, \frac{P_{mi}}{\sum_{j=1}^{m} P_{ji}}\right). \end{aligned} \tag{2.8}$$

The left side of the last equality is the entropy with mn parts in $[-1, 1]$, while the first term in the right side of the equality is the entropy with m parts. Moreover, the last term of the equality is not less than zero. Thus, the entropy with mn parts is larger than that with n parts. In other words, if there are more parts in $[-1, 1]$, the entropy will be higher.

2.10.2 Entropy vs choice of atlas: Atlases with different numbers of brain regions

In this thesis, the atlas we used was the AAL template, with 90 brain regions. we have investigated the relationship between atlas choice, the number of brain regions and the value of the functional connectivity entropy. we used different atlases with various numbers of brain regions on one sample, which was from a young healthy male, where the quality of the MRI was quite good. Figure 2.10 shows the entropy results from different atlases (red nodes) and a fit of the data by an exponential (blue line). The relationship between entropy and the number of brain regions, N, is Entropy$= 1.64N^{-0.337} + 3.305$. According to this equation, the entropy asymptotically approaches a constant as the number of brain regions tends to infinity. The limiting value of the functional connectivity entropy of this individual is 3.305.

Note that not all samples were suited to calculations of the entropy, using more than 2000 brain regions, because more brain regions lead to more noise. Thus, if we want to extract an accurate entropy with more brain regions, we need high quality MRI samples. Not all of the samples have sufficient quality, e.g., some samples are from 1.5T MRI or are affected by some head motions.

2.10.3 Entropy vs choice of atlas: Different atlases with a fixed number of brain regions

We further note that if we use different templates, but fix the number of brain regions, the results are quite stable. To see this consider Figure 2.11, where we have chosen the AAL atlas and separated it in different ways. we have considered 10 different atlases (all have 1024 brain regions) and extract the entropy of 20 normal young individuals, based on the various atlases. we have found no significant entropy differences for each sample, with various atlases. In Figure 2.11, different symbols label the entropy from different brain region atlases. The difference between the entropy from various atlases is sufficiently small that we need to amplify the scale to distinguish them. Thus, the entropy results are quite stable.

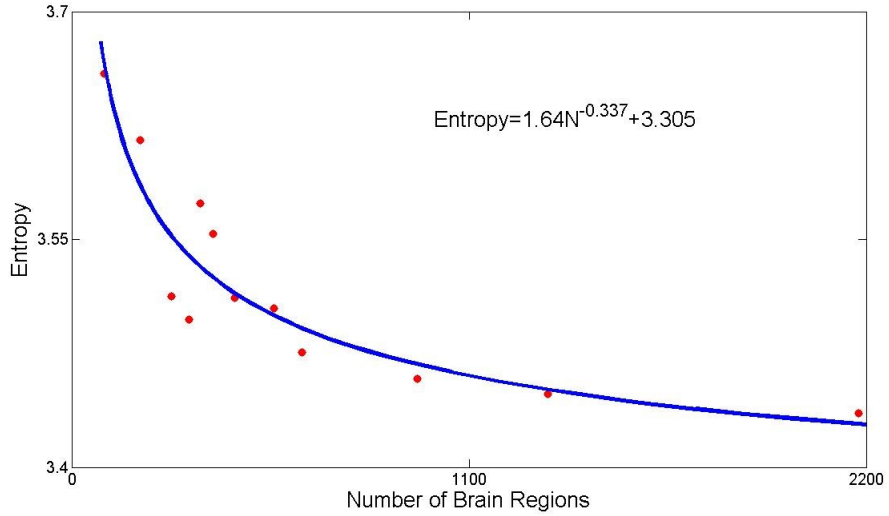

Figure 2.10: Entropy versus the number of brain regions
The red nodes are from an entropy calculation based on atlases with different numbers of brain regions. The blue line is a fit through the nodes from an exponential function.

2.10.4 A mathematical description of Functional Connectivity Entropy

Let $x(t)$ be a resting fMRI time course of the brain. This is defined on a function space (with respect to time), Θ, which is a subspace of the Lebesgue function space $L^2(T, R)$, where T can be either the continuous time set $[0, S]$ or the discrete time set $\{1, 2, , S\}$. we assume that a probability measure, P, is defined on Θ with its σ-algebra $\mathcal{F}$ induced by the norm of $L^2(T, R)$. In the following, we need not know the explicit forms of the probability distributions of the random functions, to define the entropy. One particular fMRI time course from one of the regions of interest, which were considered, is regarded as a state point in the probability space $\{\Theta, \mathcal{F}, P\}$. Let $x(\cdot)$ and $y(\cdot)$ be two independent random time courses following the same distribution. Their correlation coefficient can be regarded as a functional with respect to $\Theta \times \Theta$:

$$\rho(x, y) = \frac{\int_0^S (x(t) - \bar{x})(y(t) - \bar{y})\mathrm{d}t}{\mathrm{std}(x)\mathrm{std}(y)}, \tag{2.9}$$

with $\bar{x} = \frac{1}{S}\int_0^S x(t)\mathrm{d}t$, $\mathrm{std}(x) = \sqrt{\int_0^S [x(t) - \bar{x}]^2 \mathrm{d}t}$. The functional connectivity entropy is actually that of the random (scale) variable $\rho(x, y)$ that is induced by

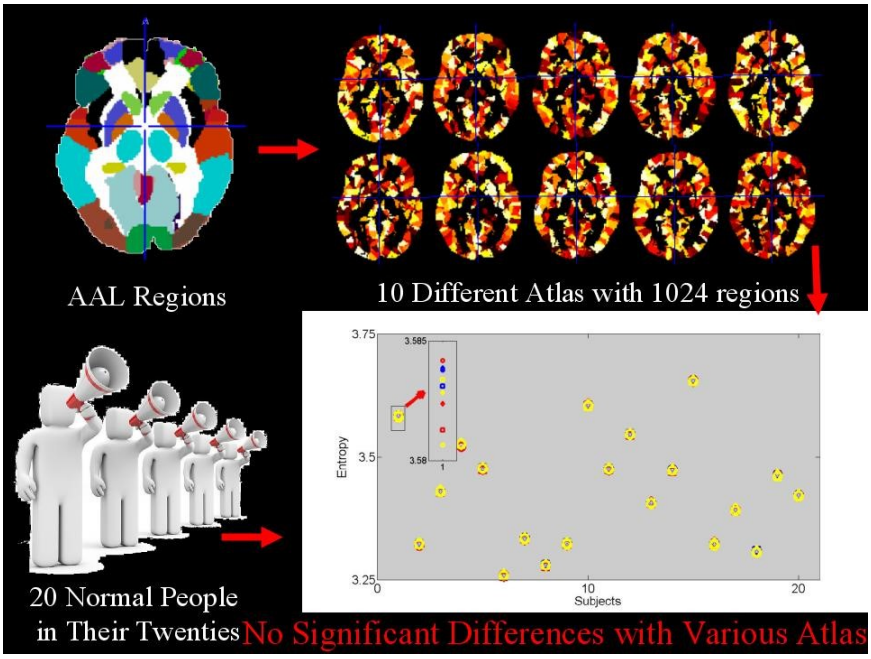

Figure 2.11: 10 different atlases were chosen to separate the AAL atlas into more parts
We calculated the entropy in samples from 20 normal people with ages in the range 20 to 26. There are no significant differences with various atlases.

the two independent random functions $x(\cdot)$ and $y(\cdot)$. Thus, we write the entropy as $H(\rho(x,y))$. The entropy of a region can be regarded as the specific conditional entropy of $\rho(x,y)$ when y is fixed, namely $H(\rho(x,y)|y = y(\cdot))$. The mean of a region's entropy can be regarded as the conditional entropy of $\rho(x,y)$ with respect to the random function $y(t)$, and we write this entropy as $H(\rho(x,y)|y)$.

To specify the meaning of the definition of functional connectivity entropy given, we restrict the function space Θ to all periodic functions with the same constant frequency, ω. Then $x(t)$ can be written as $x(t) = a \times \cos(\omega t + \varphi)$ and $y(t)$ can be written as $y(t) = b \times \cos(\omega t + \psi)$. For sufficiently large S, the mean of both x and y are approximately zero. Their correlation coefficient, as $S \to \infty$, becomes,

$$\rho(x,y) = \frac{\frac{1}{2S}\int_0^S ab \times [\cos(2\omega t + \varphi + \psi) + \cos(\varphi - \psi)]\mathrm{d}t}{ab\sqrt{\frac{1}{S^2}\int_0^S [\cos(\omega t + \varphi)]^2 \mathrm{d}t \int_0^S [\cos(\omega t + \psi)]^2 \mathrm{d}t}} \to \cos(\varphi - \psi), \tag{2.10}$$

Additionally, $\rho(x,y) = \cos(\varphi - \psi)$ also holds if S is an integer multiple of the period. Thus, the correlation coefficient between two periodic oscillations with the same period is the cosine of the phase difference. In this scenario, the function space can be embedded in a phase space (a one dimensional torus) S^1 (namely, $[0, 2\pi]$). Let $\{S^1, \mathcal{F}, P\}$ be the probability space induced by $\{\Theta, \mathcal{F}, P\}$, let φ and ϕ be two independent random variables in it, and let $z = \cos(\varphi - \psi)$. Then, the entropy of z is $H(z)$, and the region's entropy is the specific conditional entropy, $H(z|\varphi = \varphi_0)$, and the mean regional entropy is the conditional entropy $H(z|\varphi)$. Note that in the definition of the entropy, the Lebesgue measure of $z = \cos(\varphi - \psi)$ is the trivial one defined in $[-1, 1]$, denoted by $m_{\cos}(\mathrm{d}z)$. The difference between the entropy of z and its conditional entropy is clearly the mutual information between φ and z:

$$I(z, \varphi) = H(z) - H(z|\varphi). \tag{2.11}$$

Let $\theta = |\varphi - \psi|$, then, z is equivalent to Θ, considering the torus S^1 with $\theta \equiv 2\pi + \theta$. With a properly-defined Lebesgue measure of θ, i.e., the measure induced by that of z, namely $m_{\cos}(\cdot)$, the entropy and conditional entropy of θ then equal those of z. Pick the measures of these variables, in order to define the (relative) entropy. That is: First, pick a joint measure of (φ, ψ) (denoted by $m_1(\mathrm{d}\varphi, \mathrm{d}\psi) = m(\mathrm{d}\varphi)m(\mathrm{d}\psi)$, a joint measure of two independent and identical measures, where $m(\cdot)$ is determined below), and a joint measure of $(\varphi, \varphi - \psi)$, denoted by $m_2(\mathrm{d}\varphi, \mathrm{d}(\varphi - \psi))$, such that they are preserved through the transformation between them, (i.e., letting T be the transform from (φ, ψ) to $(\varphi, \varphi - \psi)$, then for

any measurable set A in the space of $(\varphi, \varphi - \psi)$, $m_2(A) = m_1(T^{-1}(A))$ holds); Second, pick the measure $(\varphi, \theta = |\varphi - \psi|)$ induced by $m_1(\mathrm{d}\varphi, \mathrm{d}\psi)$ and denoted by $m_3(\mathrm{d}\varphi, \mathrm{d}\theta)$; Finally, $m(\cdot)$ is chosen to guarantee that the embedded measure of θ equals to $m_{\cos}(\mathrm{d}z)$. Thus, we have,

$$\begin{aligned} 2D(\varphi||m(\cdot)) &= D(\varphi, \psi||m_1(\cdot,\cdot)) = D(\varphi, \varphi - \psi||m_2(\cdot,\cdot)) \\ &\geq D(\varphi, \theta||m_3(\cdot,\cdot)) = D(\theta|\varphi||m_3(\cdot,\cdot)) + D(\varphi||m(\cdot)). \end{aligned} \tag{2.12}$$

We conclude that $D(\theta|\varphi||m_3(\cdot,\cdot)) \leq D(\varphi||m(\cdot))$. This implies that the mean regional entropy is a lower-bound of the entropy of the phase random variable under the measure preserving transformation. In addition, if different measures were picked, there would be constant differences in the above inequality induced by the expectation of the derivative of different Lebesgue measures.

In particular, if we pick the trivial measure on the torus, S^1, and let $f(\varphi)$ be the probability density function (pdf) of φ, then after simple algebra, we have the conditional pdf of θ with respect to φ as

$$p(\theta|\varphi) = f(\varphi - \theta) + f(\varphi + \theta), \qquad \pi \geq \theta \geq 0. \tag{2.13}$$

Then we have,

$$H(\theta|\varphi) = \mathrm{E}\{\log\left[f(\varphi - \theta) + f(\varphi + \theta)\right]\}. \tag{2.14}$$

2.11 Mean, entropy and global signal

As described in the data preprocessings, the global signals were regressed out from the BOLD signals. This has the effect of making the mean correlation in the functional connectivities approximately zero, and there are both positive and negative correlations in the functional connectivity matrix [Fox et al., 2009].

Global signal regression, as mentioned in Chen et al. [2012] work, 'is a preprocessing technique, is intended to eliminate undesired global noise, i.e. non-neural noise that has a global effect on the RfMRI signal. It was hypothesized that R-fMRI signals may cancel each other out in the global average, while the global noise may be additive and dominate the global-averaged signal. Practically, the global signal is obtained by averaging all brain voxel time courses.' Moreover, as described in Fox et al. [2009] work, the exact formula of global signal regression is:
'Let the BOLD data be represented as the $n \times m$ array, B, where n is number of time points (frames) and m is the number of voxels. The global mean time course,

g, is an $n \times 1$ column vector, $g = (1/m)B1_m$, where 1_m is the $m \times 1$ column vector of all 1 s. Voxelwise regression of the BOLD data on g generates,

$$\beta_g = g^+ B, \tag{2.15}$$

where g^+(a $1 \times n$ array) is the pseudoinverse of g. Thus $g^+ = [g^T g]^{-1} g^T$ and $g^T g = 1$. Furthermore, β_g is a $1 \times m$ array (image). Regressing out the global signal gives the new volumetric times series,

$$B' = B - g\beta_g.' \tag{2.16}$$

Here, we use analysis of the data of two randomly picked individuals (one patient (SCZD), one control, both are females aged 24) from the sample to show the effect of global signal regression on the relationship between the correlation coefficients and the FCE. In Figure 2.12, we represent the correlation coefficient distributions with and without the global signals removed. As shown in Figure 2.12 a and b, the correlation distribution will move from the positive to the negative side, which is consistent with the data of Fox et al. [2009]. In Figure 2.12 c and d, we represent the differences between the patient and the control groups before and after removing the global signal. It should be emphasized that the distribution of the 4005 functional connectivity correlation measures in schizophrenia is narrower than in the controls in both situations (Entropy: SCZD vs control, 3.5 vs 3.9, without global signal removed; 3.6 vs 3.8, with global signal removed). Thus, the entropy measure for the patient is lower than for controls independently of whether we remove the global signal or not. On the other hand, the mean of the functional connectivity correlations with the global signals removed is higher in the schizophrenia group than the controls, and it will go in the opposite direction if the global signal is not removed. This shows how the entropy measure is useful, and is independent of whether the global signal is removed or not.

Figure 2.12 demonstrates that the mean correlation coefficient will show opposite results before and after removing the global signal. However, the entropy will show similar effects before and after removing the global signal. The entropy in the patients is lower than in the controls. The effects of global signal removal on FCE change in schizophrenia discussed in Section 4.5.1 in detail.

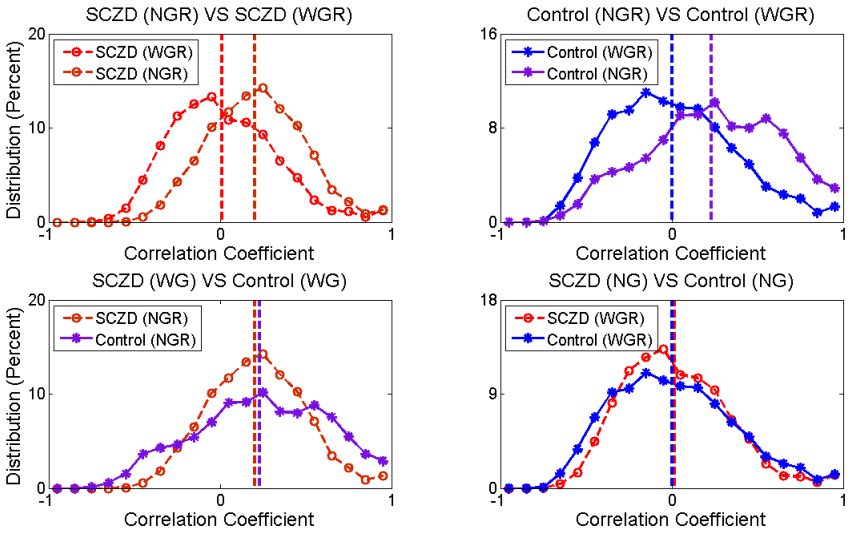

Figure 2.12: Correlation coefficient distributions in patients and controls with global signals removed (WGR) and without global signals removed (NGR)
The distribution of the correlation coefficients of the control (blue) and the patient (denoted SCZD; red) with and without the global signal. The dashed lines represent the mean correlation coefficients.
This figure is reproduced from Yao et al. [2015].

Chapter 3

Results

The results in Section 3.1 have already been published on Yao et al. [2014], while those in Section 3.4, 3.5 and 3.6 have been published on Yao et al. [2015].

3.1 Functional Connectivity Entropy Origin: Ageing Problem

We have carried out a full analysis to determine the functional connectivity entropy in all individuals in all data sets. Figure 3.1a shows the functional connectivity entropy of the full data set as a function of age, without taking into account gender differences. In Figure 3.1b we present a running average of the functional connectivity entropy for males and females, with an averaging window of 25 years. In Figures 3.1c and 3.1d, we give the results for the functional connectivity entropy in males and females separately, which are different at birth (3.5336 bits in males, 3.5547 bits in females) and which have different rates of change (0.0015 bits/year in males, 0.0011 bits/year in females). The Pearson correlation between entropy and age is strongly significant (r=0.23, N = 610, $p = 5.6 \times 10^{-9}$ for males and r=0.15, N=634, $p = 1.51 \times 10^{-4}$ for females). These lead to the crossover that can be seen in Figure 3.1b, at an approximate age of 50 years.

3.2 Functional Connectivity Entropy Results in Schizophrenia

To make the results clear, the distributions of functional connectivities in patients with schizophrenia and controls is shown first (Figure 3.2), and then the functional

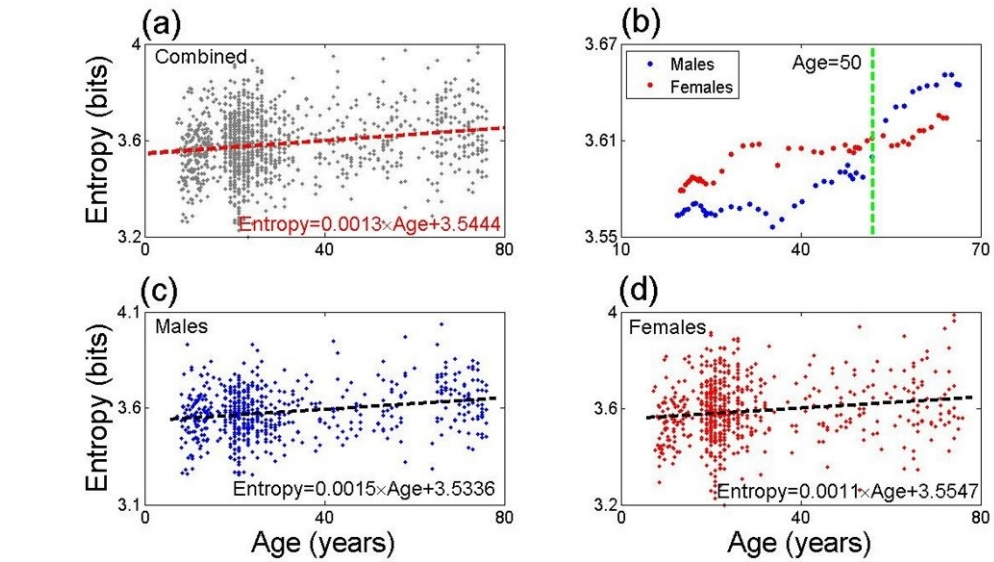

Figure 3.1: Functional connectivity entropy vs Age
Panel (a) is a plot of the functional connectivity entropy of individuals versus their age (pooling results from males and females). A mean rate of increase of the entropy of 0.0013 bits/year was found from the data. Panel (b) contains a plot of the running average of the entropy, versus age, with a window of width of 25 years adopted. There is a crossover in the male/female entropies in the vicinity of 50 years of age. Panels (c) and (d) plot the entropy versus age of males and females. Males have a lower initial value of the entropy than females, but a faster mean rate of increase. The linear correlation between entropy and age is strongly significant ($p = 5.6 \times 10^{-9}$ for males and $p = 1.51 \times 10^{-4}$ for females, r equals 0.23 for males and 0.15 for females, degree of freedom: 610 and 634, respectively.)
This figure is reproduced from Yao et al. [2014].

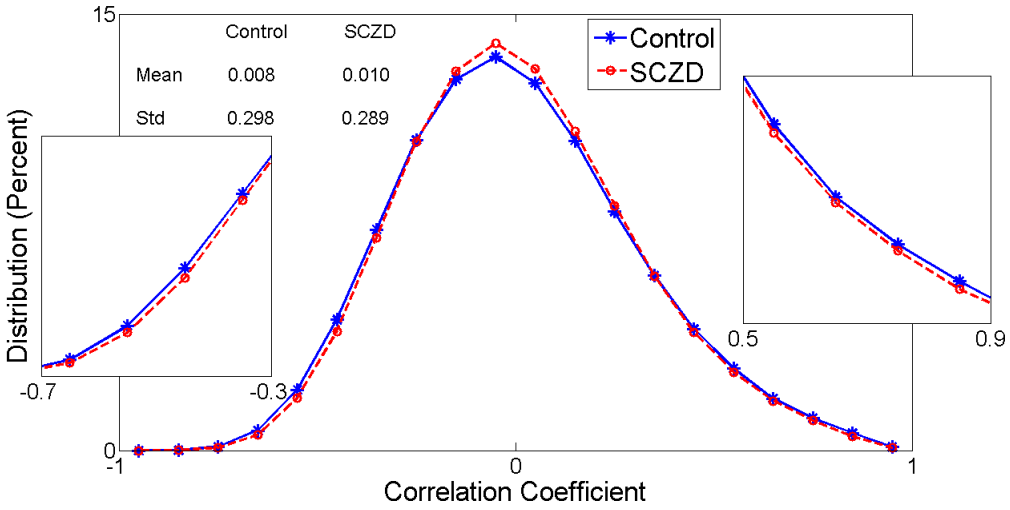

Figure 3.2: Distribution of the functional connectivity correlation coefficients
Distribution of the functional connectivity correlation coefficients of resting-state fMRI between 90 AAL brain regions for patients with schizophrenia (red, denoted SCZD) and controls (blue).
In the figure, 'Mean' stands for the average and 'Std' stands for the standard deviation of the correlation coefficients respectively.

connectivity entropy distributions are shown in Figure 3.3, as they are based on the functional connectivities shown in Figure 3.2.

3.2.1 Frequency distribution of functional connectivities

As shown in Figure 3.2, there were more low values (both positive and negative) of the functional connectivities in the patients with schizophrenia than in the controls. Statistical analyses confirmed the narrow distribution of correlation coefficients in patients when compared to controls (the standard deviation was 0.289 in patients and 0.298 in the controls, $t = 3.299$, $p = 0.001$). The shape of the distributions was very significantly different (Kolmogorov-Smirnov test = 0.013, $p = 8.52 \times 10^{-55}$). Further, for each of the bins based on functional connectivity strength (correlation coefficients) between r = -0.1 and r = 0.3, patients with schizophrenia differed significantly from controls (t tests; all p values < 0.0027).

3.2.2 Functional connectivity entropy

As shown in the frequency histogram Figure 3.3, patients with schizophrenia had significantly lower functional connectivity entropies than the controls ($t = 3.12$, df

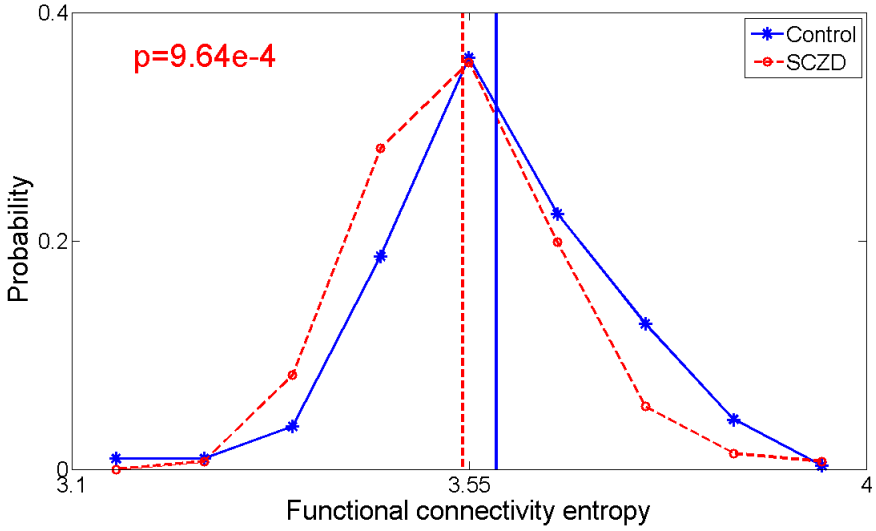

Figure 3.3: Functional connectivity entropy (FCE) for patients with schizophrenia and controls
A histogram of the functional connectivity entropy values for the control (blue) and schizophrenia (red) groups. The data points were the functional connectivity entropy values calculated for all 90×90 connections for all subjects. The mean entropy of the schizophrenia and control groups was significantly different (two-sample t test, t = 3.12, df = 466, p = 9.64×10^{-4}). The term 'SCZD' stands for patients with schizophrenia.

= 466, p = 9.64×10^{-4}).

3.2.3 Correlation of the functional connectivity entropy with the clinical symptoms

To examine the relationship between FCE and clinical symptoms, we correlated the FCE values for subjects with the positive symptom scores, the negative symptom scores, and the general symptom scores [Kay et al., 1987]. As shown in Figure 3.4, a decrease in the FCE is very significantly positively correlated with an increase in the positive (r = -0.453 p = 3.02×10^{-7}, df = 124), negative (r = -0.351, p = 1.72×10^{-4}, df = 124), and the general psychopathology (r = -0.344, p = 2.40×10^{-4}, df = 124) scores of the PANSS (Bonferroni corrected p-values).

There were some missing values for the symptom and severity scores, and that this is reflected in the degrees of freedom. In addition, to exclude any effects of age, we performed a partial correlation procedure that removed any age-related effects from the correlations, and found that the significant results described above

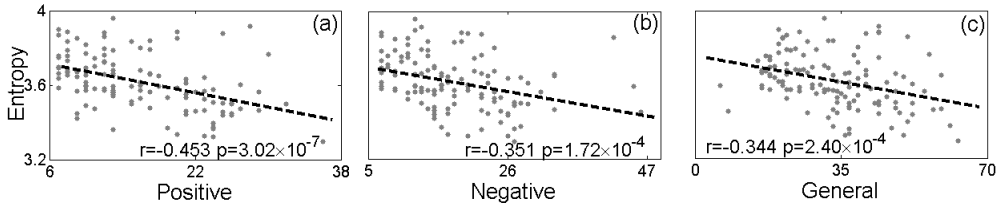

Figure 3.4: Functional connectivity entropy correlated with the severity of different symptoms in the schizophrenia group
The correlations, with the p values, are listed in black. Panel (a) with the positive score from the PANSS, (b) with the negative score, (c) with the general score from the PANSS.
Appendix Figure A.1 is the enlarged version of this figure.

still hold: FCE was still negatively correlated with positive symptom score (r = -0.401, p = 1.09×10^{-5}, df = 124), negative symptom score (r = -0.325, p = 6.58×10^{-4}, df = 124) and general severity score (r = -0.303, p = 0.0018, df = 124). Therefore, FCE is clearly a marker significantly related to the wide variety of symptoms seen in patients with schizophrenia.

In addition, to exclude any effects of age, we performed a partial correlation procedure that removed any age-related effects from the correlations, and found that the significant results described above still hold: FCE was still negatively correlated with positive symptom score (r = -0.401, p = 1.09×10^{-5}, df = 124), negative symptom score (r = -0.325, p = 6.58×10^{-4}, df = 124) and general severity score (r = -0.303, p = 0.0018, df = 124). Therefore, FCE is clearly a marker significantly related to the wide variety of symptoms seen in patients with schizophrenia.

3.2.4 Strength of functional connectivity

To identify the pattern of pairwise functional correlations that contributed most to the changes in functional connectivity entropy (FCE) of the whole brain we compared the functional connectivity matrix between patients with schizophrenia and controls, as shown in Figure 3.5. Figure 3.5 left shows the connectivity in the controls, Figure 3.5 middle shows the connectivity in the patients with schizophrenia, and Figure 3.5 right the difference (patients with schizophrenia - controls). we grouped the AAL regions into resting state networks (RSNs) based on the community structure. For the resulting 6 RSNs, we examined both within-RSN and between-RSN connectivity patterns. Figure 3.5 left shows that the connections

within a resting state network (RSN) tend to be larger than those between the RSNs. The values shown in Figure 3.5 right are color coded as follows: values that are closer to 0 in patients are shown in blue; and values that are further from 0 in patients than controls are shown in red. (Thus weaker connections, whether they are positive or negative, are shown in blue.) Figure 3.5 shows that the functional connectivity values within each RSN (i.e. the boxes on the diagonal) in the patients tend to move towards 0, from what are in general positive values normally (Figure 3.5 left). The absolute value of these within-RSN connectivities showed an average 5.4% reduction in patients (controls = 0.2648; patients = 0.2506, t = -5.44, p = 3.8×10^{-8}). The within-RSN abnormalities were most significant for RSNs 1 (the default mode network), 3 (the attention network) and 4 (the visual recognition network). An 11.5% reduction was seen within RSN1 (mean connectivity in controls = 0.252, patients= 0.223, p = 4.8×10^{-9}). A 9.3% reduction was seen within RSN3 (mean connectivity in controls = 0.214, patients= 0.194, p = 1.1×10^{-4}). A 4.6% reduction was seen within RSN4 (mean connectivity in controls = 0.432, patients = 0.412, p = 0.003).

The absolute values of the between-RSN connectivities showed an average 29.8% reduction in patients (controls = -0.0452; patients = -0.0317, t = 13.75, p $< 10^{-322}$). Specifically, the strength of 10 of 15 inter-RSN connectivities (between six communities) had a significant reduction in patients with schizophrenia (lowest p-value < 0.00001, highest p-value, 0.012).

Overall, the main result of this analysis is that in patients with schizophrenia relative to controls, the absolute values of the inter-RSN connectivities were more greatly reduced than were the intra-RSN connectivities. The implication is that the long-range connections between different networks are those that become reduced most in patients with schizophrenia relative to controls, and this implies that the connections between different major brain systems become reduced in patients relative to controls. Thus the disconnectivity that may be found in schizophrenia is more that between different major brain systems than within them. For the within-RSN functional connectivities, both the default mode and the attention networks showed relatively large decreases in functional connectivity, consistent with the roles of the brain regions comprising these networks in the cognitive symptoms of schizophrenia which include short-term memory and attention deficits. (For the default mode network, the main brain regions include the superior frontal gyrus; and for the attention network the areas include the middle frontal gyrus and superior parietal gyrus).

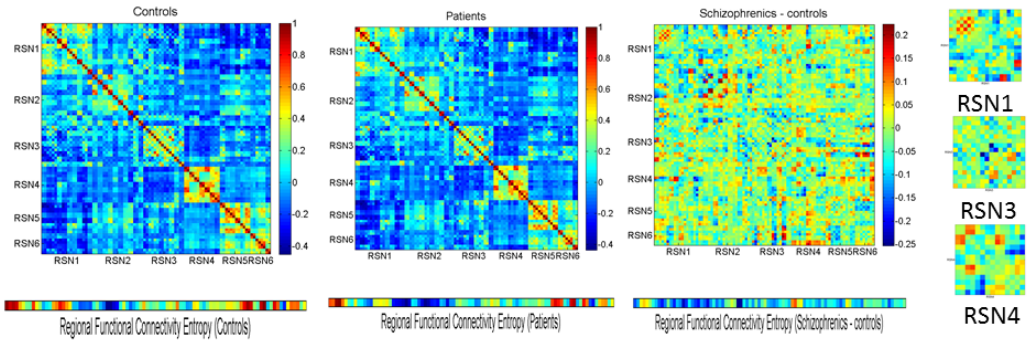

Figure 3.5: Functional connectivity matrix
Top Left Panel: Connectivity diagram of controls between the 90 regions identified in the AAL atlas. The regions are ordered according to the six resting state networks identified on the basis of the community structure [Tao et al., 2013]: RSN1 (Default Mode Network), RSN2 (Subcortical Network), RSN3 (Attention Network), RSN4 (Visual Recognition Network), RSN5 (Auditory Network) and RSN6 (Sensory-motor Network). Top Middle Panel: Connectivity diagram of patients between the 90 regions identified in the AAL atlas.
Top Right Panel: Difference of connectivity values between patients and controls. The values shown are coded by colours as follows: values that are closer to 0 in patients are shown in blue; and differences that are further from 0 in patients than controls are shown in red. (Thus weaker connections, whether they are positive or negative, are shown in blue.)
Moreover, we also enlarge the results of RSN1 (Default Mode Network), RSN3 (Attention Network) and RSN4 (Visual Recognition Network) in the rightmost of the figure.
Appendix Figure A.3 is the enlarged version of this figure.

3.2.5 Summary

In this first ever study to investigate the whole brain and regional diversity of functional connectivity in schizophrenia in a large sample of subjects, the section has shown that the dispersion of the functional connectivity measured using FCE is significantly narrower in patients with schizophrenia and the reduction in FCE is correlated with a broad spectrum of psychopathology including positive, negative and general PANSS scores.

3.3 Computational Model

As shown in Section 2.7.1, we have used a computational model [Deco and Jirsa, 2012] based on diffusion tensor imaging (DTI) data to investigate the origins of the relationship between functional connectivity entropy and age. Extensive experimental data indicates that there is significant loss of neuron number with age, and this is accompanied by the excitatory receptor number (especially NMDA) decreasing with age [Morrison and Hof, 1997]. The computational model yields a brain entropy that decreases when the excitatory connection strength and neuron number in each brain region are simultaneously reduced.

This simulation offers a realistic mechanistic model, at the level of each single brain area, which is based on spiking neurons and realistic AMPA, NMDA, and GABA synapses. The global architecture of the model is shown in Figure 3.6a. After obtaining the neuronal dynamics in each brain region, the fMRI BOLD signal was simulated by means of the Balloon-Windkessel hemodynamic model [Friston et al., 2003]. we found that the functional connectivity entropy increases with decreasing excitatory connection strength (AMPA and NMDA) within the excitatory population of each brain region, shown in Figure 3.6b. To match functional connectivity entropy of the human data, we determined a reliable range of connection strengths [1.78, 1.81] (indicated by two red dashed lines in Figure 3.6b) by comparing the two least-square lines in Figure 1.5a and Figure 3.6b. Figures 3.6c and 3.6d illustrate the simulated BOLD signal with two different connection strengths; the distribution of the correlation coefficients is broader for the smaller connection strength. Specifically, Figure 3.6c, with a larger connection strength is similar to the result for young people in Figure 1.5a, while Figure 3.6d, with a smaller connection strength, is similar to that of elderly people in Figure 1.5c. Additionally, assuming a positive correlation between excitatory neuron number and connection strength (Section 2.7.1), we find that the excitatory neuron number in each brain region decreases from 1130 to 888 (approximately a 20% loss). It is know from

experiments that both the neuron number and excitatory receptors number in the human brain reduce with age. Thus we conclude that this simplified computational model does lead to a relationship between functional connectivity entropy and age that is similar to that observed.

Then we found that the functional connectivity entropy decreased when the excitatory NMDA connection strength between the neurons was decreased. The effects found when the NMDA synaptic conductivity from the excitatory population of each brain region to the inhibitory population of each brain region was reduced are shown in Figure 3.7c. The linear correlation between the functional connectivity entropy and the connection strength was statistically significant (r=-0.85, $p<10^{-10}$, df=40). Figure 3.7d illustrates the distribution of correlation coefficients with two different reductions of the NMDA connection strength; the distribution is narrower for the smaller connection strength. Specifically, the shape of the functional connectivity distribution with an 8% reduction of the NMDAR synaptic conductivity below the starting value for the simulations is similar to that shown in Figure 3.2 for schizophrenics. In comparison, a reduction of 6% in the NMDAR synaptic conductivity produces a connectivity distribution which is similar to that for controls shown in Figure 3.2. That is, with smaller NMDAR conductivities (reduced by 8% below the simulation baseline), the functional connectivity (correlation coefficients) is more likely to be distributed with small absolute values, while with larger NMDA synaptic conductivities (reduced by 6%), the functional connectivity is more likely to be distributed with large absolute values (>0.1 or <-0.3). we show with further results in Section 2.7.2 that this reduction of excitatory-to-inhibitory (E-to-I) conductivity is associated with an increase in the mean firing rates of the excitatory neurons.

3.4 Structural paths

Using the path definitions based on DTI, in 96% of subjects (64 out of 66), all 4005 possible structural links could be classified into primary, secondary or tertiary structural paths. In 27 subjects (14 patients and 13 controls), there were no more than seven pairs of regions that required more than two intermediate linked structures to form an indirect path. On average we obtained 27.8% primary, 68.9% secondary and 3.4% tertiary structural paths in controls. In patients, 27.4% primary, 69.5% secondary and 3.1% tertiary structural paths were noted, with no significant difference between the two groups (Figure 3.8). Of the 4005 possible connections, 3774 were in the same category (primary, secondary or tertiary) when comparing patients and

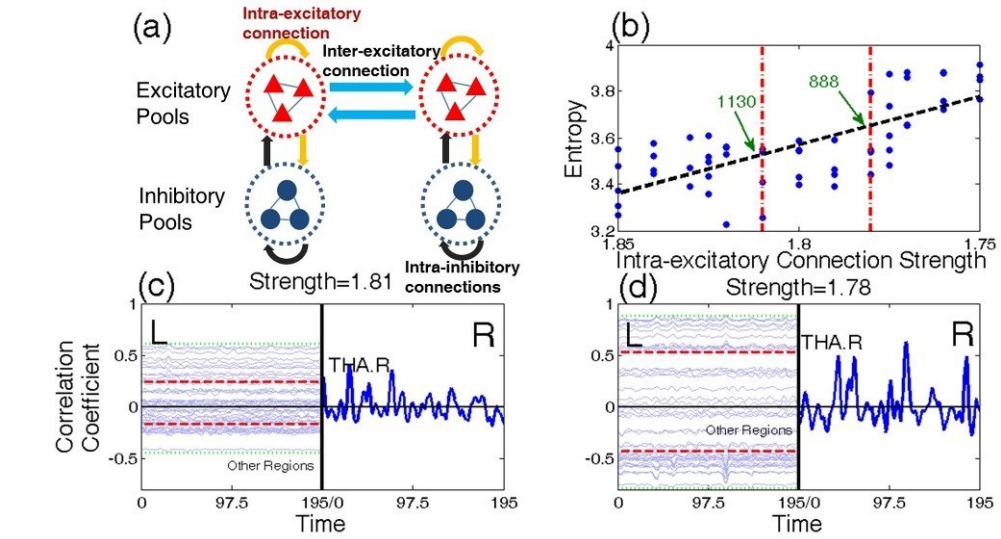

Figure 3.6: Computational Model Demonstration
Panel (a): Schematic representation of brain network. Each brain region is comprised of excitatory pyramidal cells (red triangles) and inhibitory interneurons (blue circles). Yellow and black arrows describe excitatory and inhibitory connections between neurons in each brain region respectively, and blue arrows show excitatory connections between neurons in different brain regions. Panel (b): Functional connectivity entropy versus intra-excitatory connection strength. The black dash line represents the least-square line of blue dots (different trials), and the linear correlation between functional connectivity entropy and connection strength is statistically significant (1×10^{-10}). The two red dashed lines show a range of connection strengths, [1.78, 1.81], which make the corresponding functional connectivity entropy match the human data. From the relationship between strength and excitatory neuron number (see Section 2.7.1), the neuron number range is limited to [888, 1130] (indicated by green arrows). Panel (c) and (d): Time series of simulated BOLD signal. Similar to Figure 1.5, the left hand sides of panels (c) and (d) contain 45 time series arising from brain regions in the left hemisphere. The time series are vertically located, according to their phase difference with the right thalamus. The corresponding connection strength in (c) and (d) is 1.81 and 1.78, respectively. (c) is similar to the result of young people and (d) is similar to that of elderly people. This figure is reproduced from Yao et al. [2014].

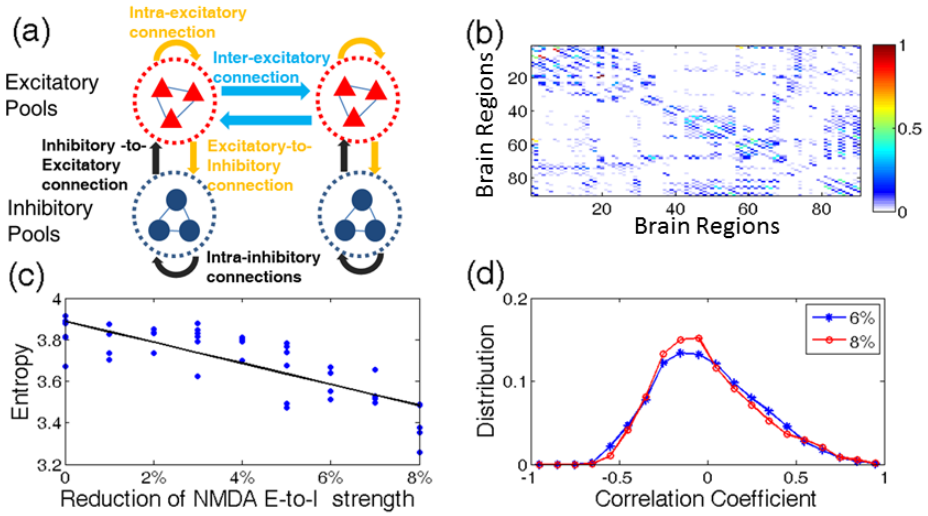

Figure 3.7: Computational Model in Schizophrenia
Panel (a): Schematic representation of the brain network. Each brain region consists of excitatory pyramidal cells (red triangles) and inhibitory interneurons (blue circles). Yellow and black arrows describe excitatory and inhibitory connections between neurons in each brain region respectively, and blue arrows show excitatory connections between neurons in different brain regions. Panel (b): Neuroanatomical connectivity matrix, obtained by DTI after averaging across 10 human subjects. Panel (c): Functional connectivity entropy versus percent reduction of NMDA connection strengths from excitatory to inhibitory (E-to-I) neurons. The black dashed line represents the least-squares fit of the different simulation runs each indicated by a blue dot, and the linear correlation between the functional connectivity entropy and the connection strength is statistically significant (r = -0.85, $p < 1 \times 10^{-10}$, df = 40). Panel (d): The distribution of the correlation coefficients for the resting state connectivity across the 90 brain regions when the percent reduction of E-to-I strength is 6% and 8%, respectively.

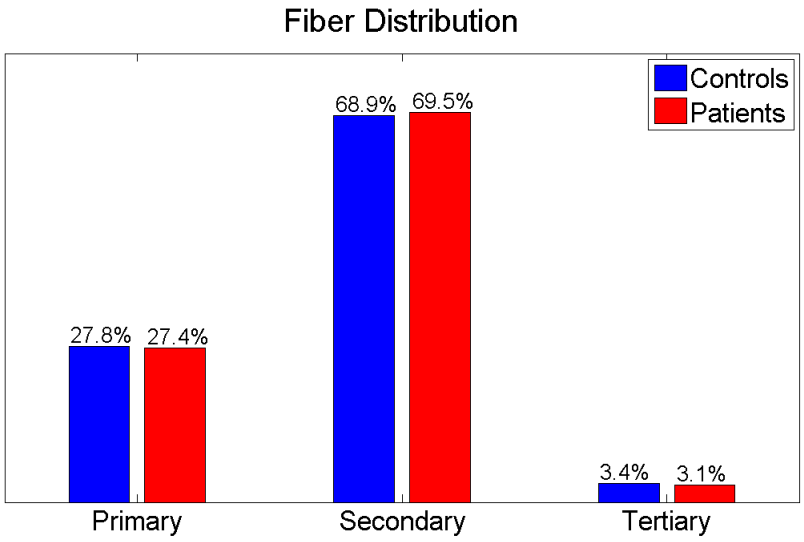

Figure 3.8: Distribution of the structural paths in patients and controls
This figure is reproduced from Yao et al. [2015].

controls. A substantial degree of agreement was noted across the three categories of connections when the two groups of subjects were compared. 95.4% of primary, 91.5% of secondary and 75.6% links are classified in the same group in both patients and controls.

We also examined the anatomical distribution of the primary, secondary and tertiary paths using the conventional distribution of Resting State Networks observed in previous studies. This is presented in Section 3.4.1.

3.4.1 Distribution of the structural paths

In Section 3.4, we separated primary, secondary and tertiary links based on every individual and calculated corresponding FCE. Thus, when we calculated FCE, the same link could be put into different groups, primary, secondary or tertiary. Figure 3.8 showed averaged calculations in patients and controls. If a link was considered to be primary in most patients, then it was counted as a primary link. So did secondary and tertiary links.

In total, 1100(27.4%), 2782(69.5%) and 123(3.1%) links were counted as primary, secondary and tertiary ones in patients, while 1113(27.4%), 2757(68.9%) and 135(3.4%) in controls. For patients, on average, links considered as primary were primary in 81.7% subjects, secondary pathways were secondary in 79.8% of subjects and tertiary pathways were tertiary in 68.5% of subjects, while for controls, the

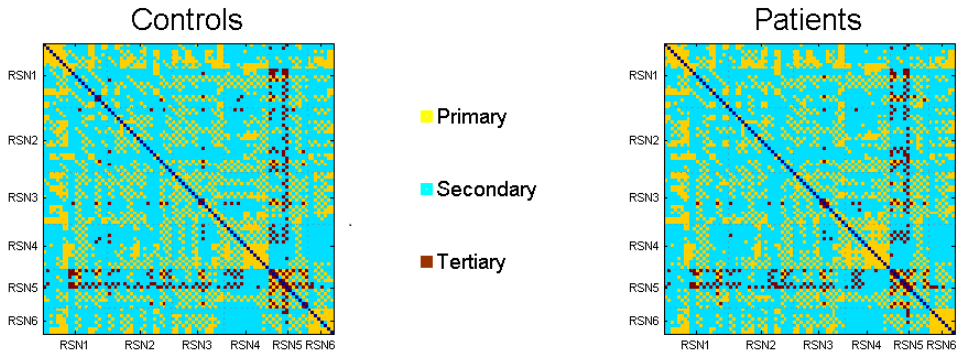

Figure 3.9: Anatomical Distribution of Direct and Indirect structural paths
Direct and Indirect structural paths ordered in accordance with the 6 Resting State Networks in patients (right panel) and in controls (left panel). RSN1 (Default Mode Network), RSN2 (Subcortical Network), RSN3 (Attention Network), RSN4 (Visual Recognition Network), RSN5 (Auditory Network) and RSN6 (Sensory-motor Network).
The diagonal elements are zero and not considered in the analysis.
Appendix Figure A.2 is the enlarged version of this figure.
This figure is reproduced from Yao et al. [2015].

respective percentages were 80.8% for primary, 80.4% for secondary and 69.5% for tertiary pathways.

Of the 4005 possible connections, 3774 were in the same category (primary, secondary or tertiary) when comparing patients and controls. A substantial degree of agreement was noted across the three categories of connections when the two groups of subjects were compared. 95.4% of primary, 91.5% of secondary and 75.6% links are classified in the same group in both patients and controls.

3.4.2 Anatomical Distribution of Structural Paths

An average correlation matrix in controls and patients, with brain regions organised on the basis of the six Resting State Networks (RSNs) [Guo et al., 2014][Tao et al., 2013] is shown in Figure 3.9 below. Table 3.1 shows the distribution of the primary secondary and tertiary paths among the links within each RSN (intra-RSN links) and between the RSNs (inter-RSN links). More information about the community structure of the RSNs observed in functional connectivity studies using AAL parcellations can be found elsewhere [Guo et al., 2014][Tao et al., 2013].

Table 3.1 shows that the RSN1 (Default Mode Network) is the major network with primary structural paths (26%) closely followed by RSN3 (Attention Network).

In contrast, for indirect secondary paths, RSN2 (subcortical) is the major substrate (24%). A substantial number of tertiary paths belong to RSN5 (Auditory Network including insula and superior temporal gyrus for >50%).

3.5 Changes in Functional Connectivity Entropy

Patients did not significantly differ in the whole brain FCE from controls when considered as a single group ($p = 0.5$). But when stratified according to illness duration, whole brain FCE was significantly higher in patients with early stage illness ($p = 0.01$, $d = 0.91$) and lower in those with chronic illness ($p = 2 \times 10^{-6}$, $d = 1.69$) in comparison with age and sex-matched controls.

Both patients in the early stage of schizophrenia ($p = 0.0002$, $d = 1.46$) and chronic illness ($p = 1 \times 10^{-17}$, $d = 4.66$) showed a significant reduction in the FCE of tertiary paths when compared to age and sex-matched controls. FCE of secondary paths was increased in those with early stage schizophrenia ($p = 0.003$, $d = 1.12$), but significantly reduced in patients at a more chronic stage of illness ($p = 2 \times 10^{-5}$, $d = 1.47$). FCE of primary paths showed a trend towards an increase in patients with chronic illness ($p = 0.084$, $d = 0.44$) but not in those with early stage illness when compared to matched controls. (Figure 3.10 panel B). Moreover, we used a permutation test to clarify the robustness of the findings. All the p values were still significant while they were a bit larger than those from two-sample t tests.

3.6 Functional Connectivity Entropy Versus Patient Severity Score

In the early stage of schizophrenia, higher whole brain FCE was associated with higher symptom burden measured using the total SSPI score ($r = 0.705$, $p = 0.034$); this was mostly driven by the increased FCE of secondary paths which was significantly related to the symptom burden($r = 0.74$, $p = 0.023$), while the FCE of primary and tertiary paths did not show any significant relationships. In those with chronic illness, lower whole brain FCE was associated with higher symptom burden ($r = -0.543$, $p = 0.024$); this was driven by the FCE of both primary ($r = -0.64$, $p = 0.006$) and secondary paths ($r = -0.51$, $p = 0.036$) being negatively correlated with the symptom burden, while tertiary paths showed no significant relationship (Figure 3.11).

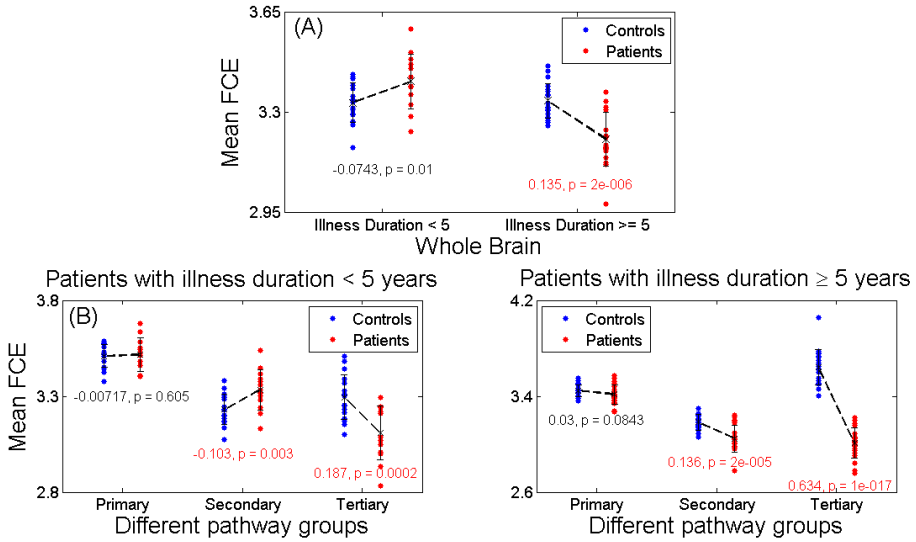

Figure 3.10: Functional connectivity entropy in different fiber pathway
(A): In patients < 5 years, the functional connectivity entropy (FCE) was slightly increased in patients (-0.0743, $p = 0.01$, $d = 0.91$), and significantly decreased (0.135, $p = 2 \times 10^{-6}$, $d = 1.69$) in patients ≥ 5 years comparing with controls.
(B): Left panel: In patients < 5 years, the functional connectivity (FCE) entropy was almost unchanged (-0.00717, $p = 0.605$, $d = 0.10$) in primary pathways, significantly increased (-0.103, $p = 0.003$, $d = 1.12$) in secondary ones and significantly decreased (0.187, $p = 0.0002$, $d = 1.46$) in tertiary ones comparing with controls.
Right panel: In patients ≥ 5 years, the functional connectivity entropy (FCE) was close to significantly decreased (0.03, $p = 0.0843$, $d = 0.44$) in primary pathways, significantly decreased (0.136, $p = 2 \times 10^{-5}$, $d = 1.47$) in secondary and most significantly decreased (0.634, $p = 1 \times 10^{-17}$, $d = 4.66$) in tertiary when compared with controls.
All the effects of age, sex and dose have been removed.
This figure is reproduced from Yao et al. [2015].

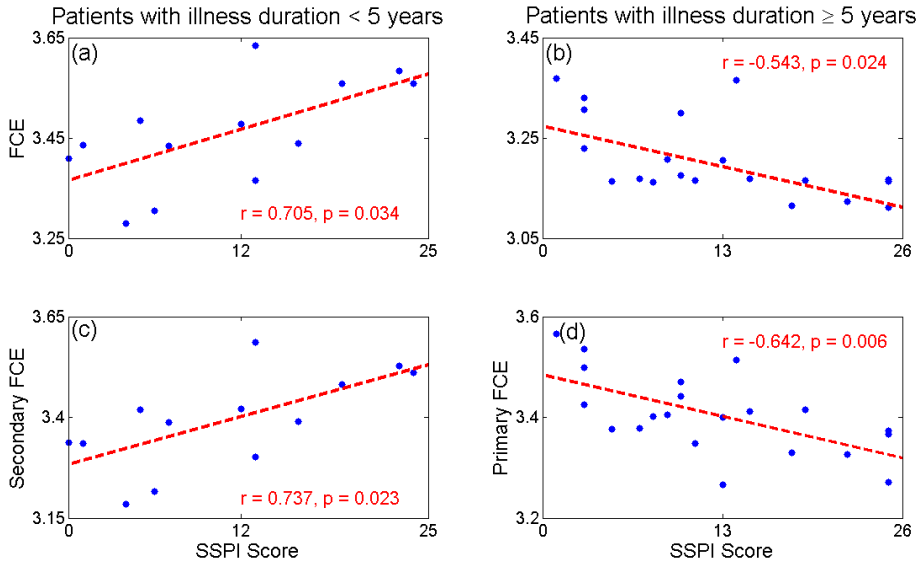

Figure 3.11: Functional Connectivity Entropy VS SSPI score
Panel (a) & (b): The functional connectivity entropy (FCE) held a significantly (r = 0.705, p = 0.034) positive correlation with SSPI score in patients $<$ 5 years (left panel), while it displayed a significantly (r = -0.543, p = 0.024) negative correlation in those $\geq$ 5 years (right panel). Panel (c) & (d): The secondary functional connectivity entropy showed a significant (r = 0.737, p = 0.023) positive correlation with SSPI score in patients $<$ 5 years (left panel), while the primary functional connectivity entropy displayed a significant (r = -0.642, p = 0.006) negative correlation in those $\geq$ 5 years (right panel).
Linear effects of age, sex and dose have been removed.
This figure is reproduced from Yao et al. [2015].

Table 3.1: Distribution of the primary, secondary and tertiary paths across the 6 Resting State Networks
In the first row, the proportion of all primary, secondary and tertiary paths that involves at least one brain region from the RSN indicated in the column header has been shown. Subsequent rows show the proportion of inter-RSN and intra-RSN links. Data for controls and patients are displayed separately.
This table is modified from Yao et al. [2015].

		Primary/Secondary/Tertiary (Number of inter- and intra-RSN links expressed as a proportion of all primary, secondary or tertiary paths within each group)		
		RSN1 (Percent %)	RSN2 (Percent %)	RSN3 (Percent %)
Total	Controls	26; 22; 13	19; 24; 16	21; 17; 10
	Patients	24; 22; 13	19; 24; 14	20; 17; 12
RSN 1	Controls	7; 4; 1	5; 5; 1	5; 4; 1
	Patients	7; 4; 0	5; 5; 0	5; 4; 1
RSN 2	Controls	5; 5; 1	4; 5; 1	4; 4; 1
	Patients	5; 5; 0	4; 5; 0;	4; 4; 1
RSN 3	Controls	5; 4; 1	4; 4; 1	4; 3; 1
	Patients	5; 4; 1	4; 4; 1	4; 3; 2
RSN 4	Controls	3; 4; 1	3; 4; 1;	3; 3; 1
	Patients	3; 4; 0	3; 4; 0	3; 3; 1
RSN 5	Controls	2; 3; 10	1; 3; 12	3; 2; 6
	Patients	2; 3; 12	2; 3; 12	3; 2; 7
RSN 6	Controls	2; 2; 0	2; 2; 0	2; 1; 0;
	Patients	2; 2; 0	2; 2; 0	2; 2; 0
		RSN4 (Percent %)	RSN5 (Percent %)	RSN6 (Percent %)
Total	Controls	16; 16; 8	11; 13; 51;	10; 9; 1
	Patients	17; 16; 7	11; 13; 52;	10; 9; 2;
RSN 1	Controls	3; 4; 1	2; 3; 10	2; 2; 0
	Patients	3; 4; 0	2; 3; 12	2; 2; 0
RSN 2	Controls	3; 4; 1;	1; 3; 12	2; 2; 0
	Patients	3; 4; 0	2; 3; 12	2; 2; 0
RSN 3	Controls	3; 3; 1	3; 2; 6	2; 1; 0;
	Patients	3; 3; 1	3; 2; 7	2; 2; 0
RSN 4	Controls	6; 1; 0	1; 1; 6	0; 1; 0
	Patients	6; 1; 0	1; 2; 5	0; 2; 0
RSN 5	Controls	1; 1; 6	2; 1; 16	1; 1; 1
	Patients	1; 2; 5	2; 1; 14	1; 1; 1
RSN 6	Controls	0; 1; 0	1; 1; 1	2; 0; 0
	Patients	0; 2; 0	1; 1; 1	3; 0; 0

Chapter 4

Discussion

4.1 Results Summary

Wntropy is used to characterize intrinsic ageing properties of the human brain. Analysis of fMRI data from a large dataset of individuals, using resting state BOLD signals, demonstrated that a functional connectivity entropy associated with brain activity increases with age. During an average lifespan, the entropy, which was calculated from a population of individuals, increased by approximately 0.1 bits, due to correlations in BOLD activity becoming more widely distributed. This is attributed to the number of excitatory neurons and the excitatory conductance decreasing with age. Incorporating these properties into a computational model leads to quantitatively similar results to the fMRI data. The dataset involved males and females and significant differences were found between them. The entropy of males at birth was lower than that of females. However, the entropies of the two sexes increase at different rates, and intersect at approximately 50 years; after this age, males have a larger entropy.

In addition, the connectivity between different brain areas provides evidence about normal function and dysfunction. Changes are described in the distribution of these connectional strengths in schizophrenia using a large sample of resting-state fMRI data. The functional connectivity entropy, which measures the dispersion of the functional connectivity distribution, was lower in patients with schizophrenia than in controls, reflecting a reduction in both strong positive and negative correlations between brain regions. The decrease in the functional connectivity entropy was strongly associated with an increase in the positive, negative, and general symptoms. Using an integrate-and-fire simulation model based on anatomical connectivity, it is shown that a reduction in the efficacy of the NMDA mediated excitatory synaptic

inputs can reduce the functional connectivity entropy to resemble the pattern seen in schizophrenia.

When compared to healthy controls, the whole brain FCE is higher in the early stages of schizophrenia indicating an increase in unpredictability and spatial randomness of functional connectivity, especially in those with more severe illness. A pronounced reduction in whole-brain FCE is seen in the later stages of schizophrenia, indicating that the underlying pathophysiological process may be associated with an indistinct, non-specific mode of brain operation at rest. As hypothesized originally, we note that the most significant changes in the randomness of functional connectivity in schizophrenia occur in indirect paths that do not have a direct axonal linkage. In particular, we note that the variability of connectivity in tertiary paths shows a striking reduction in both early and late stages of schizophrenia, not altered by the severity of symptoms, suggesting that this is an invariant, 'trait-like' feature of the illness.

Section 4.3 and 4.5 have already been published on Yao et al. [2015], while chapter 4.6 has been published on Li et al. [2016].

4.2 Functional Connectivity Entropy in Schizophrenia

The presence of reduced FCE in patients provides important insights into the pathophysiology of schizophrenia. Firstly, this reflects an overall reduction in the occurrence of strong connectivity links (both positive and negative) between brain regions in patients with schizophrenia. The implication is that in schizophrenia, the ability for both synchronization of some brain areas and anti-correlated activations in other brain areas (within the fMRI time scale) are likely to be affected. This resonates with the observations that cerebral recruitment during task performance is inefficient in schizophrenia [Liddle et al., 2002], resulting in widespread but weak engagement of several brain regions. In healthy controls, the strongest positive correlations exist within large-scale networks (RSNs) while the negative correlations (anticorrelations) exist between RSNs. Our findings suggest that the inter-network communications are more significantly affected in schizophrenia. In this context, the changes of functional connectivity we describe could affect the capacity to employ brain networks towards functional roles that simultaneously require engagement of a selected set of brain regions along with the disengagement of the others. we note that the reduced functional connectivity entropy in patients with schizophrenia illustrated in Figure 3.3 reflects a decrease in the strong positive and negative functional connectivity values as illustrated in Figure 3.2, and is consistent with a reduction in the under-

lying synaptic connectivity, without necessarily implying that the dispersion of the underlying synaptic connectivity is changed. This interpretation is supported by the finding that reducing the NMDA synaptic conductance in the model reduced the simulated FCE.

Despite the large number of neurobiological abnormalities noted in schizophrenia, very few relate meaningfully to the everyday symptom burden [Katsnelson, 2010]. The failure to identify biomarkers that relate to the construct of schizophrenia as a whole, has in part contributed to the challenges posed to the validity of schizophrenia as a diagnostic entity. Nevertheless, epidemiological data continue to endorse the above-chance probability of clustering of the classical symptoms of schizophrenia and the stability of this diagnostic construct [Owen et al., 2010]. We find that reduced FCE is correlated with the positive, negative and general psychopathology seen in patients with schizophrenia. This indicates that the reduction in brain connectivity is likely to be a cardinal neural feature that could explain the myriad of seemingly distinct but nevertheless clustered clinical features of this illness.

It was found that in patients with schizophrenia relative to controls, the absolute values of the inter-RSN connectivities were more greatly reduced than the intra-RSN connectivities (Figure 3.5). For the within-RSN functional connectivities, both the default mode and the attention networks showed relatively large decreases in functional connectivity.

Our approach of employing an entropy measure from information theory to study the change in functional connectivity in schizophrenia has provided, for the first time, a novel framework that integrates the large-scale network-level abnormalities in schizophrenia with molecular synaptic models. In combination with other approaches to study neural complexity, we anticipate that the current findings will ultimately aid in offering a core mechanistic explanation as to why a cluster of seemingly unrelated mental states such as hallucinations, anhedonia and cognitive disorders co-occur in certain individuals and lead to marked functional deterioration that characterizes the construct of schizophrenia [Rolls, 2012][Rolls et al., 2008][Rolls and Deco, 2010]. Furthermore, by identifying disturbances in the diversity of brain connectivity as a potential factor associated with the burden of clinical symptoms, it raises the question as to whether treatments that enhance this diversity could provide symptomatic relief to patients.

The dysconnectivity hypothesis of schizophrenia [Friston and Frith, 1995] is that some connections are abnormal between brain regions, without necessarily specifying whether this is an increase or decrease of functional connectivity, with both

being found [Pettersson-Yeo et al., 2011]. The new findings in this thesis show that overall there is a reduced dispersion of the functional connectivity values as measured by functional connectivity entropy, and this reflects overall a reduction in the strength of the positive and negative functional connectivity values. This reduction was shown by the modelling to be consistent with an overall decrease in connectivity such as might be produced by a reduction in NMDA receptor functionality / glutamatergic neurotransmission. An important aspect of this investigation is that the reduction of functional connectivity entropy was related to a wide range of the symptoms of schizophrenia. This is consistent with the hypothesis that reductions of glutamate transmission, including effects of this that may be mediated by reduced drive to GABA neurons, may, when present in different brain regions, provide an account of the different symptoms of schizophrenia [Rolls, 2012][Rolls et al., 2008]. According to this hypothesis, the cognitive symptoms (including reduced short-term memory and attention) may be related to reductions in excitatory transmission in the dorsolateral prefrontal cortex, the negative symptoms (including reduced affect) to decreases in excitatory transmission in the orbitofrontal and anterior cingulate cortex, and the positive symptoms (such as hallucinations and psychotic thoughts) to reduced GABA in the temporal lobes [Rolls, 2012][Rolls et al., 2008].

FCE uniquely captures the uncertainty introduced by bidirectional deviations (both increase and decrease) of connectivity strength occurring in schizophrenia. It provides an intuitive measure of the overall randomness in the distribution of connectivity, irrespective of the mean strength of the functional links, changes in which can be nullified by the bidirectional changes across the brain. Though FCE has not been previously employed a lot in the investigation of schizophrenia, the issue of spatial diversity of functional connections was investigated in two previous studies. Both Lynall et al. [2010] and Bassett et al. [2012] quantified the average of the variance in the pairwise connections within each brain region (column-wise variance across brain regions in the functional connectivity matrix) and reported an increase in the dispersion of functional connectivity in schizophrenia. Unlike variance, entropy is an index of diversification and uncertainty that does not depend on the absolute values of the underlying metric (in this case, functional connectivity), and uses more information about the probability distribution than variance, especially relevant in the presence of fat-tailed distributions [Schwarz and McGonigle, 2011][Skudlarski et al., 2010]. Higher entropy within a system suggests that the whole provides more information than the sum of its parts [Tononi et al., 1994]. Variance does not capture the unpredictability when the values taken by a variable are similar to each other (i.e. narrow distribution range) [Bach and Dolan, 2012]. FCE is a more intuitive index

of uncertainty when a subtle randomization is expected, as in schizophrenia. Our observations suggest that FCE is a relevant measure in this context that is sensitive to both the clinical stage and severity of schizophrenia.

4.3 Inspirations from Different Structural Path Results

FCE is reduced in tertiary paths in both groups, and across all pathways and in the whole brain in those with chronic illness. One exception to the observation of predominant FCE reduction is the increased FCE in secondary paths, which annuls the effect of FCE reduction seen in tertiary links, contributing to a lack of group difference with controls, when whole brain FCE is considered in the early stage illness. One may speculate that the increase in FCE seen in the secondary paths in early stages may reflect a compensatory effort against the process driving a predominant reduction in FCE; the observation that those with more severe illness in early stages show a higher FCE in secondary paths, supports this speculation.

Patients with chronic schizophrenia showed reduced variability in secondary paths, with a trend towards reduced variability in primary paths as well. Both of these changes in the primary (most significant) and secondary paths were more pronounced in those with more severe illness. One may speculate, on this basis, that any compensatory increase in FCE seen in secondary paths at early stages, 'decays' over the course of the illness as the process of FCE reduction now extends to the secondary and primary pathways in those with a more chronic illness. On the basis of this observation, we speculate that in the backdrop of pervasive alteration in tertiary (highly indirect) links, the dynamic pathophysiological process that contributes to clinical severity may progressively 'penetrate' the less indirect (secondary) and more direct (primary) pathways. As this sample is not longitudinal, we are not able to draw any firm conclusions on the progressive nature of these changes. Nevertheless, we can infer a continuum of dysconnectivity on the axis of anatomical connectedness associated with varied clinical severity and persistence of schizophrenia.

Unlike the indirect paths, the primary structural paths showed no significant alteration in the early stages, and only a mild reduction in FCE reaching trend level significance in the chronic illness. If one assumes that the pathophysiology of schizophrenia primarily affects the functional relationship among brain regions, then this observation suggests that the relationship among brain regions that have a direct axonal linkage is less susceptible, at least in the early stages of the illness. In fact, several crucial alterations in functional connectivity relevant to the pathophysiology of schizophrenia have been noted between regions that do not have direct anatom-

ical linkage. To consider an example, consistent functional connectivity between insula and anterior cingulate cortex has been observed using resting state fMRI, constituting a Salience Network [Menon and Uddin, 2010][Seeley et al., 2007][Taylor and Seminowicz DADavis, 2009]. But to date, no consistent direct axonal linkage has been noted between these two regions Cerliani et al. [2012][Cloutman et al., 2012][van den Heuvel et al., 2009]. Several studies have now shown that the abnormalities within this 'indirect' functional network, is a key feature of psychosis [Manoliu et al., 2013][Palaniyappan et al., 2013][Pu et al., 2012][White et al., 2010]. As shown in Section 3.4.2, the largest proportion of tertiary paths involved a network that included the insula. Focused investigation of the anatomical distribution of indirect functional links is warranted in future studies.

Poor spatial coherence between structural and functional connectivity has been previously reported in schizophrenia [Skudlarski et al., 2010], implying functional dysconnectivity involving anatomically unconnected regions. Indirect paths indicate the presence of weaker links in the functional connectivity architecture [Goñi et al., 2014]. While most previous investigations of the connectome used thresholding procedures to discarded weaker links from analysis, the importance of weak links is being increasingly appreciated in recent times [Gallos et al., 2011][Schwarz and McGonigle, 2011]. The integrity of weaker links relate to global cognitive capacity in healthy individuals [Santarnecchi et al., 2014]. Bassett et al. [2012] have also shown that in schizophrenia abnormalities involving the weaker links are likely to be more specific to the illness process and relate to both cognitive abnormalities and symptom severity in schizophrenia. Our results also suggest that while there is a substantial overlap in the anatomical similarity of primary and secondary paths between patients and controls, 24.4% of all identified tertiary paths were present only in one group of subjects, highlighting that the weaker, indirect links are more prone to spatial redistribution, in addition to reduced variability in the strength of connectivity.

Functional connectivity of secondary but not tertiary paths can be attributed to connections mediated by a third region either by directed polysynaptic linkage [Lu et al., 2011] or shared afferents [Adachi et al., 2012]. As tertiary pathways do not share common afferent/efferent links, the observed connectivity in these paths are likely to be related to the emergent properties of the network-level architecture [Adachi et al., 2012][Goñi et al., 2014]. Uncovering the processes beyond physical connections that bring about functional correlation across time to 'bind' a distributed set of brain regions is likely to be a crucial step to understand the pathophysiology of psychosis.

4.4 Limitations

The novelty of this thesis includes the categorization of functional links using DTI-based structural paths, the measurement of an unbiased estimate of unpredictability associated with functional connectivity, and the investigation of the effect of illness stage and severity on the structure-function relationship. Several limitations must be considered when interpreting our observations. To study the effect of illness duration, we used an arbitrary cut-off point of 5 years. From the multitude of neuroimaging studies investigating the effect of illness duration, no single period has emerged as the time of stabilization of brain changes after the onset. Nevertheless, existing evidence suggests that amount of dynamic (supposedly progressive) changes are most pronounced immediately before onset and in the first five years of illness. Moreover, we have done analysis with small changes of the illness duration (4 and 6 years). All the results are still valid with small changes of statistical test values. We studied a medicated sample of patients; antipsychotic treatment alters functional connectivity of brain regions in schizophrenia [Bolding et al., 2012][Stephan et al., 2001]. Given the suspected confound, we adjusted for the current dose of prescribed antipsychotics. we did not have information on cumulative antipsychotic exposure, but unlike volumetric changes that become more pronounced with cumulative exposure, functional dysconnectivity normalizes or returns to baseline levels on using antipsychotics [Abbott, 1999]. As a result, functional dysconnectivity in medicated samples are likely to be an underestimate of the true effect. In the absence of investigations focusing on the effect of antipsychotics on indirect functional links, caution is warranted when interpreting these results. Further, when computing the spatial variability of functional connectivity, we have assumed stationarity of the functional architecture within the time scale of fMRI. The unpredictability introduced by non-stationarity (dynamic 'making and breaking' of functional dependencies) [Messé et al., 2014] is beyond the scope of this work.

4.5 Resting fMRI Preprocessing Discussion

4.5.1 Global Signal Correction

At present, there is no consensus in the field with regard to the removal of global signal when computing functional connectivity related metrics. Global signal removal has been shown to reduce physiological noise from resting fMRI, thus improving its reliability [Fox et al., 2009][Hayasaka, 2013][Yan et al., 2013], though it can increase the frequency of pairwise negative correlation coefficients across the brain [Saad

et al., 2012]. we employed several procedures to ensure that the results are robust to this issue.

The major argument against the removal of global signal is the introduction of spurious negative correlations; this problem occurs especially when the global signal is of high magnitude and is correlated negatively with a large number of voxels. A data-driven solution for this problem was recently proposed by Chen et al. [2012] who advocate a metric called Global Negative Index (the proportion of all voxels in the brain that show negative correlation with the global signal expressed as a percentage). A GNI value of 3 or greater in a dataset indicates that the removal of global signal using regression will induce a number of spurious negative correlations. For values less than 3, the propensity for spurious anticorrelations will be very low and global signal regression will indeed be advantageous in removing the non-neural sources of the signal. Using this approach we determined the GNI for this sample. The mean GNI was 2.79, indicating that global regression would be advantageous in this dataset. Secondly, in line with Murphy et al. [2009], we have refrained from interpreting negative correlation coefficients as representative of anticorrelations. Thirdly, by definition, FCE is a measure that does not depend on the absolute value of the functional connectivity strength. This is illustrated in Figure 4.1, on the data obtained from a single random subject. As shown here, while the mean of functional connectivity shifts towards zero upon the removal of global signal, the probability density function shows no change. So, irrespective of whether global signal is retained or removed, FCE values remain the same.

4.5.2 Head Movement Correction

In addition to the precautions taken during image acquisition, several other measures were employed to control for movement-induced artefacts. Firstly, motion parameters in three planes were assessed for each participant, and participants with >3 mm or 3^o movement were excluded from the analysis. Secondly, displaced frames (defined as frames with summed displacement across all six rigid body motion parameters exceeding 0.5mm or root-mean-square of volume signal intensity difference that exceeded ± 3 standard deviation of the average across all scans), along with 1 preceding 2 succeeding frames were replaced using a nearest (unaffected) neighbour interpolation method using ArtRepair software (`http://cibsr.stanford.edu/tools/human-brain-project/artrepair-software.html`). Thirdly, to remove the variance in functional connectivity spuriously introduced by head motion, we used the head motion parameters as nuisance covariates when extracting the timeseries of BOLD signals. Fourthly, we compared the overall framewise displacement levels

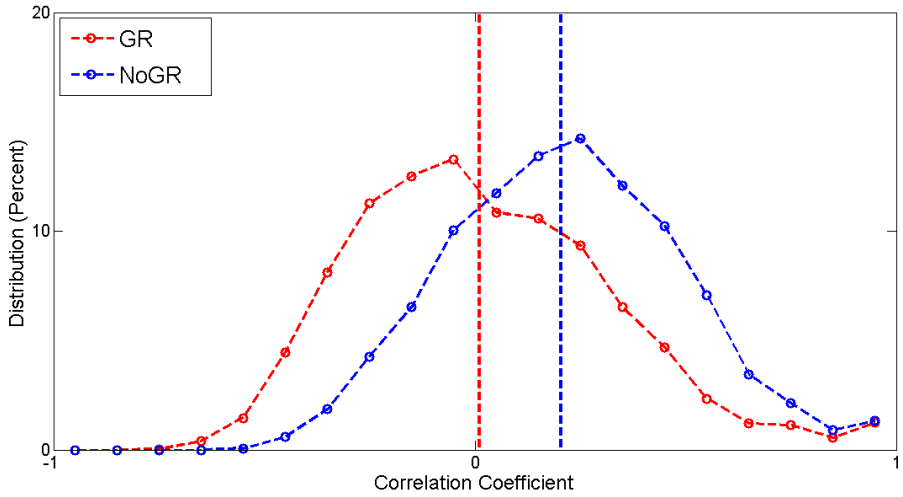

Figure 4.1: Effect of global signal on Functional Connectivity Entropy
Correlation coefficient distribution for one subject with global signal regression (GR) and without global signal regression (NoGR).

between the two groups to detect the possibility of systematic differences in head motion. Finally, we correlated the proportion of displaced frames in each subject with whole brain FCE in each group separately to study the influence of head motion on the group differences in FCE.

No significant difference was noted in the total proportion of frames with displacement (proportion of frames (SD) displaced >0.5mm in controls = 1.2%(0.6%); patients = 6.8%(2%); p=0.13) and for the mean displacement across the 3 translation and 3 rotation axes, quantified in accordance with Power et al. [2012] (framewise displacement (SD) in controls = 0.061 (0.29); patients = 0.077(0.54); p=0.14). No significant correlation was noted between mean framewise displacement and FCE of whole brain (r=0.12, p=0.51), primary (r=0.20, p=0.26) secondary (r=0.07, p=0.68) or tertiary (r=0.13, p=0.46) paths in patients.

4.5.3 Streamline Threshold Effects

In the primary analysis, we used a minimum threshold of one streamline connecting 2 regions to define a structural path. While the streamline count is often used as a proxy measure of connection in DTI studies, the neurobiological substrate of DTI-based streamlines is unclear. White matter bundles with low FA may have fewer streamlines than those in the regions with higher FA, despite being equally well

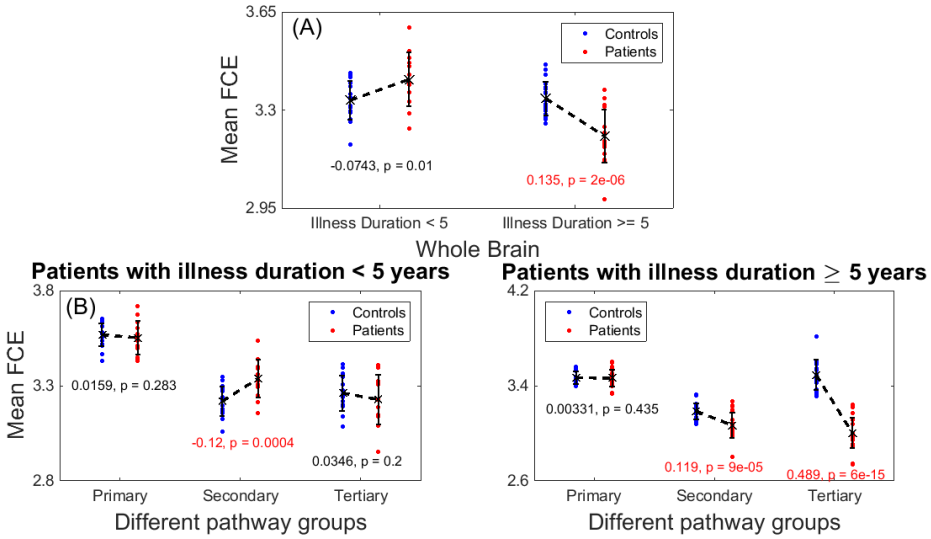

Figure 4.2: Results of using streamline threshold=2
This figure is reproduced from Yao et al. [2015].

connected. Nevertheless, it is possible that a low minimum threshold might have introduced some spurious paths.

We tested the effect of varying the streamline threshold by repeating the primary analysis with a threshold of 2 and a threshold of 3. we found that there were no major changes in the pattern of FCE distribution across the two groups for the different pathways; though the values of statistical significance were altered to some extent, the direction of the results was preserved. These are shown in Figure 4.2 and 4.3, in line with the Figure 3.10 in Results.

It should be emphasized that the use of minimum thresholds is crucial to identify tertiary paths. When a threshold of 10 or more streamlines is used, there would be very few or no tertiary paths that could be identified in the brain. Furthermore, the use of one streamline as a threshold is in line with several DTI-based graph theory applications that generate connection matrices binarised on the basis of having at least one streamline connection between 2 regions [Batalle et al., 2012][Tymofiyeva et al., 2013][van den Heuvel and Sporns, 2011].

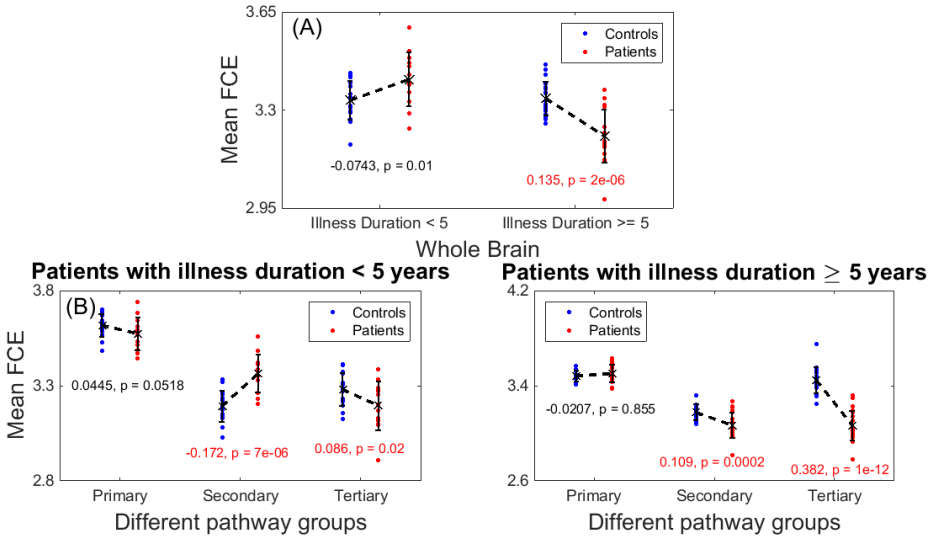

Figure 4.3: Results of using streamline threshold=3
This figure is reproduced from Yao et al. [2015].

4.6 Functional Connectivity Entropy in Cognitive Training (Further Applications)

In this thesis, we used functional connectivity entropy to do some analysis on schizophrenia. Actually, there are a list of further applications. For example, the entropy idea could be applied in the cognitive training project described below.

4.6.1 Summary

Background: The neural mechanisms underlying the restorative effects of cognitive training on aging brains remain unclear. To address this issue, we examined the relationship between changes in spontaneous brain activity and cognitive performance that occur after cognitive training.

Methods: Participants were older adults who were part of a randomized control trial within a larger longitudinal cognitive training study. Doctors conducted single-domain and multi-domain cognitive training in two respective intervention groups. Participants trained for one hour, twice a week, for 12 weeks. Cognition was assessed in all participants and magnetic resonance images were obtained at baseline and one year after training. To assess spontaneous fluctuations in brain activity, resting-state fMRI data was acquired. Functional connectivity entropy was used to measure

the effects of training. Functional connectivity entropy increases with aging, and indicates disruptions in functional connectivity.

Results: Seventy participants completed the study: 26 in the multi-domain cognitive training group (mean age: 70.38 yrs), 27 in single-domain group (mean age: 70.48 yrs), and 17 in a control group (mean age: 68.59 yrs). Functional connectivity entropy increased significantly less in the multi-domain ($p = 0.047$) and single-domain groups ($p = 0.51 \times 10^{-4}$) compared with the control group.

Conclusions: Cognitive training can induce plastic changes in neural functional connectivity of healthy older people, and these changes may underlie the positive effect of cognitive training.

4.6.2 Introduction

Normal aging of the brain is associated with memory loss and cognitive impairments. These can interfere with daily routines [Hedden and Gabrieli, 2004] and affect the capacity of the elderly to live independently. In addition, cognitive impairment is associated with a higher mortality risk [van Gelder et al., 2007]. Clarifying the mechanisms of cognitive aging and dementia may ultimately prevent the aging crisis [Voss et al., 2010]. In the past few decades, some preventative studies in this field have been carried out, such as cognitive training and physical exercise [Geda and Roberts, 2012][Lautenschlager et al., 2008]. The effectiveness of cognitive training has been verified by randomized controlled trials [Sylvie et al., 2011][Mahncke et al., 2006][Willis and Schaie, 2009][Wolinsky et al., 2007][Yan et al., 2012][Anguera, 2013]. However, the possible neural mechanisms underlying restorative effects of cognitive trainings on aging individuals remain unclear and are the subject of debate [Owen et al., 2010][Katsnelson, 2010]. The essential difficulty, as pointed out in Owen et al. [2010] work, lies in the difficulty in finding any evidence of the transfer of the effects of cognitive trainings to untrained tasks. One promising way to fully assess the impact of cognitive trainings on aging individuals and explore its mechanisms, which is now possible, is by studying cortical changes or neural plasticity via neuroimaging techniques [Willis and Schaie, 2009][Sylvie et al., 2011]. Such studies provide an objective and quantitative way of analysing cognitive trainings.

Intrinsic brain activity that is coherent is an important feature of healthy brain functioning. This is manifested, in resting-state functional magnetic resonance imaging (fMRI), as temporal correlations of blood oxygenation level dependent signals (BOLD) [Fox and Raichle, 2007]. There is increasing evidence that temporal fluctuations in resting state fMRI, in particular, in low frequency components (<0.1Hz), arise primarily from spontaneous fluctuations of the brains metabolism

and intrinsic neuronal activity [Fox and Raichle, 2007][Yan et al., 2009]. Increasingly, researchers agree that spontaneous neuronal activity plays a fundamental role in brain function, and maintains the brains integrity and capacity to deal effectively with future demands [Pizoli et al., 2011][Uddin et al., 2010].

To assess the effects of cognitive trainings, we have employed functional connectivity entropy. The functional connectivity of fMRI data is used to characterize the temporal coherence of the activity of distant brain areas, either during task performance or in the resting state Bullmore and Sporns [2009]. For the present party, we focused on resting-state functional connectivity. The notion of functional connectivity entropy, which has been recently introduced and found to increase with age in a population of healthy individuals [Yao et al., 2014], was employed to the cognitive training data of the present work. Interestingly, both single and multiple domain training reduced the rate at which the functional connectivity entropy increased in the control group.

Taken together, the results indicate that cognitive training could induce plasticity of the intrinsic activity in the elderly, mainly through modifications of the resting-state functional connectivity and brain structure. These are thus likely to be some of the neural mechanisms underlying the effects of cognitive training.

4.6.3 Methods

The study was approved by the Human Research Ethics Board of Tongji Hospital in Shanghai, China. Informed consent was obtained from all participants before the experiment (LL(H)-09-04).

Participants

All participants were healthy elderly adults, with normal functional capacity, that were living independently in the community. The participants were recruited from three community centers around Tongji Hospital in Shanghai through a dispatched notice/broadcasting by the local institute of community service from March 2008 to April 2008. Eligibility criteria included: 65 *leq* age *leq* 75 years; educational level *geq* 1 year; absence of significant hearing, vision, or communication difficulties; absence of severe physical diseases or psychotic disorders; no obvious evidence of cognitive decline (on the Chinese version of the Mini-Mental State Examination, this required a score of 19 or above [Li et al., 2006]. Exclusion criteria included: obvious cognitive decline such as AD; history or clinical evidence of neurological diseases or psychiatric disorders such as brain cancer, major depressive disorders,

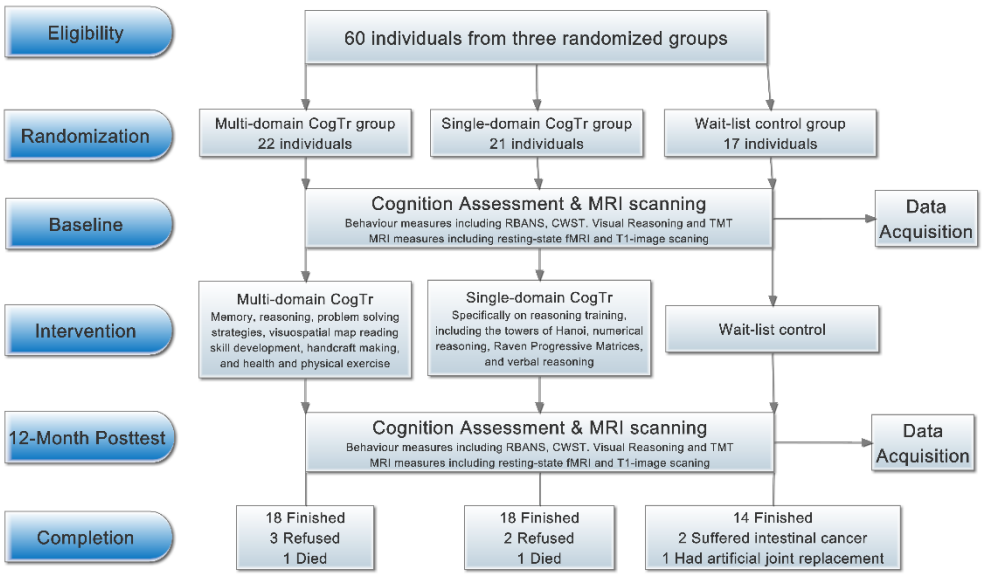

Figure 4.4: Flowchart in the trials
'Refused' due to lack of interest in continuing, repeatedly missed appointments, scheduling conflicts. 'Died' includes cancer, stroke, cardiac sudden death.
This figure is reproduced from Li et al. [2016].

and schizophrenia. Because the training-related changes predicted in this part have no relation with handedness [M. et al., 2013], both right and left-handed participants were enrolled. In the multi-domain training group, one participant, out of a total of 22, was left-handed, and in the single-domain training group, two participants were left-handed, out of a total of 21.

Study design

In this part, we used controlled design to test the effect of cognitive trainings on spontaneous brain activity and cognitive capacity. All subjects were selected from three randomized groups [Yan et al., 2012]. The schematic diagram of study design and the flowchart of trials are illustrated in Figure 4.4.

Interventions

The three groups included one control group, and two intervention groups. Either single-domain or multi-domain cognitive trainings were conducted on the two intervention groups. Participants undertook 12 weeks of training, twice a week, for 24 sessions (each session was 60 minutes). The multi-domain cognitive trainings in-

cluded aspects of: memory, reasoning, problem-solving, visual-spatial map-reading skills, handcraft, health and physical exercise. The single-domain cognitive trainings focused specifically on reasoning training, including the 'towers of Hanoi', numerical reasoning, Raven Progressive Matrices, and verbal reasoning. The non-training control group was used as a match for the social contact associated with cognitive trainings. All participants were given a lecture about healthy living every two months (more details in the previous study [Yan et al., 2012].

MRI acquisition

All people underwent functional scanning using a Siemens Trio 3T scanner at East China Normal University, Shanghai, China. Foam padding was used to minimize head motion for all subjects. Functional images were acquired using a single-shot, gradient-recalled echo planar imaging sequence (repetition time = 2000 ms, echo time = 25 ms and flip angle = 90 degrees). Thirty-two transverse slices (field of view = 240 $\times$ 240 mm^2, in-plane matrix = 64 $\times$ 64, slice thickness = 5 mm, voxel size = 3.75 $\times$ 3.75 $\times$ 5 mm^3), aligned along the anterior commissureCposterior commissure line were acquired. For each subject, a total of 155 volumes were acquired, resulting in a total scan time of 310s. Subjects were instructed simply to rest with their eyes closed, not to think of anything in particular, and not to fall asleep. Subsequently, high-resolution T1-weighted anatomical images were acquired in the sagittal orientation using a magnetization-prepared rapid gradient-echo sequence (repetition time = 1900 ms, echo time = 3.43 ms, flip angle = 9, field of view = 256 $\times$ 256 mm^2, matrix size = 256 $\times$ 256, slice thickness = 1 mm, voxel size = 0.9375 $\times$ 0.9375 $\times$ 1 mm^3 and 160 slices) on each subject.

Cognitive testing

All participants were, initially, given a cognitive capacity assessment, and this was taken as the baseline for any changes. One year after intervention another cognitive capacity assessment was made. The assessment included the Repeatable Battery for the Assessment of Neuropsychological Status [Randolph et al., 1998] (RBANS, Form A) which has good reliability and validity in a sample of elderly Chinese individuals that live in the community [Cheng et al., 2011], the Color Word Stroop test (CWST) [van Boxtel et al., 2001], the visual reasoning test [Xiao et al., 2002] and the trail making test (TMT) [Ashendorf et al., 2008].

Data Preprocessing

The first 10 volumes of these datasets were discarded, to allow for scanner stabilization and the subjects' adaptation to the environment. fMRI data preprocessing was then conducted by Statistical Parametric Mapping [Frackowiak et al., 2003] (SPM8) and a Data Processing Assistant for Resting-State fMRI [Yan and Zang, 2010] (DPARSF). The remaining functional scans were first corrected for within-scan acquisition time differences, between slices, and then realigned to the middle volume, to correct for inter-scan head motions. Subsequently, the functional scans were spatially normalized to a standard template [Fonov et al., 2011] (Montreal Neurological Institute) and resampled to $3 \times 3 \times 3$ mm^3. Data was then smoothed, and after normalization and smoothing, BOLD signals of each voxel were firstly detrended, to remove any linear trend, and then passed through a band-pass filter (0.01-0.08 Hz) to reduce low-frequency drift and high-frequency physiological noise. Finally, nuisance covariates including head motions, global mean signals, white matter signals and cerebrospinal signals were regressed out from the BOLD signals. After data preprocessing, the time series were extracted in each ROI by averaging the signals of all voxels within that region and then linearly regressing out the influence of head motion and global signals. In this thesis, the automated anatomical labeling atlas Tzourio-Mazoyer et al. [2002] (AAL) was used to parcellate the brain into 90 regions of interest (ROIs) (45 per hemisphere). The names of the ROIs and their corresponding abbreviations are listed in Table 2.2.

4.6.4 Results

Demographic information

There were 60 individuals who initially took part in fMRI scanning: 22 from the multi-domain training group, 21 from the single-domain training group, and 17 from the control group. One year after the intervention, 50 individuals finished the cognitive assessments and fMRI scanning while 10 individuals withdrew, including 2 participants, who suffered intestinal cancer, 1 participant requiring artificial joint replacement and 2 participants who died during the research period. A total of 5 participants rejected the scanning one year after the intervention. The flowchart of trials through the entire data collection is illustrated in Figure 4.4. The intervention groups were comparable with the control group with regard to age, gender and education composition at each assessment. Characteristics of subjects are summarized in Table 4.1.

Table 4.1: Characteristics of the trials
A Chi-squared test was used to test gender differences, while the F test was used to test age and education differences. No significant age, gender and education differences were found in the multi-domain cognitive trainings, single-domain cognitive trainings and control groups.
This table is modified from Li et al. [2016].

	Multi-domain cognitive trainings (n = 18)	Single-domain cognitive trainings (n =18)	Control group (n = 14)	χ^2/F	P value
Age (x(_) ± SD)	72.28 ± 3.46	71.61 ± 3.97	70.93 ± 3.63	0.527	0.594
Education (x(_) ± SD)	11.67 ± 3.20	9.39 ± 4.22	10.71 ± 3.34	1.78	0.180
Gender (male:female)	13:5	8:10	9:5	3.042	0.218

Cognitive capacity

The RBANS test score was found to be significantly improved (t = 2.75, p = 0.007) in the multi-domain cognitive training group. However, the single-domain cognitive training group showed no significant changes in the RBANS. In addition, the RBANS test score was improved especially in language (t = 2.13, p = 0.024), attention (t = 1.95, p = 0.034) and delayed memory (t = 2.74, p = 0.007) in the Multi-domain cognitive training. Moreover, the CWST and TMT scores showed no significant improvements in both groups. Lastly, the visual reasoning test score was not significantly improved, but the result was close to significance (t = 1.61, p = 0.063) in the multi-domain training group. By contrast, the single-domain training group exhibited a significant improvement (t = 2.32, p = 0.017).

Spontaneous brain activity

The mean rate of increase of the functional connectivity entropy was significantly reduced in both the multi-domain cognitive trainings (t = 1.77, p = 0.047) and the single-domain cognitive training group (t = 3.67, p = 9.51×10^{-4}), as shown in Figure 4.5.

4.6.5 Discussion

In the Results, we analyzed changes of the entropy of functional connectivity from resting-state fMRI. The trend of the functional connectivity entropy to increase, as observed in healthy individuals, was significantly reduced in both cognitively trained groups, as shown in Figure 4.5.

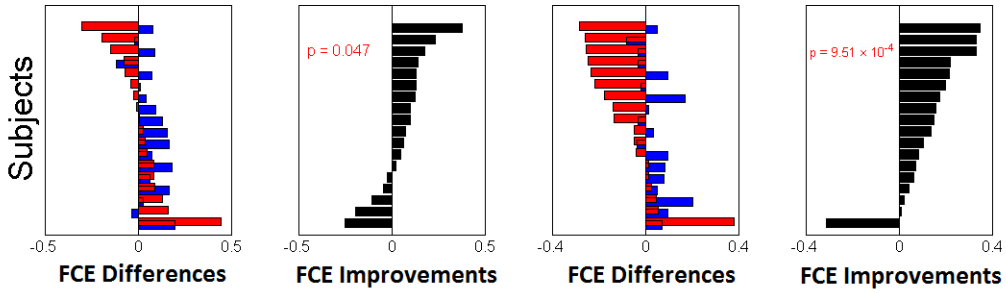

Figure 4.5: Entropy change rate in cognitive training groups
The entropy differences (black bars) between the predictions (blue bars) and actual values (red bars) indicated the cognitive training effect on the entropy measures. The functional connectivity entropy increase rate was significantly reduced in both the multi-domain cognitive trainings ($t = 1.77$, $p = 0.047$) and the single-domain Cognitive training groups ($t = 3.67$, $p = 9.51 \times 10^{-4}$).
Subjects are ranked according to the entropy values.
This figure is reproduced from Li et al. [2016].

The results confirm that cognitive training is transferable, thereby answering a long-term debate in the area. Combining the analysis of the cognition data, it could be concluded that both types of cognitive trainings could improve cognitive capacity in elderly individuals, but the multi-domain cognitive trainings has more advantages in the cognitive domains it affects.

Note that Owen et al. [2010] obtained negative results for the transferability of cognitive trainings, while positive results found here. This may be related to the longer training time in this section, where subjects were cognitively trained for a total of 24 hours, over 6 weeks, in contrast to the total training time of 4 hours in Owen et al. [2010] study. The present results are compatible with results in the area of mental disorder, where schizophrenic patients have benefited from extended periods of cognitive training (more than 50 hours).

It should be emphasized that the results are mainly based on an informational concept, namely functional connectivity entropy. To have a direct comparison with more conventional approaches, we have analyzed the change of the functional connectivity of the 4005 links in the different groups. we found that in the multi-domain training group, there is one link which can survive the Bonferroni correction ($p = 7.2 \times 10^{-6} < 0.05 \ / \ 4005$) as shown in Figure 4.6. This implied the link was significantly improved with Multi-domain training.

The results also suggest that the target of cognitive trainings should be the

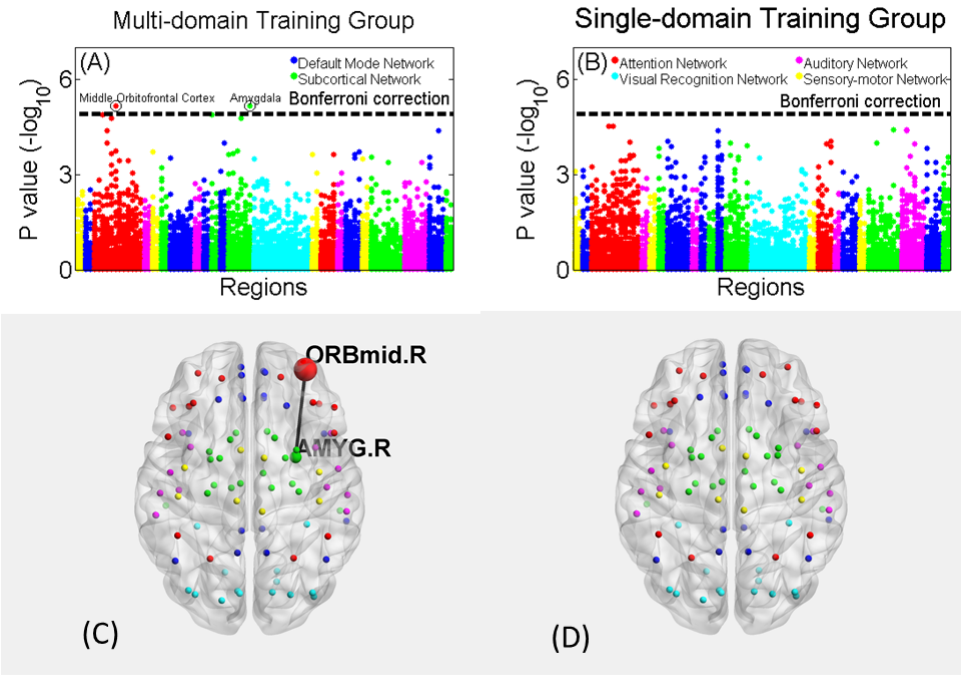

Figure 4.6: Functional Connectivity Change in training groups
Panels (A) & (C) In the Multi-domain training group, the p value of the link from Amygdala (Right hemisphere) to Middle Orbitofrontal Cortex (Right hemisphere) can pass the Bonferroni correction ($p = 7.2 \times 10^{-6} < 0.05 / 4005$).
Panels (B) & (D) In the single-domain training group, there are no links whose p value can pass the Bonferroni correction.
This figure is reproduced from Li et al. [2016].

dysfunction of cortical circuits which have been assumed to play a role in cognitive aging [Decarli et al., 2012][Andrewshanna et al., 2007]. The logic is given below. Extensive experimental data indicates that there is significant loss of neuron number with age, and this is accompanied by the excitatory receptor number (especially NMDA) decreasing with age [Morrison and Hof, 1997].

To summarise, cognitive trainings could induce the plasticity of intrinsic activity patterns in the elderly, mainly by modifying the resting state functional connectivity, which is thus likely to be one of the neural mechanisms underlying the cognitive trainings effect. Multi-domain cognitive trainings demonstrated more advantages than single-domain cognitive trainings, perhaps because multi-domain cognitive trainings involves more regions relative to cognition. Larger sample sizes are urgently needed to test the cognitive training-induced changes of brain activity, cognition capacity and their relationship.

Chapter 5

Conclusions

To conclude, we used entropy to characterize intrinsic ageing properties of the human brain. Analysis of fMRI data from a large dataset of individuals, using resting state BOLD signals, demonstrated that a functional connectivity entropy associated with brain activity increases with age. During an average lifespan, the entropy, which was calculated from a population of individuals, increased by approximately 0.1 bits, due to correlations in BOLD activity becoming more widely distributed. In addition, the connectivity between different brain areas provides evidence about normal function and dysfunction. Changes are described in the distribution of these connectional strengths in schizophrenia using a large sample of resting-state fMRI data. The functional connectivity entropy, which measures the dispersion of the functional connectivity distribution, was lower in patients with schizophrenia than in controls, reflecting a reduction in both strong positive and negative correlations between brain regions. The brain BOLD signals could be simulated by a computational model. After brain functional connectivity network construction, the increase FCE with age and decrease FCE in schizophrenia could be simulated.

In a healthy brain, the resting connectional architecture (system as a whole) accommodates a higher degree of variability in functional connections (constituent parts), but in established schizophrenia the variability of constituents that make up this system is limited, especially when considering those with an established illness. Our findings address a critical gap in the literature linking structure and function in schizophrenia, and demonstrate for the first time that the abnormal state of functional connectivity preferentially affects structurally unconstrained links in schizophrenia. It also raises the question of a continuum of dysconnectivity ranging from less direct (structurally unconstrained) to more direct (structurally constrained) brain pathways underlying the clinical severity of schizophrenia.

Lastly, functional connectivity entropy idea have a lot of possible future avenues of work. As shown in Section 4.6, we used FCE idea to show that cognitive training can induce plastic changes in neural functional connectivity of healthy older people, and these changes may underlie the positive effect of cognitive training. We will apply FCE more in mental health area. Moreover, in the near future, we will also try to do FCE analysis in neurological and neurosurgical diseases.

The key story of this thesis has already been published on Yao et al. [2015].

Appendix A

Appendix Figures

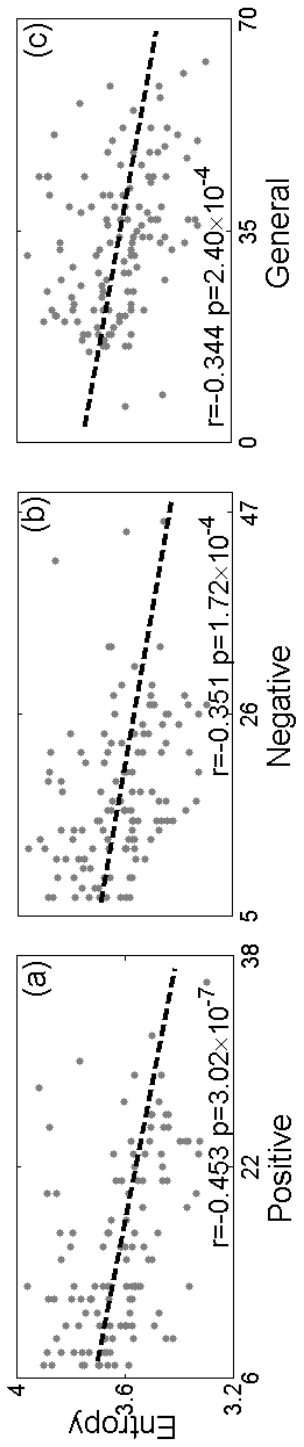

Figure A.1: Enlarged Version of Figure 3.9

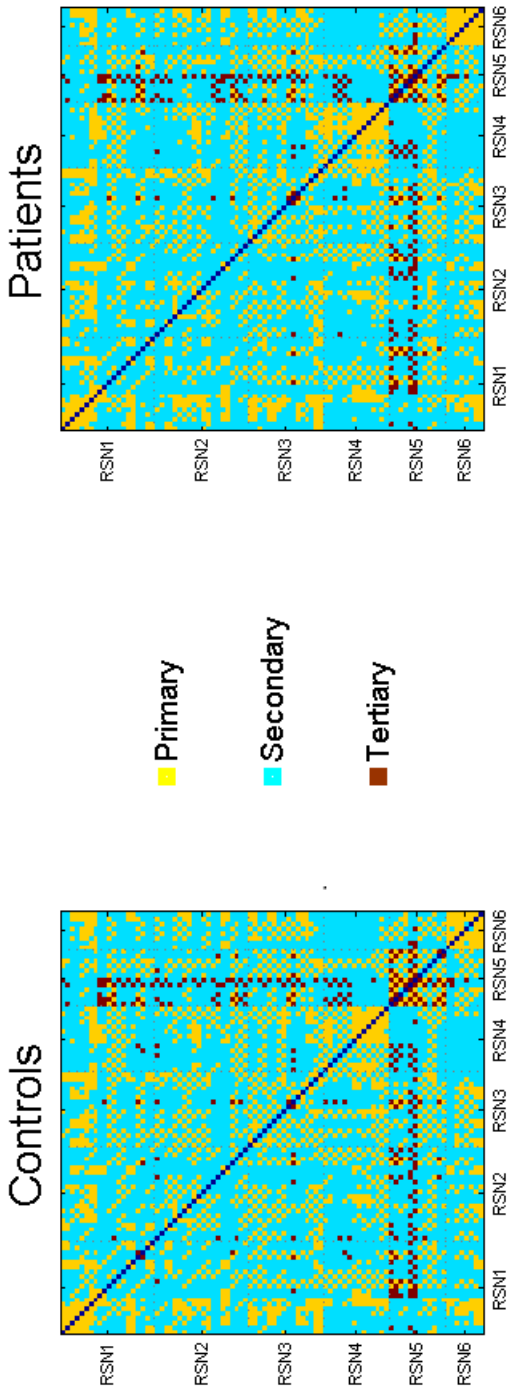

Figure A.2: Enlarged Version of Figure 3.5

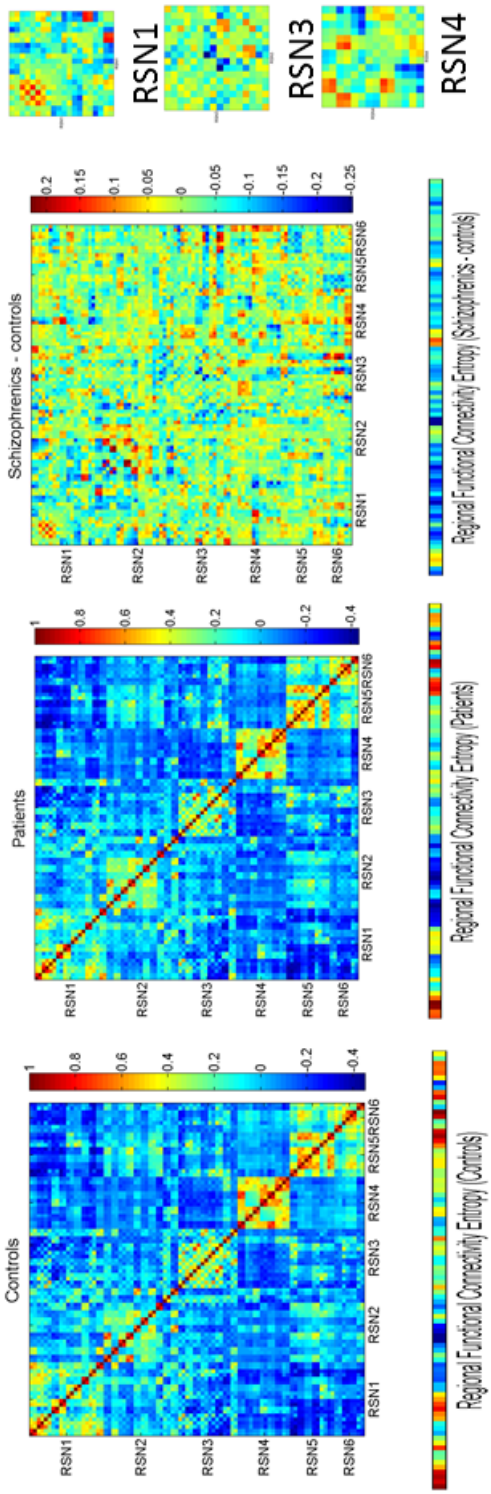

Figure A.3: Enlarged Version of Figure 3.5

Appendix B

Appendix Code

B.1 Matlab Code of Functional Connectivity Entropy

```
% Entropy of the whole brain
function [Entropy_value]=Brain_Entropy(CorrMat)
% Input is the correlation matrix of the resting state BOLD
    signal.
% Output is the entropy value.
IntervalNumber=20;% Interval number in [-1,1]

% Extract the upper triangular matrix of CorrMat
CorrMatSize=size(CorrMat);
CorrMatLength=CorrMatSize(1);
CorrList=zeros(1,CorrMatLength*(CorrMatLength-1)/2);%
    Correlation list
k=0;
i=1;
while i<=CorrMatLength
     j=i+1;
     while j<=CorrMatLength
          k=k+1;
          CorrList(1,k)=CorrMat(i,j);
          j=j+1;
     end
     i=i+1;
end
```

```
% Entropy calculation
EntropyList=zeros(IntervalNumber,1);
i=1;
while i<=IntervalNumber
    TempPosi1=find((CorrList>-1+2/IntervalNumber*(i-1))& (
        CorrList<=-1+2/IntervalNumber*i));
    EntropyList(i,1)=length(TempPosi1);
    i=i+1;
end
EntropyList=EntropyList./sum(EntropyList);
TempPosi2=find(EntropyList~=0);
Entropy_value=-sum(EntropyList(TempPosi2).*log(EntropyList(
    TempPosi2)))/log(2);
```

Bibliography

L. F. Abbott. Lapicque's introduction of the integrate-and-fire model neuron (1907). *Brain Research Bulletin*, 50(5):303–304, 1999.

Y. Adachi, T. Osada, O. Sporns, T. Watanabe, T. Matsui, K. Miyamoto, and Y. Miyashita. Functional connectivity between anatomically unconnected areas is shaped by collective network-level effects in the macaque cortex. *Cerebral Cortex*, 22(7):1586–1592, 2012.

A. F. Alexander-Bloch, N. Gogtay, D. Meunier, R. Birn, L. Clasen, F. Lalonde, R. Lenroot, J. Giedd, and E. T. Bullmore. Disrupted modularity and local connectivity of brain functional networks in childhood-onset schizophrenia. *Frontiers in Systems Neuroscience*, 4:147, 2010.

N. C. Andreasen, G. E. Berrios, B. Bogerts, H. D. Brenner, W. T. Carpenter, T. J. Crow, A. Deister, C. Eggers, H. Häfner, A. Klimke, et al. *Negative versus positive schizophrenia*. Springer Science & Business Media, 2012.

J. R. Andrewshanna, A. Z. Snyder, J. L. Vincent, C. Lustig, D. Head, M. E. Raichle, and R. L. Buckner. Disruption of large-scale brain systems in advanced aging. *Neuron*, 56(5):924–35, 2007.

J.; Rintoul J. L.; Al-Hashimi O.; Faraji F.; Janowich J.; Kong E.; Larraburo Y.; Rolle C.; Johnston E.; Gazzaley A. Anguera, J. A.; Boccanfuso. Video game training enhances cognitive control in older adults. *Nature*, 501(7465):97, 2013.

A. Anticevic, M. W. Cole, G. Repovs, A. Savic, N. R. Driesen, G. Yang, Y. T. Cho, J. D. Murray, D. C. Glahn, and X. J. Wang. Connectivity, pharmacology, and computation: toward a mechanistic understanding of neural system dysfunction in schizophrenia. *Frontiers in Psychiatry*, 4:169, 2013.

M. Argyelan, T. Ikuta, P. DeRosse, R. J. Braga, K. E. Burdick, M. John, P. B. Kingsley, A. K. Malhotra, and P. R. Szeszko. Resting-state fmri connectivity

impairment in schizophrenia and bipolar disorder. *Schizophrenia Bulletin*, 40(1): 100, 2014.

L. Ashendorf, A. L. Jefferson, M. K. O'Connor, C. Chaisson, R. C. Green, and R. A. Stern. Trail making test errors in normal aging, mild cognitive impairment, and dementia. *Archives of Clinical Neuropsychology*, 23(2):129–137, 2008.

D. R. Bach and R. J. Dolan. Knowing how much you don't know: a neural organization of uncertainty estimates. *Nature Reviews Neuroscience*, 13(8):572–586, 2012.

P. J. Basser, S. Pajevic, C. Pierpaoli, J. Duda, and A. Aldroubi. In vivo fiber tractography using dt-mri data. *Magnetic Resonance in Medicine*, 44(4):625–632, 2000.

D. S. Bassett, B. G. Nelson, B. A. Mueller, J. Camchong, and K. O. Lim. Altered resting state complexity in schizophrenia. *Neuroimage*, 59(3):2196–2207, 2012.

D. S. Bassett, M. A. Porter, N. F. Wymbs, S. T. Grafton, J. M. Carlson, and P. J. Mucha. Robust detection of dynamic community structure in networks. *Chaos: An Interdisciplinary Journal of Nonlinear Science*, 23(1):013142, 2013.

D. Batalle, E. Eixarch, F. Figueras, E. Muñoz-Moreno, N. Bargallo, M. Illa, R. Acosta-Rojas, I. Amat-Roldan, and E. Gratacos. Altered small-world topology of structural brain networks in infants with intrauterine growth restriction and its association with later neurodevelopmental outcome. *Neuroimage*, 60(2): 1352–1366, 2012.

D. J. Bates, R. Liang, N. Li, and E. Wang. The impact of noncoding rna on the biochemical and molecular mechanisms of aging. *Biochimica et Biophysica Acta (BBA)-General Subjects*, 1790(10):970–979, 2009.

B. B. Biswal. Resting state fmri: a personal history. *Neuroimage*, 62(2):938–944, 2012.

B. B. Biswal, J. V. Kylen, and J. S. Hyde. Simultaneous assessment of flow and bold signals in resting-state functional connectivity maps. *NMR in Biomedicine*, 10(45):165–170, 1997.

R. L. Bluhm, J. Miller, R. A. Lanius, E. A. Osuch, K. Boksman, R. W. J. Neufeld, J. Théberge, B. Schaefer, and P. Williamson. Spontaneous low-frequency fluctuations in the bold signal in schizophrenic patients: anomalies in the default network. *Schizophrenia Bulletin*, 33(4):1004–1012, 2007.

M. S. Bolding, D. M. White, J. A. Hadley, M. Weiler, H. H. Holcomb, A. C. Lahti, et al. Antipsychotic drugs alter functional connectivity between the medial frontal cortex, hippocampus, and nucleus accumbens as measured by h215o pet. *Front Psychiatry*, 3:105, 2012.

R. W. Brown, Y. N. Cheng, E. M. Haacke, M. R. Thompson, and R. Venkatesan. *Magnetic resonance imaging: physical principles and sequence design*. John Wiley & Sons, 2014.

E. Bullmore and O. Sporns. Complex brain networks: graph theoretical analysis of structural and functional systems. *Nature Reviews Neuroscience*, 10(3):186–198, 2009.

L. Cerliani, R. M. Thomas, S. Jbabdi, J. C. W. Siero, L. Nanetti, A. Crippa, V. Gazzola, H. D'Arceuil, and C. Keysers. Probabilistic tractography recovers a rostrocaudal trajectory of connectivity variability in the human insular cortex. *Human Brain Mapping*, 33(9):2005C2034, 2012.

G. Chen, G. Y. Chen, C. M. Xie, B. D. Ward, W. J. Li, P. Antuono, and S. J. Li. A method to determine the necessity for global signal regression in resting-state fmri studies. *Magnetic Resonance in Medicine*, 68(6):1828–1835, 2012.

Y. Cheng, W. Wu, J. Wang, W. Feng, X. Wu, and C. Li. Reliability and validity of the repeatable battery for the assessment of neuropsychological status in community-dwelling elderly. *Archives of Medical Science Ams*, 7(5):850–7, 2011.

S. A. Chong, G. J. Remington, and K. Z. Bezchlibnyk-Butler. Effect of clozapine on polypharmacy. *Psychiatric Services*, 2000.

K. Christensen, T. E. Johnson, and J. W. Vaupel. The quest for genetic determinants of human longevity: challenges and insights. *Nature Reviews Genetics*, 7(6):436–448, 2006.

L. L. Cloutman, R. J. Binney, M Drakesmith, G. J. Parker, and M. A. Lambon Ralph. The variation of function across the human insula mirrors its patterns of structural connectivity: evidence from in vivo probabilistic tractography. *Neuroimage*, 59(59):3514–3521, 2012.

H. Clow and I. R. Young. Britain's brains produce first nmr scans. *New Scientist*, 80(588):b26, 1978.

J. Cohen. Statistical power analysis. *Current Directions in Psychological Science*, 1 (3):98–101, 1992.

G. Collin, R. S. Kahn, M. A. de Reus, W. Cahn, and M. P. van den Heuvel. Impaired rich club connectivity in unaffected siblings of schizophrenia patients. *Schizophrenia Bulletin*, 40(2):438–448, 2014.

Joint Formulary Committee and Royal Pharmaceutical Society of Great Britain. *British national formulary*. Pharmaceutical Press, 2012.

J. T. Coyle. Glutamate and schizophrenia: beyond the dopamine hypothesis. *Cellular and Molecular Neurobiology*, 26(4-6):363–382, 2006.

N. Crumlish, P. Whitty, M. Clarke, S. Browne, M. Kamali, M. Gervin, O. McTigue, A. Kinsella, J. L. Waddington, C. Larkin, et al. Beyond the critical period: longitudinal study of 8-year outcome in first-episode non-affective psychosis. *The British Journal of Psychiatry*, 194(1):18–24, 2009.

Z. Cui, S. Zhong, P. Xu, Y. He, and G. Gong. Panda: a pipeline toolbox for analyzing brain diffusion images. *Frontiers in Human Neuroscience*, 7:42, 2013.

J. S. Damoiseaux and M. D. Greicius. Greater than the sum of its parts: a review of studies combining structural connectivity and resting-state functional connectivity. *Brain Structure and Function*, 213(6):525–533, 2009.

C. Decarli, C. Kawas, J. H. Morrison, P. A. Reuterlorenz, R. A. Sperling, and C. B. Wright. Session ii: Mechanisms of age-related cognitive change and targets for intervention: Neural circuits, networks, and plasticity. *Astrophysical Journal*, 311 (7):930–936, 2012.

G. Deco and V. K. Jirsa. Ongoing cortical activity at rest: criticality, multistability, and ghost attractors. *The Journal of Neuroscience*, 32(10):3366–3375, 2012.

V. Dousset, C. Delalande, L. Ballarino, B. Quesson, D. Seilhan, M. Coussemacq, E. Thiaudiére, B. Brochet, P. Canioni, and J. M. Caillé. In vivo macrophage activity imaging in the central nervous system detected by magnetic resonance. *Magnetic Resonance in Medicine*, 41(2):329–333, 1999.

R. R. Edelman and S. Warach. Magnetic resonance imaging. *New England Journal of Medicine*, 328(10):708–716, 1993.

R. M. Feldman and C. Valdez-Flores. *Applied probability and stochastic processes*. Springer Science & Business Media, 2009.

A. Fernndez, C. Gmez, R. Hornero, and J. J. Lpez-Ibor. Complexity and schizophrenia. *Progress in Neuropsychopharmacology and Biological Psychiatry*, 45:267, 2013.

M. B. First. Diagnostic and statistical manual of mental disorders. *DSM IV-4th Esdition. APA*, 1994.

V. Fonov, A. C. Evans, K. Botteron, C. R. Almli, R. C. McKinstry, D. L. Collins, Brain Development Cooperative Group, et al. Unbiased average age-appropriate atlases for pediatric studies. *NeuroImage*, 54(1):313–327, 2011.

A. Fornito, A. Zalesky, C. Pantelis, and E. T. Bullmore. Schizophrenia, neuroimaging and connectomics. *Neuroimage*, 62(4):2296–2314, 2012.

M. D. Fox and M. E. Raichle. Spontaneous fluctuations in brain activity observed with functional magnetic resonance imaging. *Nature Reviews Neuroscience*, 8(9): 700–11, 2007.

M. D. Fox, D. Zhang, A. Z. Snyder, and M. E. Raichle. The global signal and observed anticorrelated resting state brain networks. *Journal of Neurophysiology*, 101(6):3270–3283, 2009.

R. S. J. Frackowiak, K. Friston, R. Dolan, C. Price, S. Zeki, J. Ashburner, W. Penny, and C. Frith. *Human Brain Function: Second Edition.* Academic Press, 2003.

K. J. Friston. Functional and effective connectivity in neuroimaging: a synthesis. *Human Brain Mapping*, 2(1-2):56–78, 1994.

K. J. Friston. Statistical parametric mapping: The analysis of functional brain images. *Neurosurgery*, 61(1):216–216, 2007.

K. J. Friston and C. D. Frith. Schizophrenia: a disconnection syndrome. *Clinical Neuroscience*, 3(2):89–97, 1995.

K. J. Friston, L. Harrison, and W. Penny. Dynamic causal modelling. *Neuroimage*, 19(4):1273–1302, 2003.

C. Frith. Functional imaging and cognitive abnormalities. *The Lancet*, 346(8975): 615–620, 1995.

L. K. Gallos, H. A. Makse, and M Sigman. A small world of weak ties provides optimal global integration of self-similar modules in functional brain networks. *Proceedings of the National Academy of Sciences of the United States of America*, 109(8):2825–30, 2011.

Y. E. Geda and R. D. Roberts. Physical exercise, aging, and mild cognitive impairment: a population-based study. *Mayo Clinic Proceedings*, 87(5):437–42, 2012.

G. H. Glover, T. Q. Li, and D. Ress. Image-based method for retrospective correction of physiological motion effects in fmri: Retroicor. *Magnetic Resonance in Medicine*, 44(1):162–167, 2015.

J. Goñi, V. D. H. Mp, A. Avenakoenigsberger, D. M. N. Velez, R. F. Betzel, A. Griffa, P. Hagmann, B. Corominasmurtra, J. P. Thiran, and O. Sporns. Resting-brain functional connectivity predicted by analytic measures of network communication. *Proceedings of the National Academy of Sciences*, 111(2):833, 2014.

I. I. Gottesman. *Schizophrenia genesis: The origins of madness.* WH Freeman/-Times Books/Henry Holt & Co, 1991.

S. Guo, L. Palaniyappan, B. Yang, Z. Liu, Z. Xue, and J. Feng. Anatomical distance affects functional connectivity in patients with schizophrenia and their siblings. *Schizophrenia Bulletin*, 40(2):449–459, 2014.

P. Hagmann, L. Jonasson, P. Maeder, J. P. Thiran, V. J. Wedeen, and R. Meuli. Understanding diffusion mr imaging techniques: From scalar diffusion-weighted imaging to diffusion tensor imaging and beyond 1. *Radiographics*, 26(suppl_1): S205–S223, 2006.

S. Hayasaka. Functional connectivity networks with and without global signal correction. *Frontiers in Human Neuroscience*, 7, 2013.

L. Hayflick. Entropy explains aging, genetic determinism explains longevity, and undefined terminology explains misunderstanding both. *PLoS Genetics*, 3(12): e220, 2007.

T. Hedden and J. D. E. Gabrieli. Insights into the ageing human mind - a view from cognitive neuroscience. *Nature Reviews Neuroscience*, 5(2):87–96, 2004.

C. J. Honey, O. Sporns, L. Cammoun, X. Gigandet, J. P. Thiran, R. Meuli, and P. Hagmann. Predicting human resting-state functional connectivity from structural connectivity. *Proceedings of the National Academy of Sciences*, 106(6):2035–2040, 2009.

S. A. Huettel, A. W. Song, and G. McCarthy. *Functional magnetic resonance imaging.* Sinauer Associates Sunderland, 2004.

M. Jenkinson, C. F. Beckmann, T. E. J. Behrens, M. W. Woolrich, and S. M. Smith. Fsl. *Neuroimage*, 62(2):782–790, 2012.

H. Johansen-Berg and T. E. J. Behrens. *Diffusion MRI: from quantitative measurement to in vivo neuroanatomy*. Academic Press, 2013.

H. Karbasforoushan and N. D. Woodward. Resting-state networks in schizophrenia. *Current Topics in Medicinal Chemistry*, 12(21):2404–2414, 2012.

A. Katsnelson. No gain from brain training. *Nature*, 464(7292):1111, 2010.

S. R. Kay, A. Flszbein, and L. A. Opfer. The positive and negative syndrome scale (panss) for schizophrenia. *Schizophrenia Bulletin*, 13(2):261, 1987.

T. T. J. Kircher and R. Thienel. Functional brain imaging of symptoms and cognition in schizophrenia. *Progress in Brain Research*, 150:299–604, 2005.

J. Lanceta, R. A. Prough, R. Liang, and E. Wang. Microrna group disorganization in aging. *Experimental Gerontology*, 45(4):269–278, 2010.

N. T. Lautenschlager, K. L. Cox, L. Flicker, J. K. Foster, F. M. Van Bockxmeer, J. Xiao, K. R. Greenop, and O. P. Almeida. Effect of physical activity on cognitive function in older adults at risk for alzheimer disease: a randomized trial. *Journal of the American Medical Association*, 300(9):1027–1037, 2008.

D. Le Bihan, J. F. Mangin, C. Poupon, C. A. Clark, S. Pappata, N. Molko, and H. Chabriat. Diffusion tensor imaging: concepts and applications. *Journal of Magnetic Resonance Imaging*, 13(4):534–546, 2001.

J. F. Leckman, D. Sholomskas, D. Thompson, A. Belanger, and M. M. Weissman. Best estimate of lifetime psychiatric diagnosis: a methodological study. *Archives of General Psychiatry*, 39(8):879, 1982.

C. A. Levie. The schizophrenic disorders: Long-term patient and family studies. *American Journal of Psychiatry*, 136(7):1001–1002, 1979.

C. Li, W. Wu, H. Jin, X. Zhang, H. Xue, Y. He, S. Xiao, D. V. Jeste, and M. Zhang. Successful aging in shanghai, china: definition, distribution and related factors. *International Psychogeriatrics*, 18(3):551–563, 2006.

T. Li, Y. Yao, Y. Cheng, B. Xu, X. Cao, D Waxman, W. Feng, Y. Shen, Q. Li, and J. Wang. Cognitive training can reduce the rate of cognitive aging: a neuroimaging cohort study. *Bmc Geriatrics*, 16(1):12, 2016.

M. Liang, Y. Zhou, T. Jiang, Z. Liu, L. Tian, H. Liu, and Y. Hao. Widespread functional disconnectivity in schizophrenia with resting-state functional magnetic resonance imaging. *Neuroreport*, 17(2):209–213, 2006.

P. F. Liddle, E. T. C. Ngan, G. Duffield, K. Kho, and A. J. Warren. Signs and symptoms of psychotic illness (sspi): a rating scale. *The British Journal of Psychiatry*, 180(1):45–50, 2002.

Y. Liu, M. Liang, Y. Zhou, Y. He, Y. Hao, M. Song, C. Yu, H. Liu, Z. Liu, and T. Jiang. Disrupted small-world networks in schizophrenia. *Brain*, 131(4):945–961, 2008.

J. Lu, H. Liu, M. Zhang, D. Wang, Y. Cao, Q. Ma, D. Rong, X. Wang, R. L. Buckner, and K. Li. Focal pontine lesions provide evidence that intrinsic functional connectivity reflects polysynaptic anatomical pathways. *Journal of Neuroscience the Official Journal of the Society for Neuroscience*, 31(42):15065–15071, 2011.

M. E. Lynall, D. S. Bassett, R. Kerwin, P. J. McKenna, M. Kitzbichler, U. Muller, and E. Bullmore. Functional connectivity and brain networks in schizophrenia. *The Journal of Neuroscience*, 30(28):9477–9487, 2010.

Allyson P. M., Alison T. M. S., and Silvia A. B. Intensive reasoning training alters patterns of brain connectivity at rest. *Journal of Neuroscience the Official Journal of the Society for Neuroscience*, 33(11):4796–803, 2013.

H. W. Mahncke, B. B. Connor, J. Appelman, O. N. Ahsanuddin, J. L. Hardy, R. A. Wood, N. M. Joyce, T Boniske, S. M. Atkins, and M. M. Merzenich. Memory enhancement in healthy older adults using a brain plasticity-based training program: A randomized, controlled study. *Proceedings of the National Academy of Sciences of the United States of America*, 103(33):12523–8, 2006.

A. Manoliu, V. Riedl, A. Doll, J. G. Bäuml, M. Mühlau, D. Schwerthöffer, M. Scherr, C. Zimmer, H. Förstl, and J. Bäuml. Insular dysfunction reflects altered between-network connectivity and severity of negative symptoms in schizophrenia during psychotic remission. *Frontiers in Human Neuroscience*, 7(4):216, 2013.

P. D. McGorry. The recognition and optimal management of early psychosis: an evidence-based reform. *World Psychiatry*, 1(2):76–83, 2002.

P. D. Mcgorry, E. Killackey, and A. Yung. Early intervention in psychosis: concepts, evidence and future directions. *World Psychiatry Official Journal of the World Psychiatric Association*, 7(3):148–156, 2008.

W. Mendenhall, R. Beaver, and B. Beaver. *Introduction to probability and statistics*. Cengage Learning, 2008.

V. Menon and L. Q. Uddin. Saliency, switching, attention and control: a network model of insula function. *Brain Structure and Function*, 214(5):655–667, 2010.

A. Messé, D. Rudrauf, H. Benali, and G. Marrelec. Relating structure and function in the human brain: relative contributions of anatomy, stationary dynamics, and non-stationarities. *PLOS Computational Biology*, 10(3):e1003530, 2014.

A. S. Meyer-Lindenberg, R. K. Olsen, P. D. Kohn, T. Brown, M. F. Egan, D. R. Weinberger, and K. F. Berman. Regionally specific disturbance of dorsolateral prefrontal–hippocampal functional connectivity in schizophrenia. *Archives of General Psychiatry*, 62(4):379–386, 2005.

J. H. Morrison and P. R. Hof. Life and death of neurons in the aging brain. *Science*, 278(5337):412–419, 1997.

G. Morrow, S. Battistini, P. Zhang, and R. M. Tanguay. Decreased lifespan in the absence of expression of the mitochondrial small heat shock protein hsp22 in drosophila. *Journal of Biological Chemistry*, 279(42):43382–43385, 2004.

K. Murphy, R. M. Birn, D. A. Handwerker, T. B. Jones, and P. A. Bandettini. The impact of global signal regression on resting state correlations: are anti-correlated networks introduced? *Neuroimage*, 44(3):893–905, 2009.

S. Ogawa and Y. W. Sung. Functional magnetic resonance imaging. *Scholarpedia*, 2(10):3105, 2007.

S. Ogawa, T. M. Lee, A. R. Kay, and D. W. Tank. Brain magnetic resonance imaging with contrast dependent on blood oxygenation. *Proceedings of the National Academy of Sciences*, 87(24):9868–9872, 1990.

A. M. Owen, A. Hampshire, J. A. Grahn, R. Stenton, S. Dajani, A. S. Burns, R. J. Howard, and C. G. Ballard. Putting brain training to the test. *Nature*, 465(7299): 775, 2010.

L. Palaniyappan, M. Simmonite, T. P. White, E. B. Liddle, and P. F. Liddle. Neural primacy of the salience processing system in schizophrenia. *Neuron*, 79(4):814–828, 2013.

C. Pantelis, M. Yücel, E. Bora, A. Fornito, R. Testa, W. J. Brewer, D. Velakoulis, and S. J. Wood. Neurobiological markers of illness onset in psychosis and

schizophrenia: the search for a moving target. *Neuropsychology Review*, 19(3): 385–398, 2009.

W. Pettersson-Yeo, P. Allen, S. Benetti, P. McGuire, and A. Mechelli. Dysconnectivity in schizophrenia: where are we now? *Neuroscience and Biobehavioral Reviews*, 35(5):1110–1124, 2011.

C. E. Pizoli, M. N. Shah, A. Z. Snyder, J. S. Shimony, D. D. Limbrick, M. E. Raichle, B. L. Schlaggar, and M. D. Smyth. Resting-state activity in development and maintenance of normal brain function. *Proceedings of the National Academy of Sciences of the United States of America*, 108(28):11638–43, 2011.

S. Posse, S. Wiese, D. Gembris, K. Mathiak, C. Kessler, M. L. Grosseruyken, B. Elghahwagi, T. Richards, S. R. Dager, and V. G. Kiselev. Enhancement of bold-contrast sensitivity by single-shot multi-echo functional mr imaging. *Magnetic Resonance in Medicine*, 42(1):87–97, 1999.

J. D. Power, K. A. Barnes, A. Z. Snyder, B. L. Schlaggar, and S. E. Petersen. Spurious but systematic correlations in functional connectivity mri networks arise from subject motion. *Neuroimage*, 59(3):2142–2154, 2012.

W. Pu, L. Li, H. Zhang, X. Ouyang, H. Liu, and J. Zhao. Morphological and functional abnormalities of salience network in the early-stage of paranoid schizophrenia. *Schizophrenia Research*, 141(1):15–21, 2012.

C. Randolph, M. C. Tierney, E. Mohr, and T. N. Chase. The repeatable battery for the assessment of neuropsychological status (rbans): preliminary clinical validity. *Journal of Clinical and Experimental Neuropsychology*, 20(3):310, 1998.

S. Rea and T. E. Johnson. A metabolic model for life span determination in caenorhabditis elegans. *Developmental Cell*, 5(2):197–203, 2003.

G. P. Rédei. *Permutation Test (randomization test)*. Springer Netherlands, 2008.

J. L. Rodgers and W. A. Nicewander. Thirteen ways to look at the correlation coefficient. *American Statistician*, 42(1):59–66, 1988.

E. T. Rolls. Glutamate, obsessive–compulsive disorder, schizophrenia, and the stability of cortical attractor neuronal networks. *Pharmacology Biochemistry and Behavior*, 100(4):736–751, 2012.

E. T. Rolls and G. Deco. *The noisy brain: Stochastic dynamics as a principle of brain function*. Oxford Univ. Press, UK, 2010.

E. T. Rolls, M. Loh, G. Deco, and G. Winterer. Computational models of schizophrenia and dopamine modulation in the prefrontal cortex. *Nature Reviews Neuroscience*, 9(9):696–709, 2008.

D. Rose and D. J. Pevalin. *A researcher's guide to the national statistics socio-economic classification*. SAGE Publications Ltd, 2003.

M. Rubinov and E. Bullmore. Fledgling pathoconnectomics of psychiatric disorders. *Trends in Cognitive Sciences*, 17(12):641–647, 2013.

Z. S. Saad, S. J. Gotts, K. Murphy, G. Chen, H. J. Jo, A. Martin, and R. W. Cox. Trouble at rest: how correlation patterns and group differences become distorted after global signal regression. *Brain Connectivity*, 2(1):25–32, 2012.

E. Santarnecchi, G. Galli, N. R. Polizzotto, A. Rossi, and S. Rossi. Efficiency of weak brain connections support general cognitive functioning. *Human Brain Mapping*, 35(9):4566–4582, 2014.

P. Savadjiev, J. S. W. Campbell, G. B. Pike, and K. Siddiqi. *Streamline Flows for White Matter Fibre Pathway Segmentation in Diffusion MRI*. Springer Berlin Heidelberg, 2008.

A. J. Schwarz and J. McGonigle. Negative edges and soft thresholding in complex network analysis of resting state functional connectivity data. *Neuroimage*, 55(3): 1132–1146, 2011.

G. A. Seber and A. J. Lee. *Linear regression analysis*. John Wiley & Sons, 2012.

W. W. Seeley, V. Menon, A. F. Schatzberg, J. Keller, G. H. Glover, H. Kenna, A. L. Reiss, and M. D. Greicius. Dissociable intrinsic connectivity networks for salience processing and executive control. *Journal of Neuroscience the Official Journal of the Society for Neuroscience*, 27(9):2349, 2007.

P. Skudlarski, K. Jagannathan, K. Anderson, M. C. Stevens, V. D. Calhoun, B. A. Skudlarska, and G. Pearlson. Brain connectivity is not only lower but different in schizophrenia: a combined anatomical and functional approach. *Biological Psychiatry*, 68(1):61–69, 2010.

A. Stan and D. A. Lewis. Altered cortical gaba neurotransmission in schizophrenia: insights into novel therapeutic strategies. *Current Pharmaceutical Biotechnology*, 13(8):1557, 2012.

K. E. Stephan, V. A. Magnotta, T. White, S. Arndt, M. Flaum, D. S. O'LEARY, and N. C. Andreasen. Effects of olanzapine on cerebellar functional connectivity in schizophrenia measured by fmri during a simple motor task. *Psychological Medicine*, 31(06):1065–1078, 2001.

B. Sylvie, C. Francis, M. Samira, G. Brigitte, F Francine, and G. Serge. Training-related brain plasticity in subjects at risk of developing alzheimers disease. *Brain*, 134(6):1623–1634, 2011.

H. Tao, S. Guo, T. Ge, K. M. Kendrick, Z. Xue, Z. Liu, and J. Feng. Depression uncouples brain hate circuit. *Molecular Psychiatry*, 18(1):101–111, 2013.

K. S. Taylor and K. D. Seminowicz DADavis. Two systems of resting state connectivity between the insula and cingulate cortex. *Human Brain Mapping*, 30(9): 2731C2745, 2009.

G. Tononi, O. Sporns, and G. M. Edelman. A measure for brain complexity: relating functional segregation and integration in the nervous system. *Proceedings of the National Academy of Sciences*, 91(11):5033–5037, 1994.

D. S. Tuch, T. G. Reese, M. R. Wiegell, N. Makris, J. W. Belliveau, and V. J. Wedeen. High angular resolution diffusion imaging reveals intravoxel white matter fiber heterogeneity. *Magnetic Resonance in Medicine*, 48(4):577–582, 2002.

O. Tymofiyeva, C. P. Hess, E. Ziv, P. N. Lee, H. C. Glass, D. M. Ferriero, A. J. Barkovich, and D. Xu. A dti-based template-free cortical connectome study of brain maturation. *PloS One*, 8(5):e63310, 2013.

N. Tzourio-Mazoyer, B. Landeau, D. Papathanassiou, F. Crivello, O. Etard, N. Delcroix, B. Mazoyer, and M. Joliot. Automated anatomical labeling of activations in spm using a macroscopic anatomical parcellation of the mni mri single-subject brain. *Neuroimage*, 15(1):273–289, 2002.

L. Q. Uddin, K. Supekar, and V. Menon. Typical and atypical development of functional human brain networks: Insights from resting-state fmri. *Conservation Genetics*, 4(3):21, 2010.

M. P. van Boxtel, M. P. ten Tusscher, J. F. Metsemakers, B. Willems, and J. Jolles. Visual determinants of reduced performance on the stroop color-word test in normal aging individuals. *Journal of Clinical and Experimental Neuropsychology*, 23 (5):620, 2001.

M. P. van den Heuvel and O. Sporns. Rich-club organization of the human connectome. *The Journal of Neuroscience*, 31(44):15775–15786, 2011.

M. P. van den Heuvel, R. C. W. Mandl, R. S. Kahn, H. Pol, and E. Hilleke. Functionally linked resting-state networks reflect the underlying structural connectivity architecture of the human brain. *Human Brain Mapping*, 30(10):3127–3141, 2009.

M. P. van den Heuvel, O. Sporns, G. Collin, T. Scheewe, R. Mandl, W. Cahn, J. Goñi, H. E. H. Pol, and R. S. Kahn. Abnormal rich club organization and functional brain dynamics in schizophrenia. *JAMA Psychiatry*, 70(8):783–792, 2013.

B. M. van Gelder, M. A. Tijhuis, S. Kalmijn, S. Giampaoli, and D. Kromhout. Decline in cognitive functioning is associated with a higher mortality risk. *Neuroepidemiology*, 28(2):93–100, 2007.

S. V. Vaseghi. *Advanced digital signal processing and noise reduction*. John Wiley & Sons, 2008.

A. Venkataraman, T. J. Whitford, C. F. Westin, P. Golland, and M. Kubicki. Whole brain resting state functional connectivity abnormalities in schizophrenia. *Schizophrenia Research*, 139(1):7–12, 2012.

M. W. Voss, R. S. Prakash, K. I. Erickson, C. Basak, L. Chaddock, J. S. Kim, H. Alves, S. Heo, A. N. Szabo, and S. M. White. Plasticity of brain networks in a randomized intervention trial of exercise training in older adults. *Frontiers in Aging Neuroscience*, 2(1):: 32., 2010.

R. Wang, T. Benner, A. G. Sorensen, and V. J. Wedeen. Diffusion toolkit: a software package for diffusion imaging data processing and tractography. In *Proceedings of The International Society for Magnetic Resonance in Medicine*, volume 15, 2007.

V. J. Wedeen, R. P. Wang, J. D. Schmahmann, T. Benner, W. Y. I. Tseng, G. P. Dai, D. N. Pandya, P. Hagmann, H. D'Arceuil, and A. J. de Crespigny. Diffusion spectrum magnetic resonance imaging (dsi) tractography of crossing fibers. *Neuroimage*, 41(4):1267–1277, 2008.

T. P. White, V. Joseph, S. T. Francis, and P. F. Liddle. Aberrant salience network (bilateral insula and anterior cingulate cortex) connectivity during information processing in schizophrenia. *Schizophrenia Research*, 123(2-3):105–115, 2010.

S. Whitfield-Gabrieli, H. W. Thermenos, S. Milanovic, M. T. Tsuang, S. V. Faraone, R. W. McCarley, M. E. Shenton, A. I. Green, A. Nieto-Castanon, P. LaViolette, et al. Hyperactivity and hyperconnectivity of the default network in schizophrenia and in first-degree relatives of persons with schizophrenia. *Proceedings of the National Academy of Sciences*, 106(4):1279–1284, 2009.

S. L. Willis and K. W. Schaie. Cognitive training and plasticity: theoretical perspective and methodological consequences. *Restorative Neurology and Neuroscience*, 27(5):375–389, 2009.

F. D. Wolinsky, F. W. Unverzagt, D. M. Smith, R Jones, A Stoddard, and S. L. Tennstedt. The active cognitive training trial and health-related quality of life: protection that lasts for 5 years. *The Journals of Gerontology: Series A, Biological Sciences and Medical Sciences*, 61(12):1324–1329, 2007.

S. W. Woods. Chlorpromazine equivalent doses for the newer atypical antipsychotics. *Journal of Clinical Psychiatry*, 64(6):663, 2003.

N. D. Woodward, H. Karbasforoushan, and S. Heckers. Thalamocortical dysconnectivity in schizophrenia. *The American Journal of Psychiatry*, 169(10):1092, 2012.

S. Xiao, P. Yao, and M. Zhang. Neuropsychological testing profiles of patients with alzheimer's disease and mild cognitive impairment: a case-control study. *Hong Kong Journal of Psychiatry*, 12(4):2–5, 2002.

C. Yan, W. Wu, F. Wei, J. Wang, C. You, S. Yuan, Q. Li, Z. Xu, and C. Li. The effects of multi-domain versus single-domain cognitive training in non-demented older people: a randomized controlled trial. *BMC Medicine*, 10(1):30, 2012.

C. G. Yan and Y. F. Zang. Dparsf: a matlab toolbox for "pipeline" data analysis of resting-state fmri. *Frontiers in Systems Neuroscience*, 4(13):13, 2010.

C. G. Yan, B. Cheung, C. Kelly, S. Colcombe, R. C. Craddock, A. Di Martino, Q. Li, X. N. Zuo, F. X. Castellanos, and M. P. Milham. A comprehensive assessment of regional variation in the impact of head micromovements on functional connectomics. *Neuroimage*, 76:183–201, 2013.

L. Yan, Y. Zhuo, Y. Ye, S. X. Xie, J. An, G. K. Aguirre, and J. Wang. Physiological origin of low-frequency drift in blood oxygen level dependent (bold) functional magnetic resonance imaging (fmri). *Magnetic Resonance in Medicine Official Journal of the Society of Magnetic Resonance in Medicine*, 61(4):819, 2009.

Y. Yao, W. L. Lu, B. Xu, C. B. Li, C. P. Lin, D. Waxman, and J. F. Feng. The increase of the functional entropy of the human brain with age. *Scientific Reports*, 3(10):2853, 2014.

Y. Yao, L. Palaniyappan, P. Liddle, J. Zhang, S. Francis, and J. Feng. Variability of structurally constrained and unconstrained functional connectivity in schizophrenia. *Human Brain Mapping*, 36(11):4529–38, 2015.

Y. Zhou, M. Liang, L. Tian, K. Wang, Y. Hao, H. Liu, Z. Liu, and T. Jiang. Functional disintegration in paranoid schizophrenia using resting-state fmri. *Schizophrenia Research*, 97(1):194–205, 2007.

X. N. Zuo, C. Kelly, A. Di Martino, M. Mennes, D. S. Margulies, S. Bangaru, R. Grzadzinski, A. C. Evans, Y. F. Zang, F. X. Castellanos, et al. Growing together and growing apart: regional and sex differences in the lifespan developmental trajectories of functional homotopy. *The Journal of Neuroscience*, 30(45): 15034–15043, 2010.